INVESTIGATION OF HIGH TEMPERATURE STEAM GASIFICATION OF BIOMASS CHAR

by

RICK BRYAN WOODRUFF

B.S., Massachusetts Institute of Technology, 2007

A thesis submitted to the

Faculty of the Graduate School of the

University of Colorado in partial fulfillment

of the requirement for the degree of

Doctor of Philosophy

Department of Chemical and Biological Engineering

2012

This thesis entitled:

Investigation of High Temperature Steam Gasification of Biomass Char

written by Rick Bryan Woodruff

has been approved for the Department of Chemical and Biological Engineering

_____

Alan W. Weimer

_____

J. Will Medlin

Date_____

The final copy of this thesis has been examined by the signatories, and we find that both the content and the form meet acceptable presentation standards of scholarly work in the above mentioned discipline.

Woodruff, Rick Bryan (Ph.D., Chemical and Biological Engineering)

Investigation of High Temperature Steam Gasification of Biomass Char

Thesis directed by Professor Alan W. Weimer

Solar thermal gasification of biomass is a promising route to renewable fuel production. In order to design efficient solar biomass gasifiers, the kinetic rate of the char gasification step must be determined. The key advantages of solar thermal gasification are the ability to operate at temperatures significantly higher than those used in traditional gasifiers and to operate with steam instead of oxygen to produce a product stream with higher energy content. High temperature steam gasification kinetics are rarely studied in the literature, and the methods that are commonly used to measure low temperature gasification kinetics are often not applicable at high temperatures, for example due to heat and mass transfer limitations. The work presented in this thesis comprises studies designed to advance the state of the art in high temperature steam gasification by investigating char gasification kinetics, incorporating those kinetics into a CFD model, and facilitating gasification studies in aerosol flow through the development of a novel particle feeding system.

A primary goal of this work was to develop a low-cost method to obtain an empirical rate expression for steam-char gasification. A modified fixed bed reactor was used to limit the effects of heat transfer, steam consumption, and hydrogen inhibition in order to ensure that the rate was measured at known conditions. After minimizing the above effects within the constraints of our laboratory system, the reaction rate was so rapid that our factory configured non-dispersive infrared analyzer could not provide high enough temporal resolution. In analyzing the data, we observed that the outlet flow meter could respond very quickly to changes in the gasification

rate. After further analysis and testing, it was determined that the flow meter alone could be used to measure the rate of gasification within the fixed bed. This gas flow measurement technique was able to provide high resolution data with a very low cost and simple to use flow meter.

Using the gas flow measurement technique, data were collected over a range of temperatures, steam concentrations, hydrogen concentrations and degrees of conversion. The results were used to develop an empirical rate expression based on the Random Pore Model for the dependence on conversion and a Langmuir-Hinshelwood type expression for the dependence on the reactor conditions. To demonstrate the power of an accurate kinetic rate expression, a simplified CFD model of a small fixed bed gasifier was developed using the commercially available Ansys Fluent software package. Validation experiments were performed in a laboratory scale fixed bed reactor. The model was able to accurately predict the overall reaction rate throughout time, and to lend insight into steam gasification in a fixed bed configuration.

In addition to the investigation of high temperature steam char kinetics, a novel particulate feeding system was developed to aid in aerosol flow studies. Aerosol flow reactors are a valuable tool for measuring extremely fast reaction rates with very small particles, but they require the feedstock to be delivered pneumatically at a very consistent rate. The feeding system developed in this thesis is capable of feeding a variety of organic and inorganic particles with a diameter of less than 150 μm, and has successfully fed milled biomass containing a high fraction of hard to feed, high aspect ratio particles. It has been successfully used in several studies in our lab to measure gasification kinetics with a variety of feedstocks.

to my wife, Lauren

Acknowledgements

Without the help of many people, this four and a half year journey would not have been possible.

Firstly, I would like to thank my research advisor, Professor Alan Weimer. Al provided me with the resources and the encouragement necessary to excel in research at the graduate level. Al allowed me to have a significant amount of input in the direction of my research, trusting that I would make it work. He encouraged me and gave me the opportunities to share my work with the scientific community, through numerous trips to the AICHe annual meeting and my experiences with the Colorado Center for Biorefining and Biofuels (C2B2). For these things I will always be grateful.

I would also like to thank Will Medlin, Rich Noble, Frank Kreith, and Chris Perkins for taking the time to serve on my committee and provide input and advice throughout the process. I would especially like to thank Chris for laying the groundwork for my project, and the guidance he continued to provide along the way.

I am grateful for my funding sources; The USDA for funding a large portion of my project, C2B2 for allowing me to present my work and network with renewable energy companies, and the Department of Education Graduate Assistantships in Areas of National Need Program for valuable experiences with the other members of our department.

I would also like to thank Team Weimer and all of the people that have directly contributed to my graduate work; Janna for all of the modeling help no matter how busy she was with her own work, Peter Kreider for the laser imagining work with the particle feeding system, Kim

Zimmer for the SEM work, Dragan Mejic for help with numerous projects and the machining of the particle feeder, Amy Oberlin, Clay Beevers, and Alan Izar for the REU time that they spent with me, and a special thanks to Michael Kruesi who spent a 6 month period working with me to develop the framework of the CFD model presented in Chapter 4. Without Michael's help the modeling work would have taken significantly longer.

I'd like to thank my friends here in Colorado, without whom this journey would have been much less enjoyable. I will be forever grateful for the hours of board games, snowboarding, Guitar Hero, and camping adventures. I want to specifically thank Paul Lichty, who was always excited to pick up an 800 pound TIG welder from the middle of nowhere, or discuss what we would build inside that underground missile silo we'll buy someday. Paul's willingness listen through countless stories of sailboats, plug-in cars, beer brewing or whatever the topic of the week may have been made the countless hours in the windowless basement seem not so bad.

I'd like to thank my parents Rick and Paula and my sister Stephanie for all of the support they've given me over the years. My dad cultured a mechanical aptitude at an early age that has proven to be one of my most useful of skills and my mom kept me grounded and always reassured me that I would make it through whatever task was at hand.

Lastly and most importantly, I would like to thank my wife, Lauren, for all of the fun, support, and encouragement she has given me over the years. I owe my transition to chemical engineering to her, and I am so happy to have expanded my knowledge base to a new field. She always pushes me to achieve my best, and having her by my side throughout graduate school has made it all the more enjoyable. She's always there to support me in the craziest of endeavors. From remodeling a 1970's double-wide trailer, to building a yeast culturing lab at home, I am

always surprised by her enthusiasm to tackle any challenge. I look forward to many more exciting years to come.

Table of Contents

List of tables

List of Figures

Chapter 1 Motivation and Scope

1.1 Motivation

Abundant and affordable fossil fuels are the lifeblood of modern human civilization. Without access to cheap and easy to handle sources of energy, many of the conveniences we now view as necessities may not be accessible to the general public. While the future availability of fossil fuels is hotly debated, most can agree that they are a finite resource and many of us will see their decline within our lifetimes.

The end of the age of fossil fuels will not come overnight. The forces of supply and demand will dictate a price that some will view as acceptable, and an increasing number will be unable to afford. With the invention of the derivatives markets that allow for the trading of enormous quantities of energy on a moment's notice, price swings can be exacerbated far beyond the underlying forces of long term supply and demand as we saw with oil in 2008. The volatile and unpredictable nature of energy prices wreaks havoc on the consumers, some struggling at times to even heat their homes. With an economy now struggling to rebound from the worst economic downturn since the great depression, any increase in energy prices will dampen what little recovery we have seen. We may never fully recover if we cannot find a way to keep energy costs in check.

Price is of course only one of the concerns surrounding excessive fossil fuel use. Climate change is increasingly viewed as a threat to the livelihoods of hundreds of millions of people. Be it coastal dwellers who must deal with increased risk of flooding during major storms, or farmers who depend on the rains and moderate temperatures that their ancestors experienced, many are already feeling the effects of a world undergoing change. At least a portion of this change can be

directly traced to the increase in global CO2 levels generated from burning carbon that has been stored in the earth for millions of years [1]. For the sake of future generations, it is imperative that we develop alternative sources of energy that limit the net amount of CO_2 released to the atmosphere.

One can argue that as a society we consume too much energy and could be equally as happy with much less. To a certain extent this is true, and conservation must be part of any plan to reduce consumption of fossil fuels, but the numbers are striking. According to the EIA's Annual Energy Review 2010 only 8% of the energy consumption in the U.S. comes from renewable sources [2]. Even if energy usage was cut in half, a dramatic feat, renewables would only account for 16% of energy consumption in the United States. We must seek to expand the current sources of renewable energy that we have, and continue research in new and promising areas.

Hydroelectric, wind, solar and geothermal all offer a promising future for renewable electricity generation. Unfortunately, these sources do little to satisfy our insatiable demand for hydrocarbon fuels. Electric vehicles may be able to lessen the demand by allowing renewable sources of electricity to satisfy some of our transportation needs, but there will always be technologies such as flight that require a denser source of energy. It is possible that futurist batteries will someday fill that void, but in the near term we must find a way to produce hydrocarbon fuels from renewable sources. Biomass derived fuels are one of the few technologies that show promise in this field.

Utilization of biomass as an energy resource for power and fuel production has the potential to offset a sizeable portion of our current fossil fuel use. Current methods of biomass

processing include biological and thermochemical routes. Biomass with high water content or large amounts of easily digestible substrates like starches and sugars are often converted using biological methods. For feedstock with low inherent moisture content, thermochemical processing is often advantageous due to fast reaction kinetics and the ability to handle non-digestible substrates such as lignin. One of the oldest and most widely used thermochemical methods is gasification.

Biomass gasification has been used for over a century as a method to produce synthesis gas from low cost carbonaceous materials such as biomass and coal. Synthesis gas, a mixture of H2, CO, and CO2, can be used for power generation or as a feedstock for commodity chemicals and hydrocarbon fuel production. Long before the days of natural gas, "wood gas" produced from biomass gasifiers is said to have been supplied through pipelines in some big cities to provide lighting and heating. Today, gasification offers a method to utilize the carbon stored in plants during photosynthesis, breaking it down into a form that can be used to synthesize a number of fungible fuels.

Currently, the most popular route for producing hydrocarbon fuels from synthesis gas is the Fischer-Tropsch process. Hydrogen and carbon monoxide are pumped to high pressures and exposed to catalysts such as iron and cobalt to produce a distribution of hydrocarbons that range from methane to waxes [3]. Other methods such as direct methanol synthesis and microbial utilization of synthesis gas are currently being researched. Whatever the final process may be, a cheap and renewable source of synthesis gas has the potential to replace some portion of the energy dense, easy to transport hydrocarbons that we depend on [4].

In order to utilize the full potential of our biomass resources, gasification processes must be made as efficient as possible so that little of the precious stored carbon is wasted. One way to achieve this is to utilize concentrated solar thermal energy to drive the reaction, thus eliminating the need to burn some of the biomass to produce the heat needed for the reaction [5, 6]. Another is to develop a detailed understanding of the process and the physical conditions inside the reactor. Advances in computing have allowed the application of computational fluid dynamics (CFD) to gasification systems. CFD allows the engineer to identify potential design bottlenecks and optimize for the desired conditions before a full scale reactor is built. Unfortunately CFD is only as good as the inputs, and data on the gasification rate for specific biomasses under all conditions that may be encountered inside a reactor is difficult or impossible to find. A primary aim of this dissertation is to develop a method for measuring gasification reaction kinetics under conditions that are relevant to solar thermal gasification.

1.2 Gasification Background

Biomass gasification can be broken down into two semi-distinct steps. Upon heating to the range of 300-500 ºC, biomass undergoes pyrolysis to produce synthesis gas, tar, and char, a material composed mostly of carbon and ash. The tar is an undesired byproduct and must be further reacted to synthesis gas or removed in downstream processing. Pyrolysis is a thermal degradation reaction, no gaseous reactants are needed and the kinetics are very rapid at high temperatures [7].

In the second stage, char undergoes gasification with an oxidant such as oxygen or steam to produce more syngas. This reaction can be exothermic or endothermic depending on the oxidant used. The temperature range for this reaction varies greatly and is often performed in the range of 700-1000 ºC. A multitude of other reactions such as tar breakdown take place

simultaneously, but char gasification is widely accepted to be rate limiting [8]. For this reason the kinetic investigation and modeling presented in this dissertation will focus on biomass char gasification.

Two different methods of gasification exist. Autothermal and allothermal gasification differ primarily in the method by which heat is supplied to the reactor. In traditional autothermal gasification, air or oxygen is used as the oxidizer to partially combust the char and this exothermic reaction provides the heat needed for the process. Partial combustion is ideal for heat transfer because the heat is produced in the same place that it is needed. Unfortunately, partial combustion significantly reduces the amount of syngas produced per unit biomass. It has been estimated that autothermal gasification of coal will consume at least 35% of the feedstock to provide the process heat alone [9]. Not only does this decrease the process efficiency, but carbon converted to CO_2 from partial combustion will most likely be released to the atmosphere rather than stored in the final product, which increases the carbon footprint of the process. Additionally, the large quantity of CO_2 generated during the combustion process dilutes the product stream and decreases the heating value. If pure oxygen is not available on-site, the products are further diluted with nitrogen from the air, resulting in product gas with a low heating value.

Allothermal gasification is an alternative to traditional gasification that allows for a larger portion of the carbon in the feedstock to be stored as desirable products. Steam or CO_2 is used as an oxidant in the place of oxygen and heat is supplied externally to drive the endothermic reactions. If a renewable heat source such as concentrated solar thermal energy is used, it is possible to design a process in which all of the carbon in the biomass is converted to desirable products. Additionally, an intermittent renewable source of heat can ultimately be stored as a fungible commodity. One potential drawback to allothermal gasification is that heat must be

transferred into the reactor. The low inherent thermal conductivity of biomass makes this difficult.

1.3 Solar thermal gasification

Concentrated solar thermal energy was used as early as the 19th century as a method to produce steam from the sun's rays. Unlike photovoltaic cells which convert the sun's energy into electricity, concentrated solar uses large mirrors to focus the sun and generate intense heat. With the energy crisis of the 1970's came a wave of innovation in the field of renewable energy, and the idea to combine concentrated solar with gasification technology was born [5]. D. W. Gregg of Lawrence Livermore Laboratories was a pioneer in the field and developed a simple reactor design based on direct irradiation of a fixed bed of coal. He was able to show that up to 48% of the incident solar energy could be stored in the product gas, and that the energy in the product gas was 80% from the feedstock and 20% from solar [10]. M. J. Antal of Princeton University was another pioneer in the field. His work included an investigation of biomass pyrolysis in a quartz drop tube reactor located at the focal point of a large solar concentrator. A major setback was insufficient residence time. It was advised that greater attention be paid to two phase flows in future reactor designs. As a result of the limited residence time only 50% conversion efficiency was obtained [11].

Currently, the majority of the work on solar thermal biomass gasification takes place at ETH Zurich under Aldo Steinfeld and here in Alan Weimer's lab. Our group has developed a multi-tubular reflective cavity reactor that is currently undergoing testing and analysis [12]. In this reactor opaque tubes are irradiated with concentrated solar to heat a flow of aerosol particles inside the tubes. Steinfeld's group has worked with a vortex flow reactor where suspended particles are directly heated with incoming radiation [13]. Difficulties associated with keeping

the quartz window clean have led them to also investigate designs using indirect irradiation [9, 14].

Solar thermal gasification gains its advantage by leveraging the benefits of two distinct renewable energy sources. Concentrated solar is a great way to produce high quality heat, but heat alone cannot power our transportation system. Gasification traditionally produces its own heat, but in doing so valuable carbon is wasted. By using solar energy to drive the gasification process, low value carbonaceous waste can be converted into a more valuable product.

An additional advantage of solar thermal gasification is the relative ease with which high temperatures can be obtained. With concentrated solar, temperatures of 1000-1400 ºC and above are easily achievable. In contrast to the traditional gasification temperatures of 700-1000 ºC, high temperatures allow for faster reaction kinetics, higher rates of heat transfer, and reduced tar production [15]. These advantages lead to smaller reactor sizes, and a higher quality product stream that lacks high levels of N_2, CO_2, and tar.

With the advantages offered by solar thermal gasification come unknowns. The body of literature surrounding gasification at temperatures below 1000 °C is enormous. High temperature, allothermal gasification on the other hand is a relatively new field, and lacks the supporting literature needed to design a successful reactor. While there is commercial interest in large scale fuel production using solar thermal gasification, the academic community has been limited to proof of concept tests. More data is needed to predict the reaction rate of high temperature steam gasification for various biomass sources, but the traditional methods used to measure gasification rates often fail when applied to high temperature reactions.

1.4 Current methods for measuring gasification rates

The current methods for measuring gasification rates can be roughly divided into two categories, slow real-time analysis, and rapid single point analysis. Real-time analysis systems record the reaction rate continuously and provide information about how the reaction rate changes with time. Single point analysis systems record a single conversion value for a given reaction time.

The most commonly used method for taking real-time measurements is thermogravimetric analysis (TGA). TGA is used to record the mass loss of a sample that is undergoing reaction. Kinetic rates of char gasification have been extensively studied using TGA in the temperature range of up to about 1000 ºC [16, 17]. Beyond this point heat and mass transfer often has an effect on steam gasification [18] and on gasification with CO_2 [19]. The complexities associated with measuring a very small mass loss at high temperatures in an atmosphere of steam, H_2 and CO heavily influence the system cost and reliability. A high-precision balance must be housed in an environment of inert gas, requiring a purge stream that often makes it difficult to ensure an environment of 100% steam at the reaction site. Additionally, the large number of gas tight seals increases the chances of small oxygen leaks which are unacceptable when measuring steam-char kinetics. With proper use, these drawbacks can be overcome, and quality data for low temperature steam-char gasification can be obtained. At high temperatures, heat and mass transfer issues begin to dominate and the accuracy of the data begins to suffer.

In a traditional TGA, the sample is suspended in a basket or crucible in the high temperature region of a furnace and mechanically connected to a balance in a protected area. For optimal mass transfer, a mesh basket can be used to allow diffusion through the sample holder. For slow reactions, the temperature of the sample and gaseous environment around the sample

are close to the furnace temperature and reactant gas stream. As the temperature increases, the reaction rate increases along with the heat consumption, reactant consumption, and product generation. When the reaction rate becomes fast enough and the sample is no longer in equilibrium with its surroundings, the measured reaction rate shifts from the true kinetic rate to a rate dominated by external heat and mass transfer [18]. The temperature and conditions at which this shift occurs varies greatly with biomass source, but few authors use TGA to measure rates for reactions that take place in less than a minute.

The fixed bed is another commonly used reactor for measuring gasification rates [20-22]. Like TGA, fixed beds allow for the continuous measurement of reaction rate throughout time. Continuous measurement is achieved by monitoring the gas flow and product concentration exiting the system. In a fixed bed reactor, biomass char is loaded into a sample holder at a typical loading rate of several grams. The sample is heated to the desired reaction temperature and reactant gases are flowed either through or around the bed. The product gas stream is then passed through a condenser to remove residual water vapor, and often passed through a filter and tar trap. The clean gas then exits the reactor through a flow meter and the concentration of product gases is measured, most commonly with gas chromatography (GC).

Fixed bed reactors are advantageous due to their simplicity and ease of use, but several design features of traditional fixed beds limit their applicability to high temperature rapid reactions. Firstly, it is extremely difficult to ensure that temperature and gas composition are uniform throughout the reacting bed. Low thermal conductivity and high heat of reaction can lead to large temperature gradients. High reaction rates and low diffusion can lead to localized areas of low steam and high hydrogen concentrations. Beds that are designed in the flow through configuration can limit the effect of gas concentration gradients if they are run in differential

mode. By maintaining a high reactant to product ratio it is possible to ensure relatively constant gas composition throughout the bed. Unfortunately this does little to help the temperature gradients within the bed, as the latent heat of steam is only a fraction of the reaction enthalpy.

Secondly, the time constant associated with the flow system is generally large enough to severely restrict the frequency response of the system. Excess volume associated with the cooling region of the reactor, steam condenser, gas cleanup, and analysis system can lead to slow response.

Finally, one of the most accurate and widely used methods of gas composition analysis is GC. To make a GC measurement, a discrete sample of the gas stream is taken and analyzed over a period of one to several minutes. Even with a modern micro GC, the measurement frequency is limited to approximately one sample per minute, making it impossible to measure reactions on the order of a minute or two in duration. The limitation of measurement frequency can be partially mitigated through the use of a rapid sample collection system that allows for offline measurement, but these systems are difficult and expensive to operate. A promising real-time alternative to GC analysis is non-dispersive infrared (NDIR). Because it is based on an optical measurement the response of the measurement itself is nearly instantaneous, but it is limited by the flow constraints mentioned above and smoothing for signal conditioning. It cannot measure hydrogen, but reaction rate can be estimated by monitoring the carbon containing gases CO, CO_2, and CH_4. NDIR also suffers from aliasing with compounds that have overlapping spectra such as water vapor, but proper gas conditioning can reduce this effect.

Rapid single point measurements differ greatly from real time analysis. Rather than measuring the reaction rate over a period of time, single point measurements are made by

subjecting the sample to the desired reaction conditions for a specified period of time, after which the reaction is quenched and the sample is analyzed. Examples of single point measurements include wire mesh [23, 24], and drop tube reactors [25-27]. In a wire mesh reactor, the sample is sandwiched between two resistive heating elements and reactant gases are forced through the mesh. The reaction is initiated by switching on the heating elements and quenched by turning them off. Temperature is controlled by adjusting the current through the heating elements based on a thermocouple located with the sample. Jamil et al. used a wire mesh reactor to measure conversion after as little as 5 seconds [24].

Drop tube reactors are continuous flow reactors that operate with concurrent gas and particle flow from the top to the bottom of a furnace tube. The residence time that the particles spend at reacting conditions is controlled by the downward gas velocity, and the slip velocity between the particles and the gas stream. Very short reaction times are possible, and to the author's knowledge, drop tubes are the only reactors capable of measuring gasification reaction rates on the order of a second. If the particles are appropriately dispersed in the gas stream, heat and mass transfer resistances are very low.

For both wire mesh and drop tube reactors, only one conversion value is collected per experiment and populating even one reaction rate vs. conversion plot would take a large number of experiments. To develop a detailed kinetic rate expression, the kinetic rate must be measured for many different conversion values at many different reaction conditions and the number of experiments grows to an enormous task.

1.5 Objectives

The research presented in this dissertation aims to advance the state of the art in solar-thermal biomass gasification through three specific objectives:

1. Develop a measurement system for high temperature steam gasification of switchgrass char and construct and empirical rate expression to predict the kinetic rate as a function of temperature, steam and hydrogen concentration, and degree of conversion.
2. Incorporate the empirical kinetic rate expression into a simple CFD model of a fixed bed gasifier and compare to experimental results.
3. Develop a particle feeding system for pneumatic delivery of various milled biomass feedstocks with a particle diameter less than 150 μm to facilitate aerosol flow gasification studies.

1.5.1 Gas flow measurement technique

A primary goal of this dissertation is the development of a kinetic measurement system that provides a method for real time measurement of high-temperature steam-char gasification. In order to develop an empirical rate expression for a specific sample of biomass char, the system must be able to measure the reaction rate vs. the degree of conversion for a wide range of operating conditions. Attempts were made throughout the course of this dissertation to use 3 of the 4 kinetic measurement methods listed above. For one reason or another they failed to produce data that could lead to the development of a global rate expression to be incorporated into a CFD model. Work then shifted to the development of a new technique that has proved successful in providing the necessary data.

The gas flow measurement technique is based on a modified fixed bed design. The simplicity and ease of use of the fixed bed provided an excellent starting point for the development of an optimized system. The effect of mass transfer can be easily mitigated by ensuring a flow-through configuration with a high rate of reactant flow. By forcing a high rate of reactant through the bed, the reactor can be run in differential mode and it can be assumed that the gas concentration at any point in the bed is approximately equal to the inlet concentration.

At high temperature and steam concentration the gasification reaction is very rapid and the temperature of the bed plummets nearly instantaneously due to the endothermic reaction. Under these conditions the reaction becomes heat transfer limited and it is difficult to know at what temperature the kinetic rate is being measured. After much trial and error it was found that a 500:1 mass ratio of inert ZrO_2 pellets to biomass char could dramatically reduce the temperature drop during gasification.

With high reactant flow and large amounts of thermal mass the reaction of switchgrass char and steam is complete in approximately 20 seconds at a temperature of 1150 °C. At these rates the response time of our analytical system was far too long to capture the shape of the gasification curve. In analyzing the data we noticed that the outlet flow meter would respond almost instantaneously to the initiation of gasification. After an in depth investigation into the quality of data produced by the outlet flow meter, we determined that the flow meter alone could provide all of the data necessary to calculate the rate of reaction. Chapter 2 describes in detail the development of this kinetic measurement system.

1.5.2 Fixed bed steam gasification

Fixed beds can be used not only to measure kinetics, but also as a reactor design for commercial gasifiers. Fixed beds are advantageous because they decouple the gas and solid residence time, allowing for feedstocks with minimal processing to be utilized. They are commonly used for autothermal gasification, but the high endothermicity of the steam-char reaction means that the reactor design and operation must be changed considerably for steam gasification.

Heat may be transferred to the bed of particles in several ways. Direct particle irradiation can be used if the heat source is concentrated solar energy. Direct irradiation is the most efficient form of heat transfer and has been applied with success to a fixed bed of coal by D. W. Gregg [10]. Other researchers, attempting to avoid the difficulties associated with an optically transparent reactor wall, have investigated indirect particle radiation with the use of a radiation absorber/emitter [9]. Another method involves flowing superheated steam into the bottom of an adiabatic reactor, but it is very difficult to maintain high temperatures in the majority of the bed. As a result, the product stream can be polluted with large amounts of tar [28].

Another potential design is the externally heated downdraft fixed bed. In this design biomass is added at the top of a vertically oriented tube and undergoes pyrolysis and gasification as it moves toward the heated zone of the reactor. The biomass is suspended in the reactor with a high temperature movable grate that allows ash and gases to pass through while retaining larger biomass pieces. This type of fixed bed and grate has been employed with success in a similar but autothermal downdraft reactor at the pilot scale [29]. In the proposed design, steam instead of oxygen is injected at the top of the reactor and moves downward through the bed of biomass. Any tars that are produced in the pyrolysis section are carried with the steam to the high

temperature section of the reactor where they undergo secondary reactions and primarily break down into synthesis gas. The major drawback with this design is the need to conduct heat through the packed bed of biomass with low thermal conductivity.

The modeling and experimental work presented in Chapter 3 is aimed at investigating the potential of fixed bed gasification in an externally heated tube and demonstrating the usefulness of an accurate kinetic rate expression. The dimensions of the reactor are such that it could be easily incorporated into the multi-tubular reactor already in operation at NREL's high flux solar furnace [12]. Externally heated fixed bed reactors for steam gasification have been studied in the past, but little work was done to investigate the inhibiting effects of heat transfer and gas concentration on performance of the bed [30, 31].

1.5.3 Feeder development

The initial focus for this dissertation was the measurement of gasification rates of <150 μm biomass particles in a drop tube reactor. The lack of a commercial feeder capable of producing a fine dispersion of particles at the desired feed rate drove the development of a novel brush based feeding system. The background, design, and testing of the feeding system are described in Chapter 4. After preliminary testing of <150 μm particles in a drop tube, the focus of this dissertation shifted to minimally processed biomass char of a much larger particle size and the feeder system and drop tube were no longer applicable. The residence time capability of our drop tube reactor was on the order of 1 second, far too short to fully react large biomass particles. The feeder has however facilitated research by several other graduate students and undergraduates in our lab and continues to be a dependable and valuable piece of laboratory equipment.

1.6 References

1. Cox, P.M., et al., *Acceleration of global warming due to carbon-cycle feedbacks in a coupled climate model.* Nature, 2000. **408**(6809): p. 184-187.
2. *Annual Energy Review 2010*. 2010, U.S. Energy Information Administration.
3. Mark E, D., *The Fischer–Tropsch process: 1950–2000.* Catalysis Today, 2002. **71**(3-4): p. 227-241.
4. Huber, G.W., S. Iborra, and A. Corma, *Synthesis of transportation fuels from biomass: Chemistry, catalysts, and engineering.* Chemical Reviews, 2006. **106**(9): p. 4044-4098.
5. Richard J, K., *Sunfuels.* Progress in Energy and Combustion Science, 1982. **8**(2): p. 121-134.
6. Lédé, J., *Solar thermochemical conversion of biomass.* Solar Energy, 1999. **65**(1): p. 3-13.
7. Di Blasi, C. and C. Branca, *Kinetics of primary product formation from wood pyrolysis.* Industrial & Engineering Chemistry Research, 2001. **40**(23): p. 5547-5556.
8. Di Blasi, C., *Combustion and gasification rates of lignocellulosic chars.* Progress in Energy and Combustion Science, 2009. **35**(2): p. 121-140.
9. Piatkowski, N., C. Wieckert, and A. Steinfeld, *Experimental investigation of a packed-bed solar reactor for the steam-gasification of carbonaceous feedstocks.* Fuel Processing Technology, 2009. **90**(3): p. 360-366.
10. Gregg, D.W., et al., *Solar gasification of coal, activated carbon, coke and coal and biomass mixtures.* Solar Energy, 1980. **25**(4): p. 353-364.
11. Antal, M.J., et al., *Design and operation of a solar fired biomass flash pyrolysis reactor.* Solar Energy, 1983. **30**(4): p. 299-312.
12. Lichty, P., et al., *Rapid high temperature solar thermal biomass gasification in a prototype cavity reactor.* Journal of Solar Energy Engineering-Transactions of the Asme, 2010. **132**(1).
13. Z'Graggen, A., et al., *Hydrogen production by steam-gasification of petroleum coke using concentrated solar power--II Reactor design, testing, and modeling.* International Journal of Hydrogen Energy, 2006. **31**(6): p. 797-811.
14. Melchior, T., et al., *Solar-driven biochar gasification in a particle-flow reactor.* Chemical Engineering and Processing: Process Intensification, 2009. **48**(8): p. 1279-1287.
15. Han, J. and H. Kim, *The reduction and control technology of tar during biomass gasification/pyrolysis: An overview.* Renewable and Sustainable Energy Reviews, 2008. **12**(2): p. 397-416.
16. Marquez-Montesinos, F., et al., *CO2 and steam gasification of a grapefruit skin char.* Fuel, 2002. **81**(4): p. 423-429.
17. Klose, W. and M. Wolki, *On the intrinsic reaction rate of biomass char gasification with carbon dioxide and steam.* Fuel, 2005. **84**(7-8): p. 885-892.

18. Huang, Z.M., et al., *Kinetic studies of char gasification by steam and CO2 in the presence of H-2 and CO.* Fuel Processing Technology, 2010. **91**(8): p. 843-847.

19. Ollero, P., et al., *Diffusional effects in TGA gasification experiments for kinetic determination.* Fuel, 2002. **81**(15): p. 1989-2000.

20. Smolinski, A., K. Stanczyk, and N. Howaniec, *Steam gasification of selected energy crops in a fixed bed reactor.* Renewable Energy, 2010. **35**(2): p. 397-404.

21. Ahmed, I.I. and A.K. Gupta, *Kinetics of woodchips char gasification with steam and carbon dioxide.* Applied Energy, 2011. **88**(5): p. 1613-1619.

22. Yan, F., et al., *Hydrogen-rich gas production by steam gasification of char derived from cyanobacterial blooms (CDCB) in a fixed-bed reactor: Influence of particle size and residence time on gas yield and syngas composition.* International Journal of Hydrogen Energy, 2010. **35**(19): p. 10212-10217.

23. Messenbock, R., D.R. Dugwell, and R. Kandiyoti, *CO2 and steam-gasification in a high-pressure wire-mesh reactor: the reactivity of Daw Mill coal and combustion reactivity of its chars.* Fuel, 1999. **78**(7): p. 781-793.

24. Jamil, K., J.-i. Hayashi, and C.-Z. Li, *Pyrolysis of a Victorian brown coal and gasification of nascent char in CO2 atmosphere in a wire-mesh reactor.* Fuel, 2004. **83**(7-8): p. 833-843.

25. Biagini, E., M. Cioni, and L. Tognotti, *Development and characterization of a lab-scale entrained flow reactor for testing biomass fuels.* Fuel, 2005. **84**(12-13): p. 1524-1534.

26. Hayashi, J.i., et al., *Rapid conversion of tar and char from pyrolysis of a brown coal by reactions with steam in a drop-tube reactor.* Fuel, 2000. **79**(3-4): p. 439-447.

27. Matsumoto, K., et al., *Gasification reaction kinetics on biomass char obtained as a by-product of gasification in an entrained-flow gasifier with steam and oxygen at 900-1000 °C.* Fuel, 2009. **88**(3): p. 519-527.

28. Umeki, K., et al., *High temperature steam-only gasification of woody biomass.* Applied Energy, 2010. **87**(3): p. 791-798.

29. Henriksen, U., et al., *The design, construction and operation of a 75 kW two-stage gasifier.* Energy, 2006. **31**(10-11): p. 1542-1553.

30. Nipattummakul, N., et al., *High temperature steam gasification of wastewater sludge.* Applied Energy, 2010. **87**(12): p. 3729-3734.

31. Gao, N., et al., *Hydrogen-rich gas production from biomass steam gasification in an updraft fixed-bed gasifier combined with a porous ceramic reformer.* International Journal of Hydrogen Energy, 2008. **33**(20): p. 5430-5438.

Chapter 2 Kinetic measurements of high-temperature steam gasification of char using a novel measurement technique

2.1 Abstract

Solar thermal gasification of biomass is a promising technology that allows for operation at high temperature without burning a large portion of the biomass feedstock. Additionally, the process allows for solar energy to be stored and transported in chemical form. In order to design efficient solar reactors, a kinetic rate expression for high-temperature steam gasification is needed. Various methods have been used to measure the steam gasification rate of coal and biomass char at temperatures up to around 1000 °C. These conventional techniques often fail to collect accurate kinetic data at temperatures above 1000 °C due to heat and mass transfer resistance, and the time constants associated with the analysis system. In this chapter we discuss a novel measurement technique based on a modified fixed bed and data collected solely from a gas flow meter. The technique is then used to collect data over a range of reaction conditions between 1000 °C and 1150 °C. The Random Pore Model was found to adequately describe the reaction rate as a function of conversion, and the initial kinetic rate was fit to a Langmuir-Hinshelwood expression.

2.2 Introduction

Concerns about energy security and greenhouse gas emissions have driven a renewed interest in alternative sources of fuel. Gasification of carbonaceous material has been used for more than a century to produce synthesis gas, a mixture of CO, CO_2, and H_2. Synthesis gas can be burned directly for heat and electricity production, or used as a feedstock for the production of liquid fuels and commodity chemicals. One method to achieve the high temperatures needed for gasification is through the use of concentrated solar thermal energy. Using solar energy to supply the heat of reaction eliminates the need to burn a portion of the biomass and produces a higher quality synthesis gas.

Proper design of a solar thermal gasification reactor requires detailed knowledge of the kinetic rate under the varying conditions in the reactor. Unfortunately, the kinetic rate of biomass gasification is highly dependent on the biomass source and the method of preparation. Predicting accurate kinetic rates for a specific biomass source based on the available literature is difficult. It is therefore important to measure the kinetic rate of the intended biomass under the conditions expected in the reactor.

The kinetic investigation in this paper will focus on the steam-char reaction. Upon heating, biomass undergoes pyrolysis to produce synthesis gas, tar, and char, a material composed mostly of carbon and ash. In the second stage, char undergoes gasification with an oxidant such as oxygen or steam to produce more syngas. This reaction can be exothermic or endothermic depending on the oxidant used. A multitude of other reactions such as tar breakdown take place simultaneously, but the char gasification step is widely accepted to be rate limiting. It should be noted that this is an idealization and various products of pyrolysis may have an effect on the gasification rate [1].

The conventional methods for measuring gasification rates can be roughly divided into two categories; rapid single-point measurements, and slow real-time measurements. Rapid measurement techniques utilize reactors with high rates of heat and mass transfer to react the biomass for a specified amount of time, usually on the order of 1 second to several minutes. The sample is then removed and the degree of conversion is calculated. Examples of this type of reactor include drop tubes [2-4] and wire mesh reactors [5]. While this method is effective in measuring reactions that take place over a short period of time, extensive analysis over a range of temperatures, gas concentrations and degrees of conversion is difficult due to the limitations associated with measuring only one extent of conversion per experiment.

Real time measurement systems such as thermogravimetric analysis (TGA) [6-8] and fixed beds [9-13] have been widely applied to coal and biomass gasification. These methods are traditionally employed for reactions taking place over 5 minutes to an hour. For reaction times less than 5 minutes, heat and mass transfer limitations often begin to dominate, and inherent limitations with these systems become more apparent. Using TGA, care must be taken to avoid diffusional effects within the bed due to the nature of flow around the sample crucible [14]. With fixed beds, determining the reaction rate with high temporal resolution is difficult due to the time constants associated with the gas cleanup system and the analysis loop.

The authors have experimented with a fixed bed reactor utilizing non-dispersive infrared (NDIR) for real-time gas analysis. After much trial and error, the response time of the system was reduced to a point that allowed for the observation of reactions that complete in as little as 30 seconds. While this method provides a basis for approximating rapid reaction rates it is far from ideal. One modification includes increasing the gas flow through the analyzer to a level well above the manufacturer's recommendations. Additionally, aliasing of water vapor with the

CO_2 signal is an issue that is very difficult to avoid. Common desiccants such as Drierite cannot be used, and complete removal with a cold bath is difficult under the restrictions of high flow and low reactor volume. It is therefore of interest to develop an alternative to NDIR analysis that can be used to measure rapid gasification reactions.

The proposed method for measuring rapid gasification kinetics is based on a modified fixed bed designed to minimize the effects of heat and mass transfer. The gasification rate is calculated solely from the total gas flow exiting the reactor, allowing for very fast response to changes in the reaction rate. Because the only piece of analytical equipment that is required is a flow meter, the total system cost is much lower than with traditional methods. In this paper we use the gas flow technique to measure the steam-char reaction over a wide range of conditions and compare the results to select points measured with NDIR.

2.3 Methods

2.3.1 Gas flow measurement technique

The gas flow measurement technique is based on the molar flow rate of gaseous reaction products leaving the reactor. The steam-char gasification reaction can be represented as:

$$C + H_2O \rightarrow CO + H_2. \quad (1)$$

In this gasification reaction, two moles of gas are created for every one mol of carbon consumed. If the excess water is condensed, the reaction rate of carbon can be directly measured by measuring the molar flow rate out of the reactor.

In real world systems water gas shift also occurs as follows:

$$CO + H_2O \rightarrow CO_2 + H_2. \quad (2)$$

If excess steam is removed before the flow meter as it is in most reactor systems, water gas shift complicates the measurement of the reaction rate because one mol of CO generates two moles of gas. In this case three moles of gas are produced for every one mol of carbon, and the molar flow rate is not representative of the reaction rate. To counteract this effect the gas may be passed through a CO_2 scrubber that removes the CO_2 from the gas stream. If CO_2 is removed, two moles of gas are generated for every one mol of carbon regardless of the extent of water gas shift.

The suitability of this measurement technique is dependent on the residence time of the system due to the unique characteristics associated with measuring the gas flow rate. When a molecule of CO_2 is first generated in the reactor it displaces another molecule of gas already in the system. A pressure wave is transmitted very rapidly through the condenser and CO_2 removal system and registered on the outlet flowmeter as product gas. When that molecule then reaches the sorbent bed it is removed from the gas stream and subtracted from the outlet flow. Steam consumption contributes to a similar but opposite effect by not registering half of the reactant gases until they reach the condenser. When one molecule of steam reacts to form two molecules of product gas, one of the product molecules simply replaces the molecule of steam and is not registered on the outlet flowmeter until it passes through the condenser where that steam molecule would have been removed from the gas phase. To facilitate rapid steam condensation and CO_2 removal, a nitrogen stream is added after the reactor to decrease the residence time of the gas conditioning system while maintaining an environment of 100% steam in the reactor.

2.3.2 Reactor design

The theory behind the proposed measurement system is relatively simple, but the implementation requires care to be taken in many areas of the reactor system. Gas residence time and flow restrictions must be minimized to ensure accurate readings of the gas generation rate. Heat and mass transfer resistance must be minimized to provide the most accurate measurement of the kinetic rate.

The reaction chamber is an 81 cm long alumina tube with a 2.54 cm O.D. and 1.9 cm I.D. suspended in a vertically oriented tube furnace. A diagram of the reactor system is shown in Figure 2-1. Product gases exit the reactor through a 6.4 mm tube made of inconel 600 that extends into the hot zone of the furnace and terminates 2 cm below a wire mesh. The wire mesh is held in place by supports welded to the side of the central tube. The central exhaust tube creates an undesirable dead zone between the inner inconel and outer alumina tube, but sealing this area would be very difficult without the use of purge gas. On top of the mesh, zirconia beads are mixed with the biomass to provide extra thermal mass and limit the temperature drop in the bed when the reaction is initiated. An inconel gas preheater is suspended above the reaction zone to adsorb radiant energy from the reactor walls and heat the incoming gas stream. Four K type thermocouples are located in the reaction bed; two at the bottom and two at a height of 3 cm. At each vertical position one thermocouple is located in the center of the bed and one at the wall. The vertical position of the reaction tube relative to the furnace was adjusted until the temperature at all locations was close to uniform.

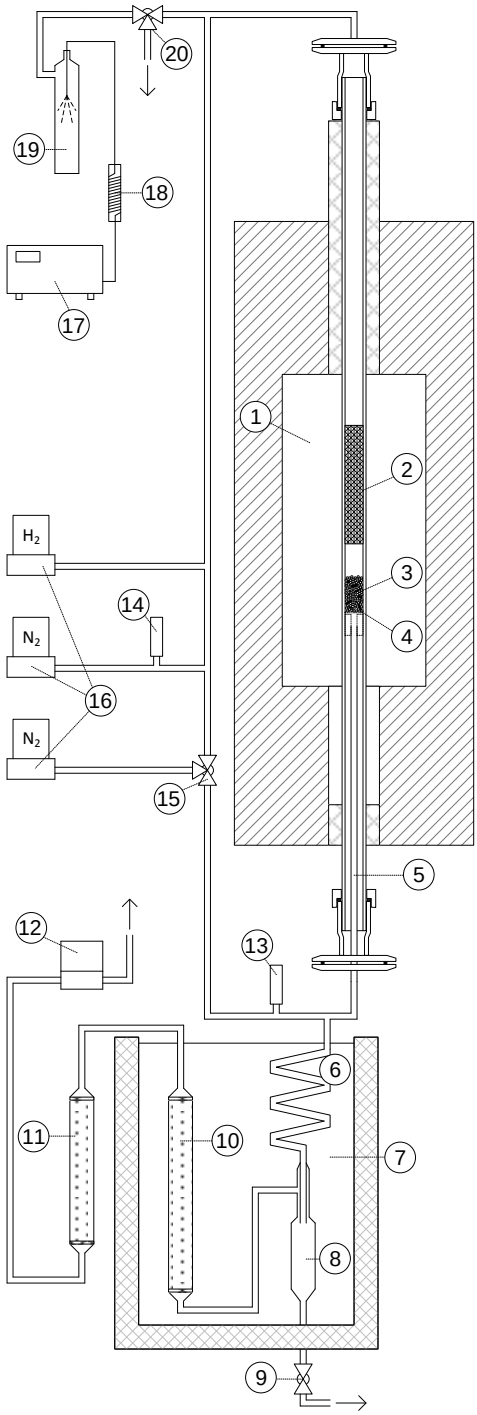

Figure 2-1: Downflow fixed bed reactor: (1) Furnace cavity; (2) Reactant preheater; (3) ZrO2 and char bed; (4) Inconel mesh; (5) Inconel outlet tube; (6) Condenser; (7) Ice bath; (8) Condensate collection; (9) Condensate drain; (10) Soda lime bed; (11) Drierite; (12) Outlet flowmeter; (13), (14) Pressure transducers; (15) Nitrogen 3-way valve; (16) Mass flow controllers; (17) High-pressure water pump; (18) Water pre-heater; (19) Steam generator; (20) Steam bypass 3-way valve.

The gas distribution system is equipped with three mass flow controllers and a custom built steam generator. Two mass flow controllers are used for nitrogen service and one for hydrogen. The system is designed such that the molar gas flow rate through the reaction tube and after the condenser is constant throughout the entirety of heat up and reaction. Constant flow ensures limited temperature changes in the bed due to changes in gas flow and quickly transports reactant gases through the analysis system. Rapid changes to the gas distribution are achieved using two 3-way valves to initiate gasification. Due to the slow response time of the mass flow controllers and steam generator, initiating steam flow by changing flow set points would be inadequate.

Gases exiting the reactor are mixed with nitrogen flow equivalent to the steam flow and enter the cleanup and analysis section. First, the flow passes through a condenser in an ice bath with a water reservoir just large enough to hold the water from the longest experiment. After the condenser, a column of soda lime is used to remove the CO_2 and Drierite is used to remove the residual water. The gas then passes through the outlet flow meter. For experiments using the NDIR, the soda lime and Drierite are replaced by a dry ice condenser to remove some of the residual water. The moisture must be reduced to limit aliasing with the CO_2 signal on the NDIR, but Drierite cannot be used due to its affinity for CO_2. Not all of the moisture is removed using this method, and the baseline CO_2 signal with steam flow is subtracted from the data.

Gas flow measurements are recorded using an Omega FMA series thermal based mass flow meter. In most cases, thermal based mass flow meters are unsuitable for measuring flows with variable concentrations. Fortunately, the calibration adjustment factor for the three main gases N_2, CO, and H_2 are all within 1% due to similar values for the product of specific heat capacity and density. Non-ideal mixing phenomena lead to a larger than predicted error when

measuring mixtures of nitrogen and hydrogen, but because the reaction rate is normalized by the total amount of gas produced, only large shifts in the CO/CO_2 production ratio would have an effect on the measured gasification rate. Experiments performed using NDIR analysis showed some shift in the ratio of CO to CO2 during the course of a reaction, but a sensitivity analysis showed little effect on the measured rate even with changes in the ratio of carbon products.

All experiments were performed at approximately atmospheric pressure. After accounting for decreased atmospheric pressure due to elevation, and slightly elevated pressure due to flow restrictions the system operates at an absolute pressure of approximately 0.95 bar.

2.3.2.1 Steam generator

Steady steam flow is a necessity in order to ensure the accuracy of measurements. No commercially available steam generators were found to deliver highly accurate steam flow in the range of 0-10 g/min at a reasonable cost. Several different steam generator designs were constructed and tested for consistency.

It is difficult to directly measure the consistency of steam flow with a time scale of several seconds. Integral measurements may be taken using a condenser weighed before and after a fixed period of time to estimate the long term accuracy. Unfortunately, little information about short term variations can be collected using this method. Measuring the steam flow directly is difficult, but the outlet flow meter on the reactor system used for gasification can be used to measure fluctuations in the nitrogen flow while passing steam through the system. The reactor system is configured the same way as in gasification tests. The steam is condensed before it reaches the outlet flow meter, but pulsations can be detected by monitoring the variations in the nitrogen flowing out of the reactor. If there is a spike in the steam flow rate, a spike in the nitrogen is

followed by a dip when the steam pulse enters the condenser. This method was used to assess the short term variation of various steam generator designs.

A syringe pump was originally used to deliver water to the reactor system by way of a capillary tube. The end of the capillary was inserted into the gas distribution system where heated nitrogen gas at roughly 150 °C was flowed past the tip. The system was extremely sensitive to changes in the steam flow rate, and often had large pulsations in flow due to a droplet forming at the outlet of the capillary tube. The droplet would continue to grow until it reached a point where it touched the heated walls of the nitrogen delivery system and it would vaporize suddenly. This issue was slightly lessened by the addition of alumina wool at the tip of the capillary to wick away some of the water, but steady flow was nearly impossible to achieve. In an attempt to further reduce the pulsations the capillary tube was also heated to approximately 150 °C. This change resulted in even worse performance. It is likely that nucleation points within the capillary tube caused liquid water to be periodically ejected from the capillary into the heated nitrogen stream. Additionally, if the pressure in the capillary rose too high, the syringe pump would stall and steam flow would cease altogether.

The failures described above led to the development of a steam generation system based on a Chromtech series 1500 high-pressure liquid pump, a liquid preheater, a nozzle, and a heated chamber. A diagram of the steam generator is shown in Figure 2-2. The HPLC pump was chosen over the syringe pump for the ability to pump water at high pressure. Operation at high pressure allowed for the use of an atomizer nozzle and a liquid preheater to bring the water to supercritical conditions before it enters the steam generator. In this system, Liquid water is pumped through a capillary tube heated to 300 ºC before passing through a nozzle and into a chamber heated to 250 ºC. Preheating the capillary under pressurized conditions ensured that no

phase transition with a discontinuous volume change would occur within the capillary. Preheating the fluid also decreased the amount of heat that was needed to be transferred from the walls inside the steam generator. Before the capillary heater was added pulsations in steam flow were observed. These pulsations were most likely due to droplets forming on the steam generator walls where the nozzle focused the majority of the spray.

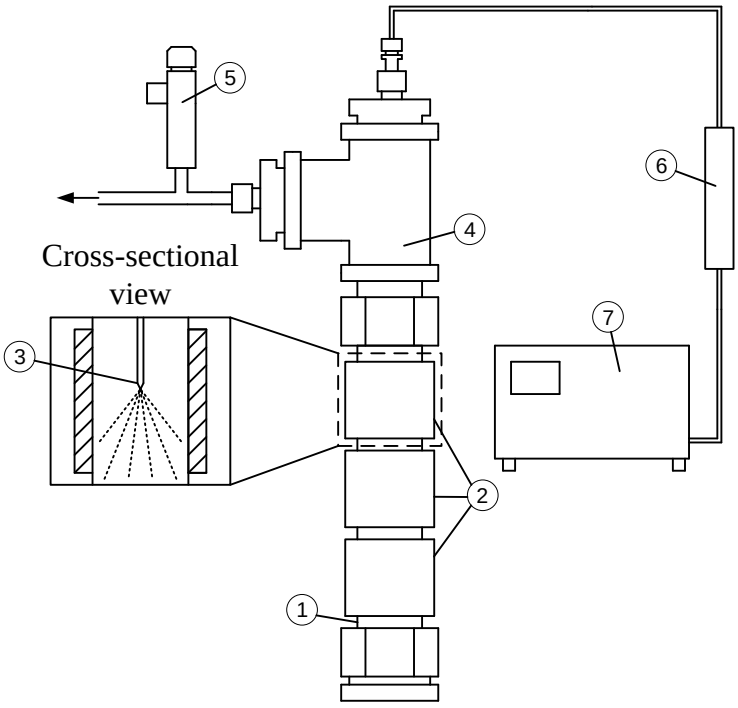

Figure 2-2: Diagram of the steam generator system. (1) 1" Copper tube; (2) Band heaters; (3) Nozzle; (4) Brass T fitting; (5) Pressure relief valve; (6) Preheater; (7) HPLC pump.

Finding a nozzle small enough to slide inside the steam generator and maintain the appropriate pressure drop was difficult. No commercially available nozzles were identified so custom nozzles were built. The nozzles were crafted by fully crimping the end of the capillary tubing and filing away the crimped portion until the pressure drop was approximately 2000 psi. Several different nozzles were made to accommodate different steam flow rates.

All lines between the steam generator and the reactor are heated to approximately 150 °C. It is important to ensure that no section of tubing drops below the condensation point of the steam. Special attention must be given to preventing condensation in the 3-way steam valve and at mounting points. In preliminary testing, one poorly insulated mounting bracket was enough to cool a small section of the steam line and greatly affect the quality of the data.

The system described above was used successfully for all experiments reported in this chapter. Steady steam flow was achieved in a consistent and repeatable manner.

2.3.2.2 CO_2 removal

As described in section 2.3.2, the gas flow measurement technique requires the removal of CO_2 from the gas stream when the water gas shift reaction occurs in any region of the reactor. Several different methods of CO_2 removal were considered.

Since CO_2 condenses into a solid form at -78.5 ºC and CO condenses at -191.5 ºC it would be possible to use a cryogenic condenser to remove the majority of the CO_2 from the gas stream. A mixture of liquid nitrogen with any of a number of other solvents could provide an appropriate temperature that would allow H_2 and CO to pass while solidifying the CO_2. As liquid nitrogen is readily available in most labs, it would be easy to replenish the cryogenic bath as needed. One drawback to this method is the dramatic temperature change and thus volume change the gas would experience when passing through the condenser. Additionally, removal of condensing solids from a high flow gas stream is very difficult and often leads to blockages. For these reasons the condensation method was not used.

NaOH was also considered due to its high affinity for CO_2. Unfortunately it also readily adsorbs water, and pellets of NaOH would quickly turn into a challenging to manage slurry.

Maintaining a high surface area would be difficult. It would be possible to deposit NaOH onto a porous inert substrate such as alumina, but an easier method was sought.

Initial testing with zeolite MS-13x showed great results for the removal of CO_2. The zeolite was preferred for its low toxicity and the ability to regenerate spent samples. Initial testing with the gasification system seemed to work, but an unexplained spike in the differential gas flow measurements raised concern. The initial spike in the product gas flow as shown in Figure 2-3 was eventually identified as an anomaly that is only present when the product gases are passed through the zeolite bed. It was initially hypothesized that the spike was due to an elevated reaction rate or unsteady steam flow.

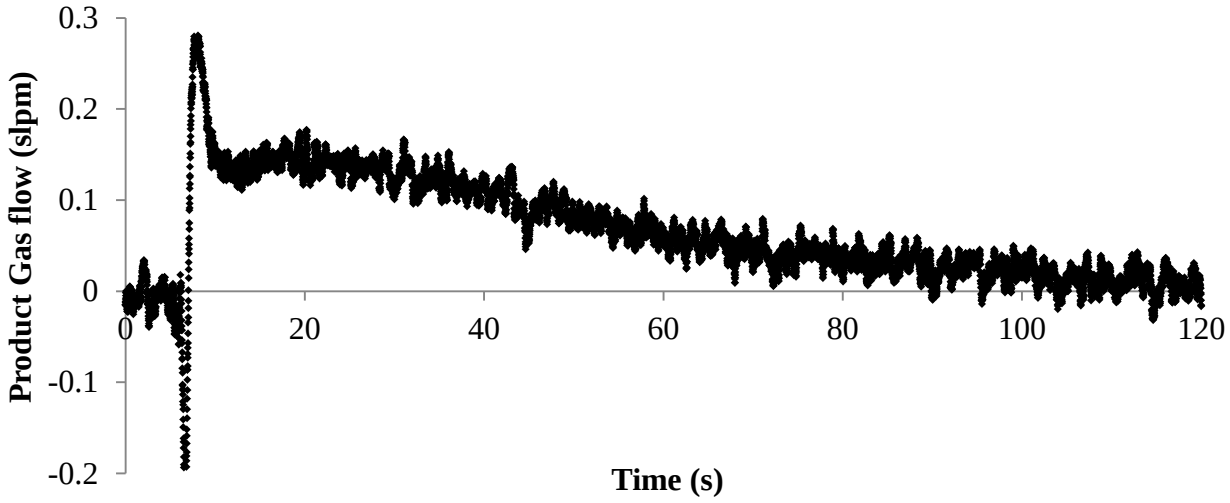

Figure 2-3: Product gas flow vs. time for gasification using the zeolite MS-13X CO_2 removal system. The large spike at the beginning of the reaction is an artifact that is caused by the presence of hydrogen in the gasification products.

The product gas flow shown in Figure 2-3 is obtained by subtracting the gas flow of a blank run from the total gas flow during gasification. Any perturbation in the adsorption/desorption characteristics of the zeolite between the gasification and blank runs

would be registered as an adjustment to the product gas flow. It was eventually determined that the introduction of a small amount of hydrogen in a background flow of nitrogen causes a spike identical to that seen during the gasification runs. The hydrogen in the gasification product stream causes the same effect, and since no hydrogen is present during the blank run, the effect is not canceled.

Soda lime was identified as a alternative to the zeolite and has performed well under all conditions. Soda lime is traditionally used to remove CO_2 from breathing gases in places like submarines and rebreathers. Because the soda lime does not also remove all of the moisture from the gas stream, a column of Drierite was used after the soda lime to remove the residual water vapor.

2.3.3 Sample preparation

Switchgrass samples were obtained from Colorado State University and chopped axially into approximately 1 cm sections. No other size reduction was performed. Samples were pyrolyzed to obtain char by heating to 1000 ºC at 20 ºC/min and holding for 20 min. Pyrolysis was performed in a separate reactor to prevent deposition of pyrolysis products in the kinetics reactor. Approximately 45 g of biomass were loaded for each pyrolysis reaction. Nitrogen at 4 slpm was used during the process to remove the majority of volatiles produced. Elemental analysis was performed by Huffman Labs of Golden, CO and is listed in Table 2-1. All results other than drying loss are reported on a dry basis. The BET surface area is 1.74 m^2/g and SEM images of two sections of char are shown in Figure 2-4.

	Switchgrass	Switchgrass char
Drying Loss	5.29%	5.74%
Carbon	43.92%	66.54%
H_2	6.21%	1.18%
N_2	0.32%	1.53%
Oxygen (diff)	45.80%	10.02%
Sulfur	0.07%	0.17%
Ash	3.68%	20.56%
HHV (BTU/lb)	7499	9782

Table 2-1: Compositional analysis of original and pyrolyzed switchgrass. All values other than drying loss are on a dry basis.

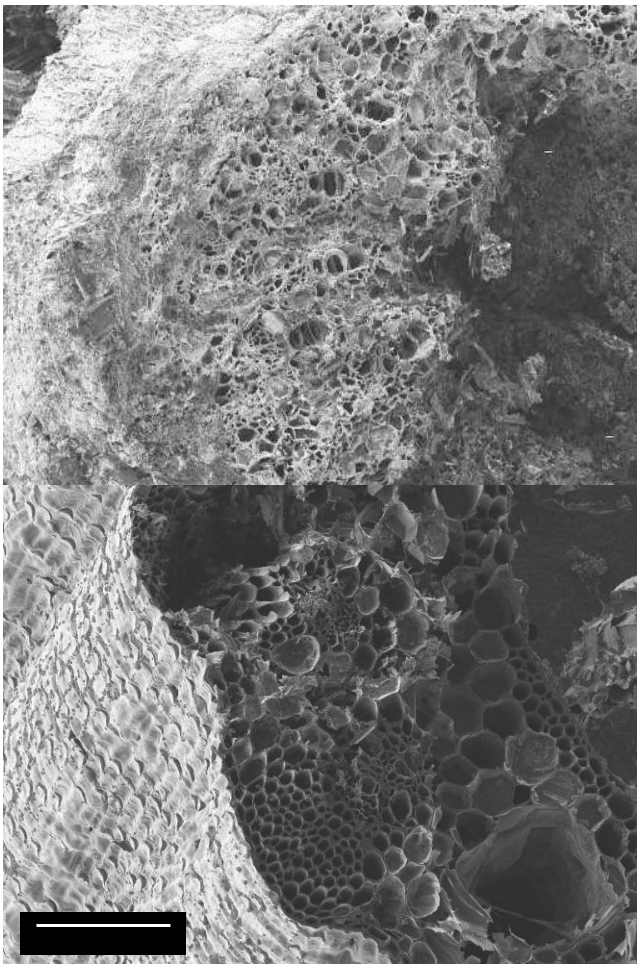

Figure 2-4 SEM image of two char sections.

2.3.4 Experimental procedure

For all experimental measurements the procedure was as follows. (1) To load the bed, 50 mg or 150 mg of char were mixed with 25 g ZrO_2 beads and loaded from the top of the reactor. 150 mg of char were used for the slowest reactions to decrease the level of noise. (2) Two mass flow controllers were used to deliver a total of 8 slpm nitrogen to the top of the reactor. One mass flow controller was set to deliver nitrogen through a 3-way valve at a set point equivalent to the desired steam flow rate. The other was set to the sum of the desired nitrogen and hydrogen flow. (3) The heat tape, steam generator, and furnace were turned on. The furnace was set to ramp at 30 K/min to the desired final temperature. (4) At a time well before the reaction was initiated, the water flow to the steam generator was started and the steam exited through a 3-way valve to bypass the reactor. (5) Once the reactor temperature had nearly stabilized, a portion of the nitrogen flow was replaced with the desired hydrogen flow and the temperature was allowed to fully stabilize. (6) To initiate the reaction, both 3-way valves were switched simultaneously. The effect of this valve actuation was to replace a portion of the nitrogen entering the reactor with an equal amount of steam, sending the replaced nitrogen to the exit of the reactor. (7) After the reaction was complete, the valves were switched back to their original position. For the gas flow measurement technique, step 6 was repeated and a baseline measurement was recorded.

2.4 Results and discussion

2.4.1 Analysis of gas flow measurements

The data collected during an experiment consist of gas flow measurements during the steam-char reaction and a blank run collected shortly after. Data from a typical run are shown in Figure 2-5. The first 10 seconds of the blank run are subtracted from the gasification data directly, after which the steady state value of the blank is used as a baseline to reduce

unnecessary noise. The large spike at the beginning of the experiment corresponds to the nitrogen in the reactor being displaced with steam. A plot of differential gas flow vs. time is shown in the bottom half of Figure 2-5.

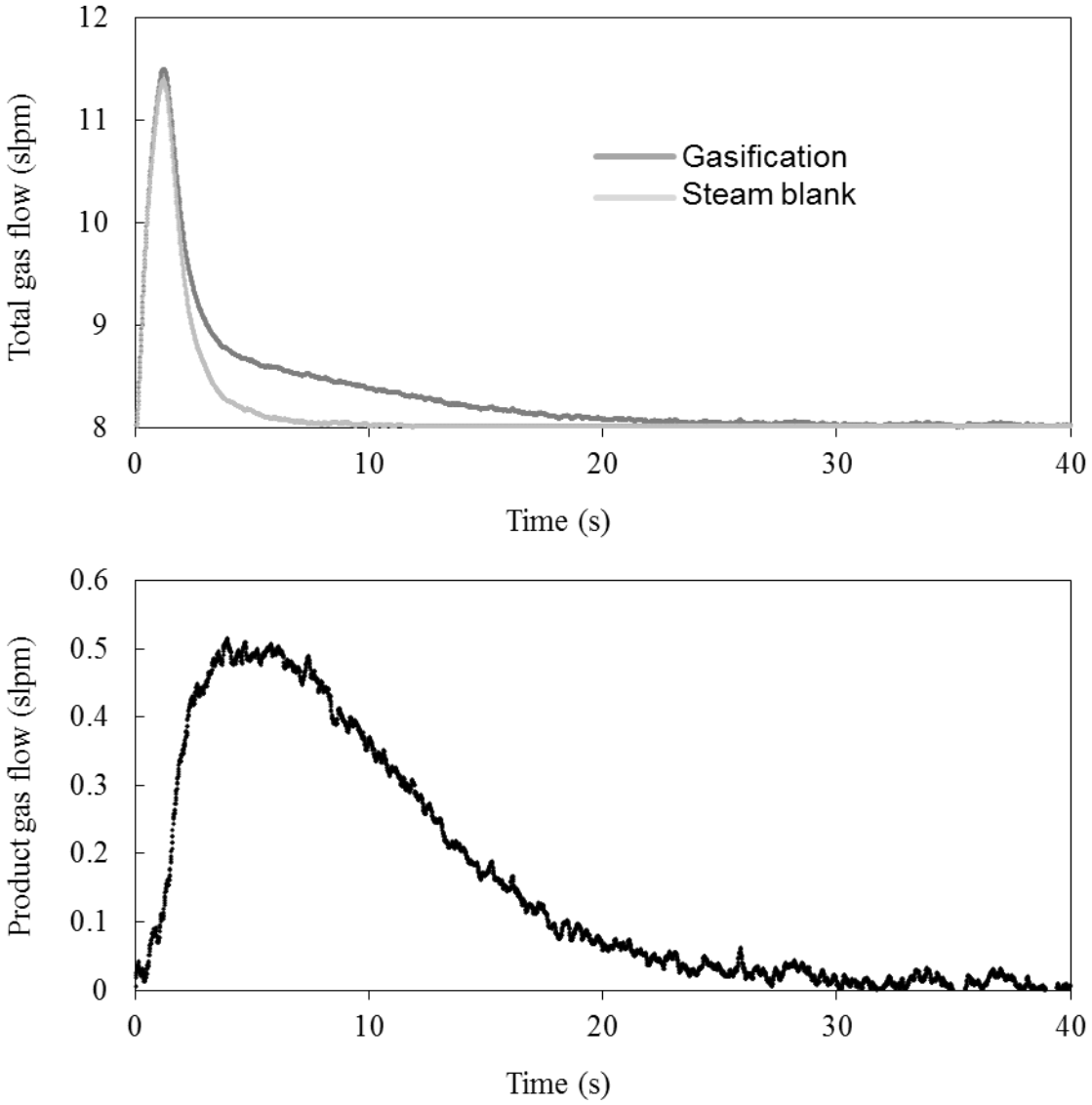

Figure 2-5: Steam gasification reaction at 1150 ºC and 100% steam at 0.95 bar. Top: Total reactor gas flow vs. time for gasification and a steam blank. Bottom: Differential gas flow corresponding to product gas generation.

The degree of conversion is calculated as follows,

$$X = \frac{V_g}{V_t} \tag{3}$$

where $V_g$is the cumulative amount of product gas at time *t* and V_t is the total amount of evolved gas for a given experiment. The reaction rate is defined as,

$$r = \frac{dX}{dt} = \frac{\dot{V}}{V_t}, \tag{4}$$

where $\dot{V}$ is the differential volumetric flow rate.

2.4.2 NDIR comparison to the gas flow measurement technique

Several data points were selected to be tested with NDIR as a comparison to the proposed measurement technique. Results from these experiments are shown in Figure 2-6 and Figure 2-7. The curves obtained using NDIR closely match the experiments using the gas flow measurement technique. For the fastest reaction rate shown in Plot A of Figure 2-6, the data from the NDIR are slower to rise and overall lower than the gas flow technique. This discrepancy is most likely due to the back mixing that occurs in the gas cleanup and analysis loop. As the response time of the system increases, the measured variables become smoothed and the apparent reaction rate decreases. It is likely that this discrepancy will continue to increase with an increase in reaction rate, giving the gas flow technique an advantage for even faster reaction rates. Unfortunately testing at higher temperatures was not possible with the current reactor design due to the materials of construction.

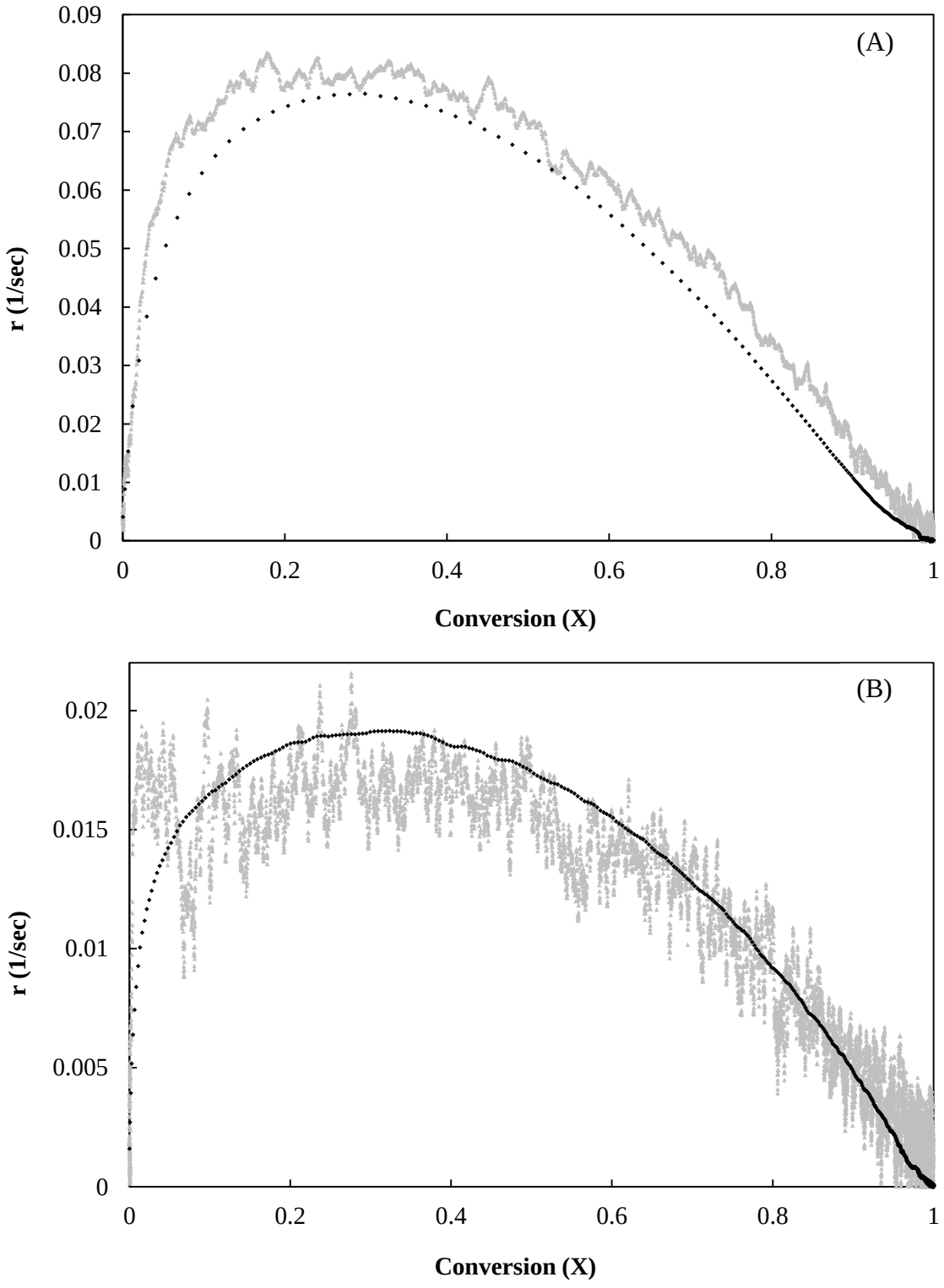

Figure 2-6: NDIR (black, foreground) vs. the gas flow measurement technique with 50 mg char loading. (A) 1150 °C, 100% H2O, (B) 1075 ºC, 20% H_2O, 80% N_2.

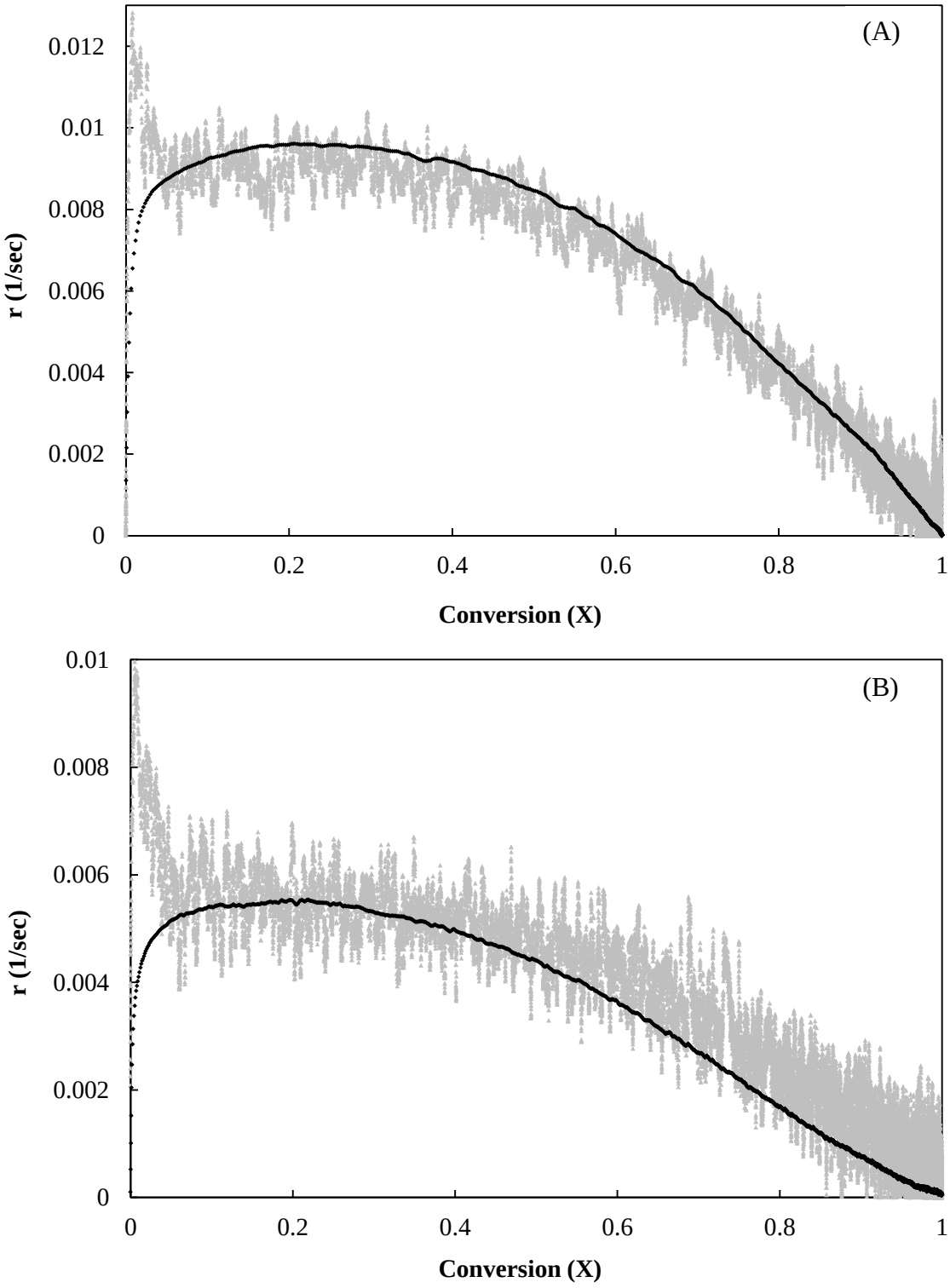

Figure 2-7: NDIR (black, foreground) vs. the gas flow measurement technique with 150 mg char loading. (A) 1000 ºC, 20% H_2O, 80% N_2, (B) 1075 ºC, 20% H_2O, 40% N_2, 40% H_2.

Although every effort was made to achieve steady steam flow, the elevated reaction rate shown in Figure 2-7 below 5% conversion is most likely due to small discrepancies in the steam flow rate. During the steam purge period shown as a large spike at the beginning of the reaction, very small differences in the steam flow are registered on the outlet flow meter. Once the system has reached equilibrium, all of the excess steam is condensed in the condenser and the baseline flow is the sum of N_2 and H_2 entering the reactor.

An inflection point can be seen at high conversion in many of the NDIR Plots. This behavior is caused from a small and slowly decreasing CO_2 signal after the majority of the reaction had completed. If the NDIR plots are created using the CO signal there is no longer an inflection point. It is likely that the small CO_2 signal is actually water vapor. While every effort was made to remove the residual water vapor from the gas stream, the dry ice condenser was not able to remove as much water as is predicted by the dew point. Some of the water vapor is condensed to ice crystals entrained in the gas stream. Every attempt to filter these ice particles resulted in a blockage before the reaction was complete. For all NDIR runs, the baseline CO_2 flow post-reaction was subtracted from the CO_2 concentration throughout the experiment.

The noise of the gas flow measurement technique increases substantially at slow reaction rates. For the slowest reactions the sample size was increased. The experiments in Figure 2-6 were performed using a 50 mg sample while those in Figure 2-7 used 150 mg. At very slow reaction rates on the order of 0.003 1/sec the gas flow technique becomes unsuitable with the current reactor configuration because the gas production rate is so small. With a larger isothermal reactor, the zirconia and char loading could be increased, and the gas flow technique could be applied to slower reactions.

2.4.3 Temperature uniformity

Due to the highly endothermic nature of the steam-char reaction, care must be taken to ensure that the reaction conditions match the desired conditions of the experiment in all regions of the bed. Initial experiments were carried out with 1 gram of char and no inert media. The temperature in the center of the bed dropped nearly 50 ºC and the reaction rate was much lower than that measured in subsequent experiments. The char loading was reduced to 50 mg, but the temperature drop observed in the bed was still too high to assume that the bed was isothermal.

In an effort to further limit the temperature drop in the bed, 25 grams of 2 mm diameter ZrO2 milling media were mixed with the char to add inert thermal mass. A maximum temperature drop of 15 ºC below the desired temperature was observed under the worst conditions of 150 mg char, 1000 ºC, and a gas composition of 20% steam and 80% nitrogen. The temperature plots for the four thermocouples located within the bed are shown in Figure 2-8.

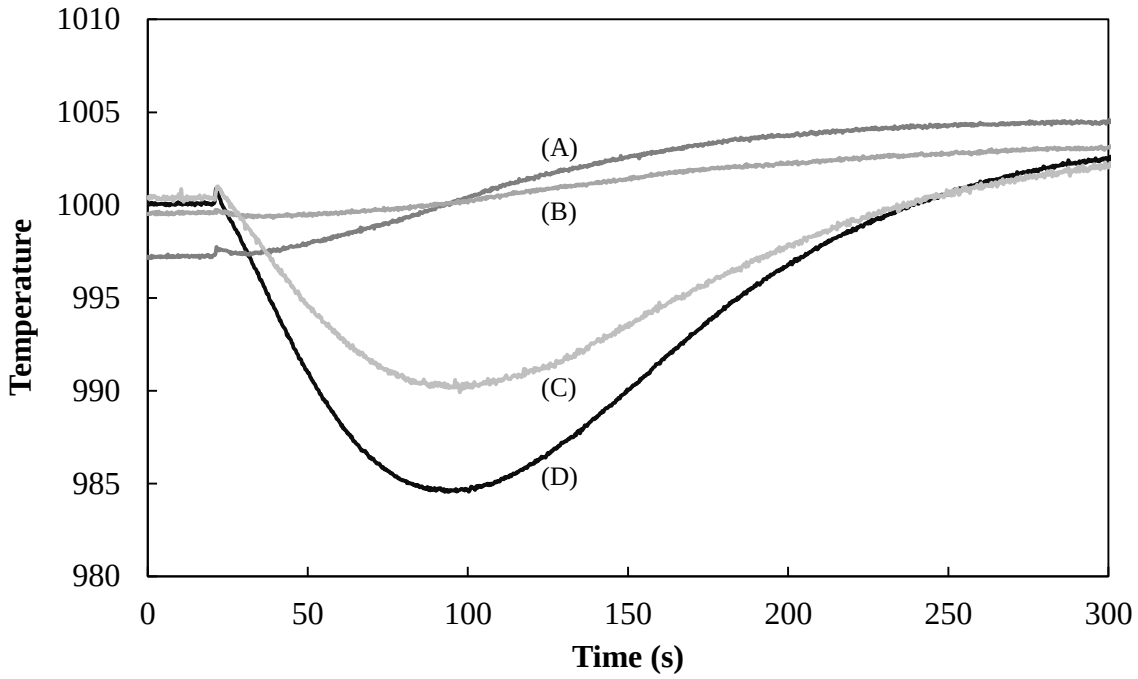

Figure 2-8: Plot of temperature vs. time at 1000 ºC, 150 mg char, and a gas composition of 20% steam, and 80% nitrogen. Thermocouple positions: (A) Top center, (B) Top wall, (C) Bottom wall, (D) Bottom center.

The highest temperature drop was observed at the bottom center of the bed.

A more typical temperature plot is shown in Figure 2-9. The majority of the bed stays within 5 ºC of the target temperature while the center reaches a maximum deviation of 8 ºC.

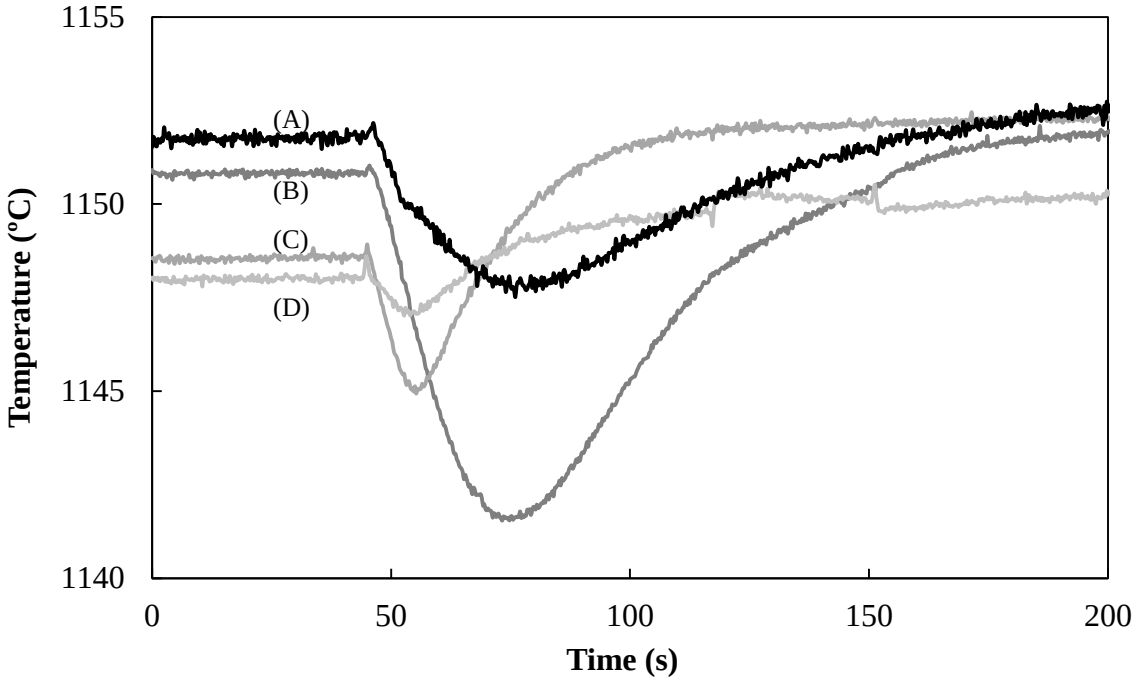

Figure 2-9: Plot of temperature vs. time at 1150 ºC, 50 mg char, and a gas composition of 70% steam, and 30% nitrogen. Thermocouple positions: (A) Bottom wall, (B) Bottom center, (C) Top center, (D) Top wall.

2.4.4 Potential sources of error

The normalization factor used in Equation (4) has a large impact on which variables introduce error into the final measurement. The value measured during the experiment is the gas flow rate with respect to time. In order to be the most useful for kinetic analysis, the gas flow rate vs. time must be converted to reaction rate vs. conversion. There are two logical candidates to use as the normalization factor. The first is the expected total gas flow as calculated based on the amount of char loaded into the reactor. The primary advantage to this method is the insensitivity to gas flow anomalies in the beginning stage of the reaction while the steam purges

the nitrogen from the system. On the other hand, all of the errors associated with predicting the amount of gas generated, measuring the flow rate accurately, and determining the mass of char in the bed at the time of reaction are propagated through to the final measurement. The char measurement is particularly important because a small and difficult to estimate amount of char is blown out of the bed by the high gas velocities before the reaction is initiated.

The second normalization method and the method used in this paper as shown in Equation (4) is performed by dividing by the total integral gas flow. Dividing by the total measured gas flow cancels all errors associated with char loading and linear variations in flow measurement. For instance, the calibration factor on the outlet flow meter could be changed by a factor of two with no effect on the calculated reaction rate. However, several sources of error remain including non-linear variations in flow measurement, flow anomalies during the purge phase, and drifting of the baseline between the gasification test and the blank run.

Non-linear variations in flow measurement can occur due to non-ideal mixing phenomena between hydrogen and nitrogen. While the calibration factor of 1.01 from nitrogen to hydrogen suggests that the two should be nearly interchangeable, this is not the case for mixtures of the two gases. Figure 2-10 shows the incremental change in gas flow when hydrogen is added to a stream of 8 slpm nitrogen. The response is linear, but the flow meter only reads 86.6% of the actual hydrogen flow. As stated above, linear variations in the calibration factor are compensated by the normalization method. If the amount of hydrogen produced per unit reaction remains constant no error is introduced, but if extent of the water-gas shift reaction changes during the experiment, errors in the measurement are possible.

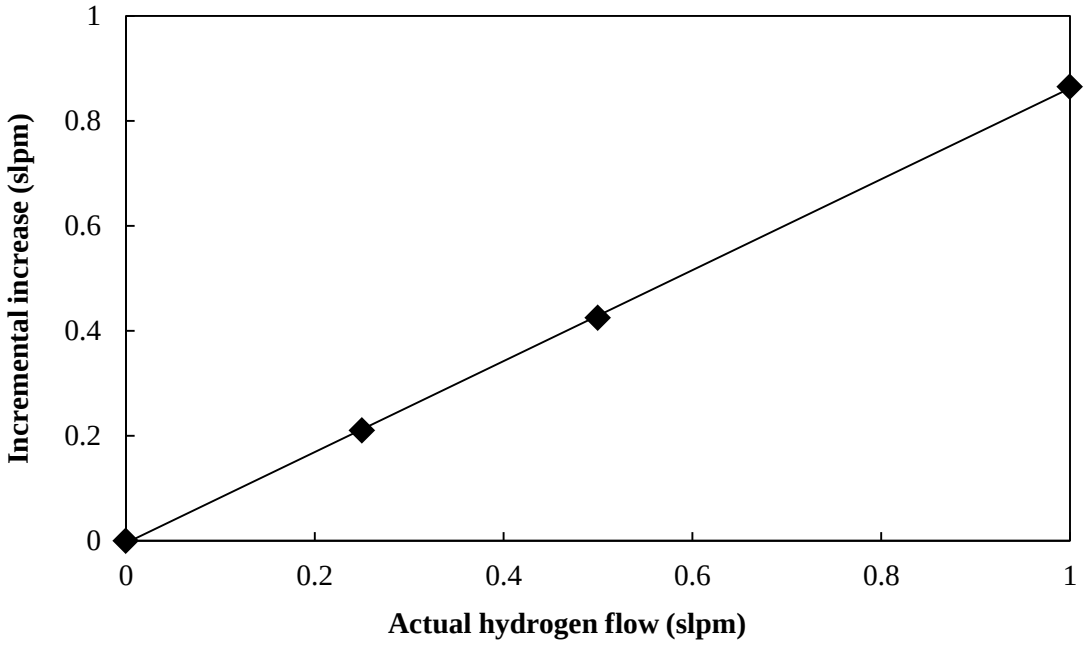

Figure 2-10: Measured vs. actual hydrogen flow with an 8 slpm nitrogen background.

Fortunately, the NDIR comparison experiments also determine how much the CO/CO_2 ratio changes during the gasification run. The change in the CO/CO_2 can then be used as a proxy for the water gas shift reaction to estimate the error introduced from changes in the hydrogen production. The gas composition data for the NDIR experiment performed at 1150 ºC and 100% steam was used to estimate the error in the instantaneous kinetic rate. The error contribution from the combination of the hydrogen calibration factor and the water-gas shift reaction is on the order of 0.4%.

Another source of error in the gas flow measurement technique is due to steam flow anomalies at the beginning of the reaction. When the reaction is first initiated, steam is directed to the inlet of the reactor and nitrogen is forced out the bottom. During this steam purge phase, small discrepancies in valve actuation timing and steam flow can lead to anomalies in the measured reaction rate. Reactions with a high rate of conversion are more affected because the

purge phase is a larger fraction of the total reaction time. Calculating a maximum error would be difficult or impossible without further knowledge of the system, but practical experience with multiple tests suggests an error up to approximately 5%. It should be noted that any steam condensation in the supply lines or unsteady steam production can greatly increase this value.

Drifting of the baseline gas flow between the gasification and the blank runs can also affect the accuracy of the measurement. Gas temperature, humidity, and particulate matter can all have an effect on the flow meter reading. With a background gas flow rate of 8 slpm, a drift of even 0.1% can have an effect on the measured reaction rate. The primary reason for baseline drift was determined to be a buildup of contaminants on the laminar flow element inside the flow meter during the reaction and better filtering of the gas stream nearly eliminated baseline drift. Given the level of noise in the flow data, a drift of approximately 0.003 slpm or greater can be detected and compensated for. For the fastest reactions, a drift of 0.003 slpm corresponds to a maximum error of approximately 2%, and for the slowest reactions it is up to 8%.

2.4.5 Model selection

In all experimental runs, the reaction rate initially increases until approximately 30% conversion. This phenomena has been observed in previous studies and is often characterized using the random pore model (RPM) [8, 11, 15]. The random pore model can be expressed as

$$r = k_0(1 - X)\sqrt{1 - \varphi \ln(1 - X)}, \tag{5}$$

where k_0 is the kinetic rate at $X = 0$, and φ is a geometric parameter. As noted by Hüttinger and Merdes, applying the RPM to gasification is only a curve fitting procedure, and it is possible that the geometry factor can change with reaction conditions even though it is based on physical parameters [13]. The exact physics that cause an increase in accessible reactive sites during our

experiments is unknown and may encompass a variety of factors including pore enlargement, a buildup of catalytic metals on the surface, or removal of pore-blocking carbonaceous deposits created during pyrolysis.

A total of 14 experimental runs were performed under the conditions listed in Table 2-2. The conditions were chosen to investigate the effect of steam alone, and to approximate the types of conditions found inside a real world reactor where the hydrogen concentration increases as steam is consumed.

Temperature (C)	Steam (%)	Hydrogen (%)	Nitrogen (%)	Char loading (mg)	k_0 (1/sec)
1150	100*	0	0	50	6.99E-02
1150	70	0	30	50	3.66E-02
1150	70	15	15	50	1.91E-02
1150	20	0	80	50	6.23E-02
1150	20	40	40	150	3.05E-02
1075	100	0	0	50	1.56E-02
1075	70	0	30	50	4.19E-02
1075	70	15	15	50	2.13E-02
1075	20	0	80	50	1.01E-02
1075	20	40	40	150	2.66E-02
1000	100	0	0	50	1.55E-02
1000	70	0	30	50	8.01E-03
1000	70	15	15	50	8.89E-03
1000	20	0	80	150	4.83E-03

*All percentage values at 0.95 bar total pressure

Table 2-2: Summary of reaction conditions and fitted kinetic parameters.

Microsoft's Excel was used to fit a single shape factor along with kinetic parameters k_0 for each run. Data were weighted to evenly represent the curve when plotted against conversion. Weighting was necessary due to the fact that time based points are more densely populated at

high values of conversion where the reaction rate is low. The data were fit over the region of 10-100% conversion; the first 10% of the reaction was ignored because it is largely affected by reactor stabilization. As can be seen in Figure 2-11 through Figure 2-15, a single shape factor of 4.3 adequately represents the data at all reaction conditions, greatly simplifying the development of an empirical rate expression. With a fixed value for the geometric parameter, only the initial kinetic rate must be fit to the reactor conditions.

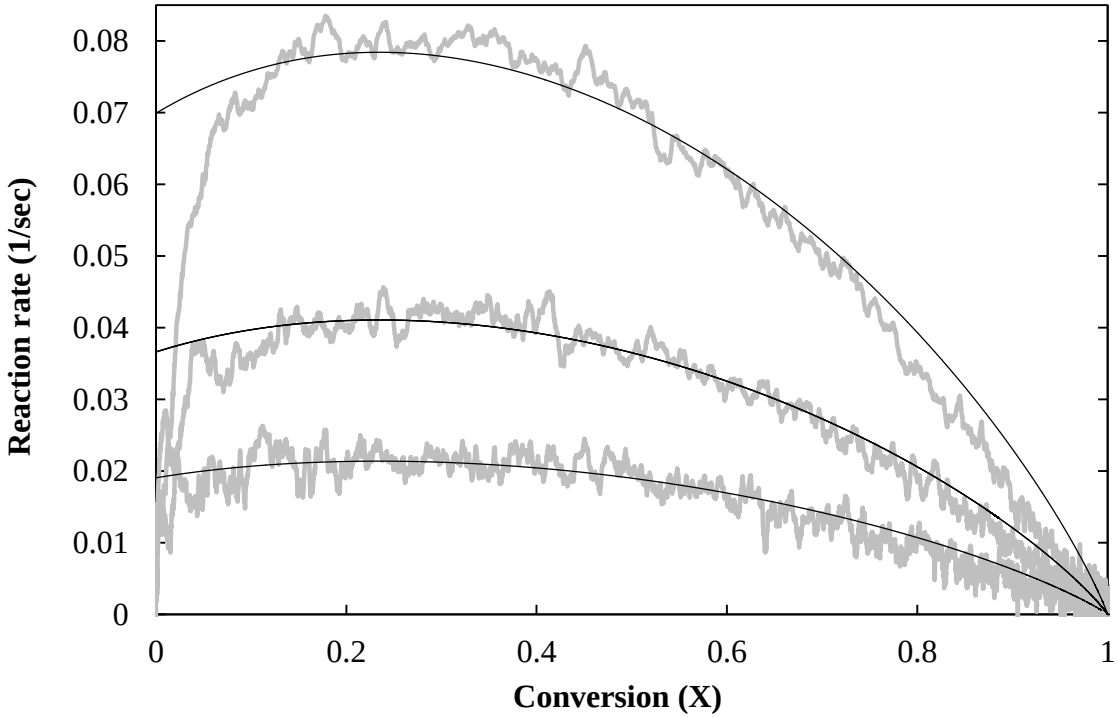

Figure 2-11: Reaction rate vs. conversion at 100% steam. Temperature: Top: 1150 ºC, Mid: 1075 ºC, Bottom: 1000 ºC. Experimental data in grey with a random pore model fit in black. For all fitted curves φ = 4.3.

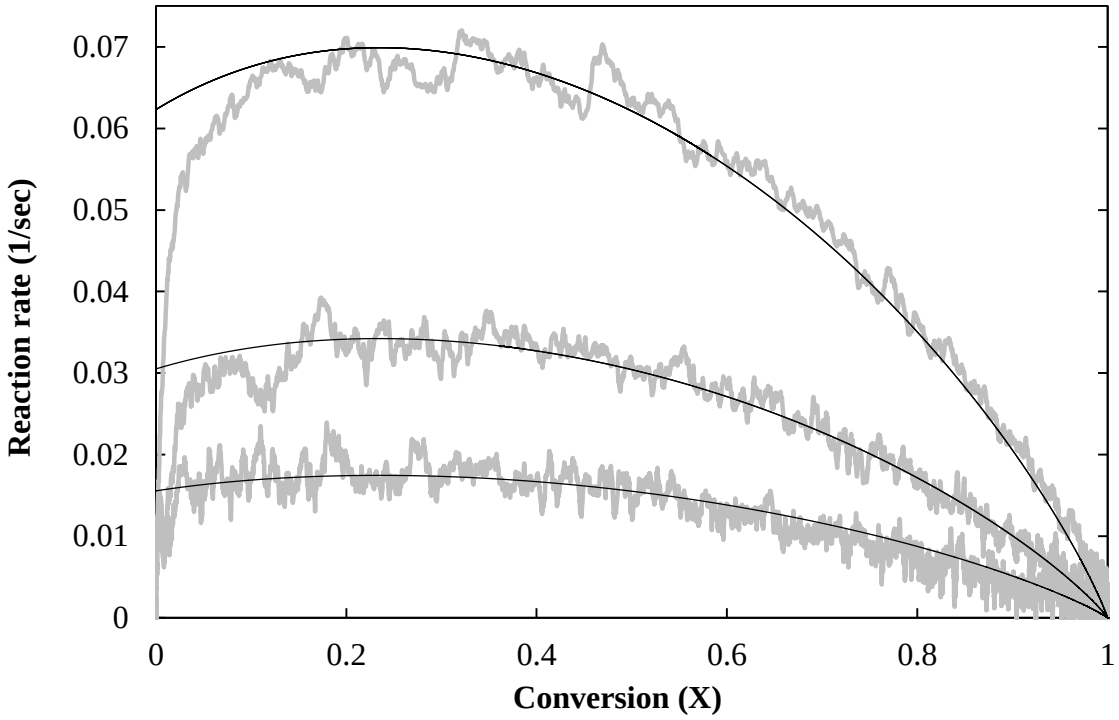

Figure 2-12: Reaction rate vs. conversion at 70% steam, 30% nitrogen. Temperature: Top: 1150 ºC, Mid: 1075 ºC, Bottom: 1000 ºC. Experimental data in grey with a random pore model fit. For all fitted curves φ = 4.3.

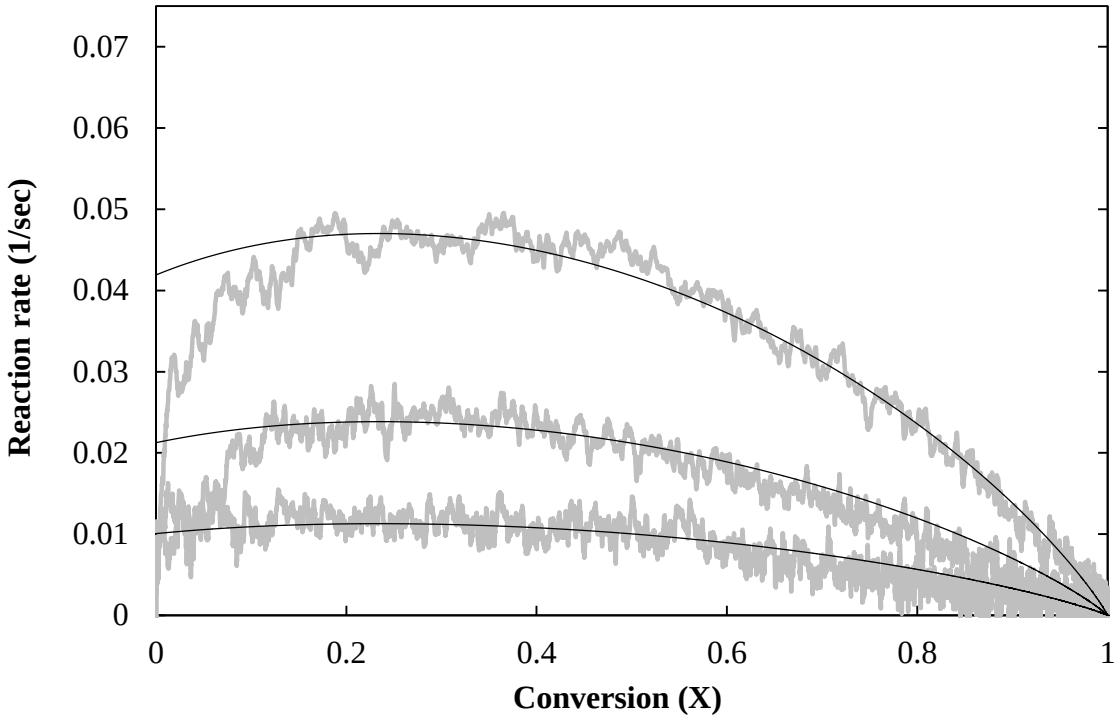

Figure 2-13: Reaction rate vs. conversion at 70% steam, 15% N_2, 15% H_2. Temperature: Top: 1150 ºC, Mid: 1075 ºC, Bottom: 1000 ºC. Experimental data in grey with a RPM fit. For all fitted curves φ = 4.3.

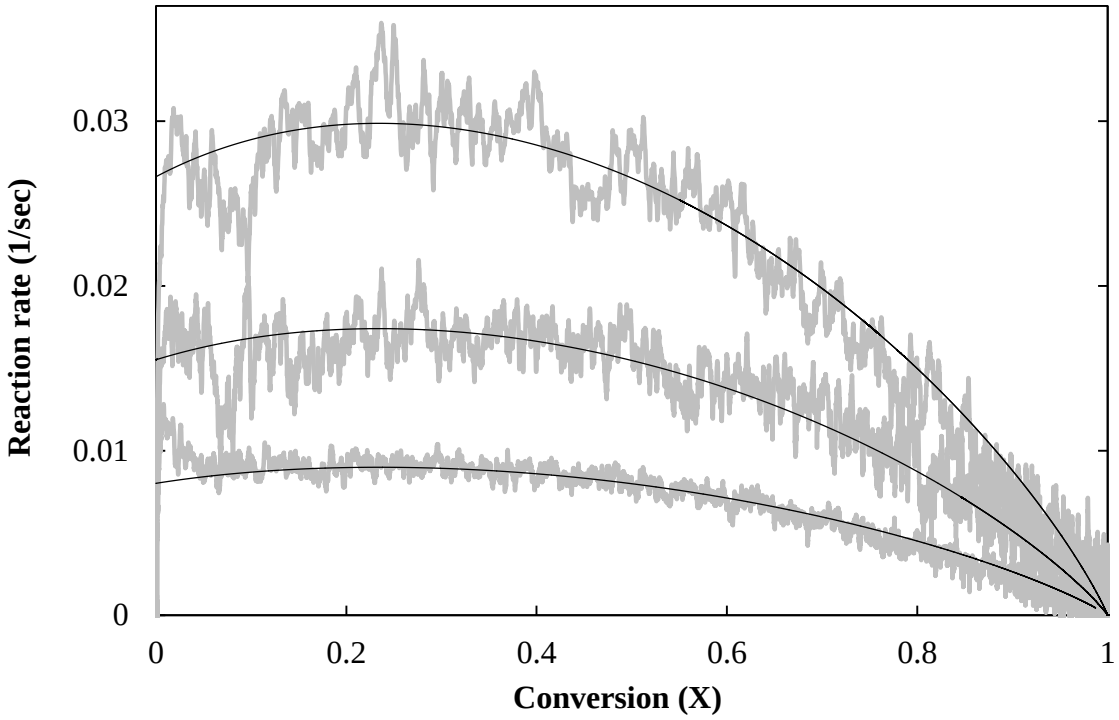

Figure 2-14: Reaction rate vs. conversion at 20% steam, 80% N_2. Temperature: Top: 1150 ºC, Mid: 1075 ºC, Bottom: 1000 ºC. Experimental data in grey with a random pore model fit. For all fitted curves φ = 4.3.

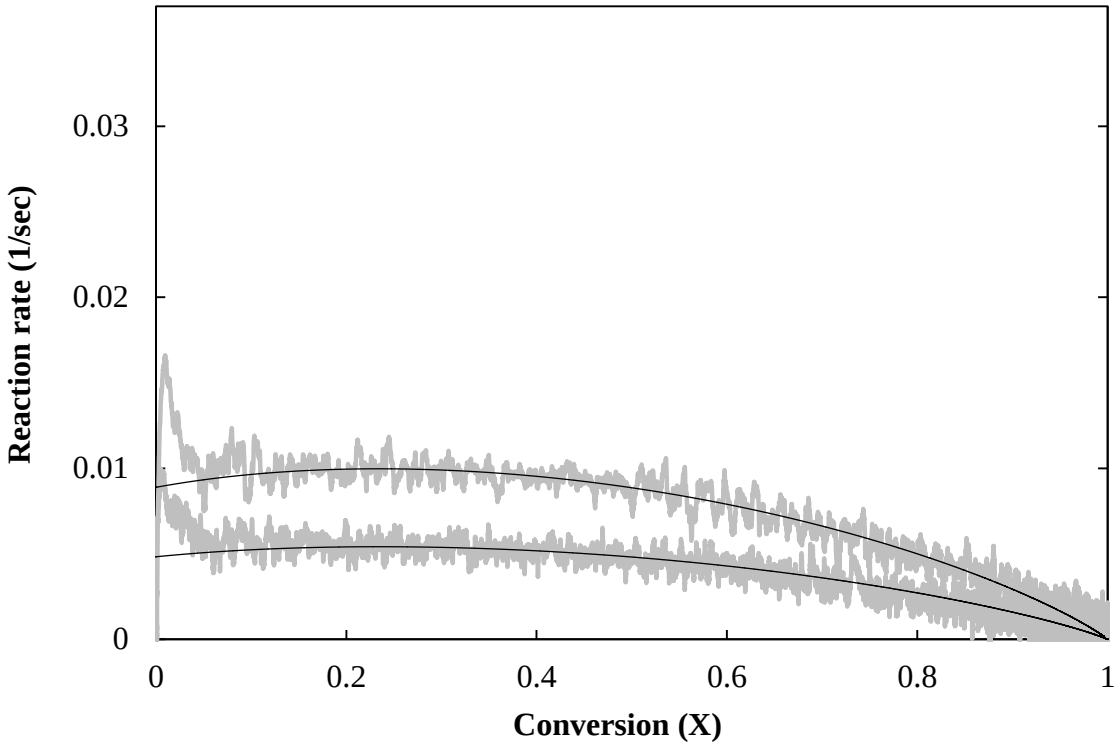

Figure 2-15: Reaction rate vs. conversion at 20% steam, 40% N_2, 40% H_2. Temperature: Top: 1150 ºC, Mid: 1075 ºC, Bottom: 1000 ºC. Experimental data in grey with a RPM fit. For all fitted curves φ = 4.3.

Modeling the kinetic rate of steam-char gasification with hydrogen inhibition is often performed using a Langmuir-Hinshelwood type expression [6, 7, 12] first described by Gadsby et al. [16]. For the case of steam-char gasification the expression takes the form of

$$k_0 = \frac{K_1 p_{H_2O}}{1 + K_2 p_{H_2O} + K_3 p_{H_2}}. \tag{6}$$

Where K_1, K_2, and K_3 are calculated using the Arrhenius type expressions,

$$K_1 = k_1 \exp(-E_1/RT), \tag{7}$$

$$K_2 = k_2 \exp(-E_2/RT), \tag{8}$$

$$K_3 = k_3 \exp(-E_3/RT). \tag{9}$$

It should be noted that while E_1 represents a single activation energy, E_2 and E_3 result from the subtraction of two activation energies.

Figure 2-16 shows the curve fit for the three pre-exponential factors and activation energies listed above. The L-H relationship provides a good fit over a wide range of concentrations and temperatures. The parameters used in the curve fit are shown in Table 2-3.

k_1	E_1	k_2	E_2	k_3	E_3
$(bar\ s)^{-1}$	kJ/mol	$(bar)^{-1}$	kJ/mol	$(bar)^{-1}$	kJ/mol
2.51E+03	112.6	6.74E-02	-37.3	3.04E-01	-36.6

Table 2-3: Fitted Langmuir-Hinshelwood parameters in equations 7-9

2.4.6 Effect of temperature and gas concentration

Figure 2-16 demonstrates the large effect that temperature has on the reaction rate. At temperatures up to 1150 ºC the reaction rate follows Arrhenius type behavior suggesting kinetic limitation rather than external heat and mass transfer.

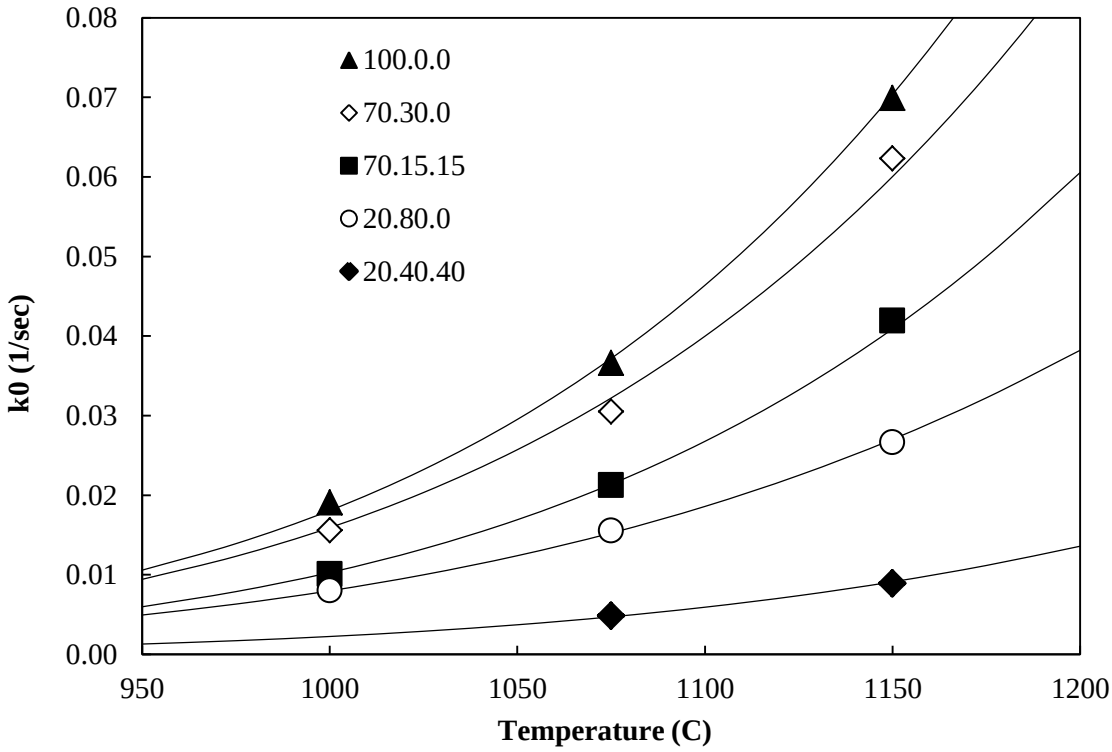

Figure 2-16: Langmuir-Hinshelwood fit for all experimental points. Reactant gas concentrations are listed as percent values in the order $H_2O.N_2.H_2$.

Steam concentration had a large positive effect under all conditions investigated. The reaction rate was measured at concentrations of 20%, 70%, and 100% with a balance of nitrogen at a total pressure of 0.95 bar.

Hydrogen was observed to have a strong inhibitory effect on the rate of steam-char gasification. For identical temperatures and steam concentrations, the supplementation of hydrogen for a portion of nitrogen dramatically lowered the reaction rate. This effect has large implications for reactor modeling due to the presence of elevated levels of reaction products in real world reactors. Unless a reactor is run with a very large excess of steam, the reaction rate in portions of the reactor will drop well below the values measured at 100% steam concentration. Strong hydrogen inhibition also suggests that some amount of excess steam is necessary to achieve high conversion without an excessively large reactor.

2.5 Conclusions

The kinetics of the steam-char reaction were investigated in the range of 1000 ºC to 1150 ºC at varying concentrations of steam and hydrogen. Experiments were performed using a novel low-cost experimental apparatus. High reactant flow rates and inert thermal mass were used to minimize the effects of heat and mass transfer. Rapid measurement of the reaction rate was achieved using thermal based flow measurements. Using this simple technique, the reaction rate was continuously measured over varying levels of conversion with high temporal resolution. Under the conditions investigated, switchgrass char gasification can be characterized using the random pore model to describe the change in reaction rate with conversion, and the initial kinetic rate can be estimated using Langmuir-Hinshelwood kinetics.

2.6 References

1. Fushimi, C., T. Wada, and A. Tsutsumi, *Inhibition of steam gasification of biomass char by hydrogen and tar.* Biomass and Bioenergy, 2011. **35**(1): p. 179-185.
2. Matsumoto, K., et al., *Gasification reaction kinetics on biomass char obtained as a by-product of gasification in an entrained-flow gasifier with steam and oxygen at 900-1000 °C.* Fuel, 2009. **88**(3): p. 519-527.
3. Simone, M., et al., *Evaluation of global biomass devolatilization kinetics in a drop tube reactor with CFD aided experiments.* Fuel, 2009. **88**(10): p. 1818-1827.
4. Biagini, E., M. Cioni, and L. Tognotti, *Development and characterization of a lab-scale entrained flow reactor for testing biomass fuels.* Fuel, 2005. **84**(12-13): p. 1524-1534.
5. Messenbock, R., D.R. Dugwell, and R. Kandiyoti, *CO2 and steam-gasification in a high-pressure wire-mesh reactor: the reactivity of Daw Mill coal and combustion reactivity of its chars.* Fuel, 1999. **78**(7): p. 781-793.
6. Huang, Z.M., et al., *Kinetic studies of char gasification by steam and CO2 in the presence of H-2 and CO.* Fuel Processing Technology, 2010. **91**(8): p. 843-847.
7. Muhlen, H.J., K.H. Vanheek, and H. Juntgen, *Kinetic-Studies of Steam Gasification of Char in the Presence of H-2, Co2 and Co.* Fuel, 1985. **64**(7): p. 944-949.
8. Alevanau, A., et al., *Parameters of high temperature steam gasification of original and pulverised wood pellets.* Fuel Processing Technology, 2011. **92**(10): p. 2068-2074.
9. Smolinski, A., K. Stanczyk, and N. Howaniec, *Steam gasification of selected energy crops in a fixed bed reactor.* Renewable Energy, 2010. **35**(2): p. 397-404.
10. Luo, S., et al., *Hydrogen-rich gas from catalytic steam gasification of biomass in a fixed bed reactor: Influence of particle size on gasification performance.* International Journal of Hydrogen Energy, 2009. **34**(3): p. 1260-1264.
11. Ahmed, I.I. and A.K. Gupta, *Kinetics of woodchips char gasification with steam and carbon dioxide.* Applied Energy, 2011. **88**(5): p. 1613-1619.
12. Lussier, M.G., Z. Zhang, and D.J. Miller, *Characterizing rate inhibition in steam/hydrogen gasification via analysis of adsorbed hydrogen.* Carbon, 1998. **36**(9): p. 1361-1369.
13. Huttinger, K.J. and W.F. Merdes, *The Carbon-Steam Reaction at Elevated Pressure - Formations of Product Gases and Hydrogen Inhibitions.* Carbon, 1992. **30**(6): p. 883-894.
14. Ollero, P., et al., *Diffusional effects in TGA gasification experiments for kinetic determination.* Fuel, 2002. **81**(15): p. 1989-2000.
15. Bhatia, S.K. and D.D. Perlmutter, *A Random Pore Model for Fluid-Solid Reactions .1. Isothermal, Kinetic Control.* Aiche Journal, 1980. **26**(3): p. 379-386.
16. Gadsby, J., C.N. Hinshelwood, and K.W. Sykes, *The Kinetics of the Reactions of the Steam-Carbon System.* Proceedings of the Royal Society of London Series a-Mathematical and Physical Sciences, 1946. **187**(1009): p. 129-151.

Chapter 3 Experimental and numerical studies of high-temperature steam-char gasification in a fixed bed

3.1 Abstract

A transient CFD model for a small fixed bed gasifier was developed to investigate the feasibility of allothermal gasification in a fixed bed. The highly endothermic nature of the reaction necessitates the use of a two-dimensional model to capture the temperature gradients within the bed. The model was developed using Ansys Fluent's porous media model with user defined functions to account for the presence of the reacting char. Although many dramatic simplifications were made in the development of the model, a set of experimental validation experiments has demonstrated that it is capable of predicting the overall bed reaction rate with a high degree of accuracy. The model's accuracy is largely possible because of an accurate kinetic rate expression developed in previous work using the same biomass char sample. The model results suggest that rapid, high temperature steam-char gasification is possible in an externally heated reactor, but careful attention must be paid to the reactor dimension tangential to the dominant direction of heat transfer. The reactor used in this study was only 19 mm in diameter, yet large radial temperature gradients developed which dramatically limited the rate of reaction in the center of the bed. Additionally, it was shown that it is exceedingly difficult to achieve high steam utilization while maintaining high reactor productivity.

3.2 Introduction

Computational fluid dynamic (CFD) modeling is a valuable tool for understanding the important parameters of gasification. The number of reactions and interactions between the gas and solid phase in real world reactors is enormous. Modeling all aspects of a working gasifier would require far more computing power than is currently available. Nonetheless, simplified models of real world systems can often predict key variables with a high degree of accuracy, and can provide valuable insight into ways of improving performance.

Traditional autothermal fixed bed reactors have been extensively studied in the literature, both experimentally and using computational modeling [1-3]. In an autothermal reactor, oxygen is used to combust a portion of the feedstock to supply the process heat. Because the heat is generated within the bed, heat transfer limitations within the bed are limited. The disadvantage of autothermal gasification is the consumption of a portion of the feedstock and the dilution of the product gases with excess CO_2. Piatkowski et. al. estimated that for autothermal coal gasification at least 35% of the feedstock must be burned to fuel the reaction [4].

Allothermal gasification uses steam instead of oxygen and offers an exciting alternative to autothermal gasification. The reaction of steam with biomass is an overall endothermic reaction and heat must be supplied externally. Because heat is added to the process, the calorific value of the product stream is higher than the feedstock, and valuable carbon resources are conserved. If the process heat is derived from a renewable source such as concentrated solar thermal energy, a completely renewable process for upgrading biomass can be realized [5]. The disadvantage of allothermal gasification is the need to transfer large amounts of energy into a material with an inherently low thermal conductivity.

Efficient heat transfer in allothermal gasifiers is often achieved through particle irradiation in an entrained flow reactor [6-8]. The radiation is provided either from the walls of the reactor or through a window using concentrated solar radiation. Most reactors of this type require a disperse cloud of particulates to achieve uniform heat transfer. This requirement limits the possible types of feedstock and often increases the feedstock processing cost. Another method, used to transfer concentrated solar thermal energy into a fixed bed, has been demonstrated with a top down concentrator design [4]. A silicon carbide plate is used to adsorb radiant energy and re-radiate to the surface of a bed of char. This design has been shown to be successful, but requires complicated concentrator optics, and the surface area for heat transfer into the bed is limited.

The latent heat of the gasifying agent can also be used to efficiently transfer heat into the char bed. Umeki et. al. have investigated the use of high temperature steam as both the gasifying agent and the heat carrier [9, 10]. The advantage of this system is that the heat transfer to the reaction site is not dependent on heat transfer through the biomass bed, effectively decoupling the heat transfer effects from the reactor diameter. Unfortunately, the large discrepancy between the heating requirements and the amount of heat carried by the steam needed for gasification requires the reactor temperature to be hundreds of degrees below the steam temperature. Experimentally, the low reactor temperature resulting from using only steam to deliver heat to the reactor was shown to result in a very high level of tar production. Additionally, the low reactor temperature will lead to very slow kinetics and an unnecessarily large reactor.

The authors have envisioned a solar reactor where particles and gas travel downward through a heated tube in a fixed bed configuration. Containing the reaction in tubes allows the use of a more traditional solar concentrating field with tower configuration and a cavity receiver. The fixed bed of biomass is suspended by a moveable grate that allows ash to pass through on a

periodic basis. Biomass is loaded from the top of the reactor and quickly pyrolyzes to form synthesis gas, tar and char. The pyrolysis reaction is very rapid, leading to a fixed bed composed primarily of char [11]. Adequate heat transfer into the reacting bed of char is the primary concern with this reactor configuration.

In this paper we investigate the feasibility of steam char gasification in an externally heated fixed bed reactor using a simplified transient model of a batch reactor and experimental validation experiments. Ansys Fluent 12.1 is used for the numerical simulations and the presence of the reacting bed is accounted for with the use of user defined functions (UDFs). A 2d axisymmetric model is used to represent the char bed and the reactor wall in the vicinity of the bed. The reaction time for the particles in a fixed bed configuration is compared to the reaction rate measured in previous work under ideal conditions.

3.3 Experimental

3.3.1 Experimental setup and procedure

The reactor system used for experimental validation is similar to that reported in Chapter 2. Only the major design points will be listed here. A diagram of the complete system is shown in Figure 3-1. The char bed rests on an Inconel mesh that is held in place with Inconel supports. Three, 0.508 mm K type thermocouples are located within the bed; two just above the mesh in the center and near the wall, and one in the center at 1.9 cm above the mesh. The support system is inserted into the bottom of a 1.9 cm diameter alumina tube and char is loaded from the top. The system is run in batch mode and ash and slag are removed after every experiment.

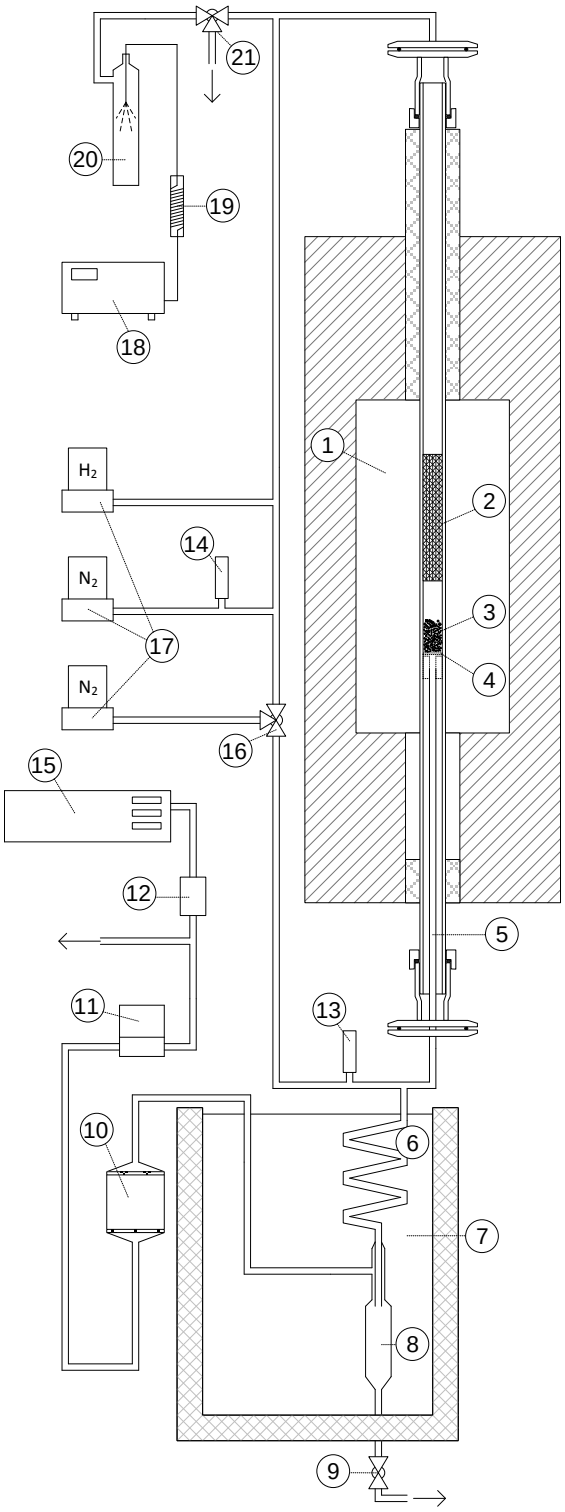

Figure 3-1: Reactor diagram: (1) Furnace cavity; (2) Reactant preheater; (3) Char bed; (4) Inconel mesh; (5) Inconel outlet tube; (6) Condenser; (7) Ice bath; (8) Condensate collection; (9) Condensate drain; (10) 0.2 µm filter; (11) Outlet flow meter; (12) Booster pump; (13), (14) Pressure transducers; (15) NDIR; (16) Nitrogen 3-way valve; (17) Mass flow controllers; (18) High-pressure water pump; (19) Water pre-heater; (20) Steam generator; (21) Steam bypass 3-way valve.

Gases exiting the reactor pass through a condenser to remove excess steam and a 0.2 μm filter to reduce particulates. The gases then pass through an Omega MFA series flow meter. After the flow meter, portion of the product stream is sent to a California Analytical Instruments ZRE model non-dispersive infrared gas analyzer (NDIR). Concentrations of CO, CO_2, and CH_4 are measured continuously and the conversion is based on the amount of carbon that has left the system. While this method of gas analysis is not as accurate as gas chromatography, real time analysis is necessary because the reactions take place over 2-5 minutes.

Char samples were identical to those used for the determination of kinetic rate reported in Section 2.3.3. The characteristics, preparation conditions, and elemental analysis can be found there. Char loading of 1 gram was used in all model validation experiments. The bed height was estimated by inserting the support platform into a clear tube of equal diameter to the reaction tube, and loading the char from the top as done before each experiment. A picture of the loaded char is shown in Figure 3-2.

Figure 3-2: Char loaded into a clear tube to measure the bed height.

To ensure more uniform bed heights, the bottom of the tube was tapped several times before all measurements and experiments. The measured bed height was 3.8 cm.

The reactor was heated to the desired set point at a rate of 30 K/min while nitrogen was flowed at 2 slpm through the bed to maintain an inert environment. Steam was supplied by a custom precision steam generator and sent to a bypass valve prior to the reaction. To initiate the reaction, the nitrogen flow was switched to the outlet of the reaction tube and steam was directed to the inlet. Rapid gas changes were achieved with the use of two 3-way valves. The reason nitrogen flow was directed to the reactor outlet rather than shut off was to facilitate efficient transport of the product gases through the analysis system.

3.3.2 Particle characterization

The density of the char particles was estimated by measuring the particle weight and approximating the void fraction in a packed bed. A cylinder of a known volume was filled with loosely packed switchgrass char. Two types of silica were added to measure the volume not occupied by the particles; ground (SIL-CO-SIL 106, 99% < 106 μm) and unground (U.S. Silica L-60, 99% < 425 μm). A char particle density of 181.0 kg/m^3 was calculated and no significant difference was found between the ground and unground silica. The standard deviation of 6 measurements was 23 kg/m^3.

Porosity of the reactor bed was calculated separately based on the packing density in the reactor tube. The porosity was estimated separately from the density measurement because the presence of thermocouples may affect how densely the particles stack. A porosity of 0.487 was calculated using a particle density of 181.0 kg/m^3, a measured bed height of 3.8 cm, 1.9 cm diameter, and a char loading of 1.00 g.

An equivalent spherical diameter was estimated using image analysis. Particles were loosely spread over a white sheet of paper with a printed grid of a known size. Images were analyzed with ImageJ software. ImageJ returns the length and width of an ellipse with an equivalent surface area. Since the majority of the particles are rectangular when viewed lying flat, these numbers were adjusted to fit a rectangle of equal area. Particles were then counted and weighed to determine an average particle weight. Using the previously calculated density of 181 kg/m^3, an average particle volume was calculated. Assuming rectangular cuboid particles, a mean thickness and surface area was calculated. A sphere with the equivalent surface are to volume ratio was found to have a diameter of 0.77 mm.

3.4 Model

Ansys Fluent is a powerful tool for performing numerical simulations in reacting flow systems. The goal of our current modeling work is to develop a model to assess the feasibility of steam-char gasification in a fixed bed.

In this model, the presence of the char bed is represented using Fluent's porous media model and a set of user defined functions (UDFs). The following assumptions are made:

- Incompressible flow
- Uniform particle size, porosity, and char composition
- Bed properties (porosity, particle size, specific heat) except the solid density do not change over time
- Thermal equilibrium between the particles and gas

The governing equations are covered in extensive detail in the Fluent operator's manual [12]. Fluent's code allows for the definition of properties, boundary conditions and source terms through simple C programs that can access the variables used in the simulation. These functions

were used to define the kinetic rate, effective thermal conductivity, and heat and mass source terms. Mass source terms were used to account for the consumption of steam and generation of hydrogen and carbon monoxide. An enthalpy source term was used to account for the heat of reaction. In addition, a user defined scalar (UDS) was defined to track the degree of conversion for all areas of the bed.

The development of the UDFs for the effective thermal conductivity, the heat of reaction, char heat capacity, and the porous media constants can be found in Appendix A. Michael's work was performed at the University of Colorado under my guidance for the fulfillment of a master's degree in mechanical engineering under Aldo Steinfeld at ETH Zurich.

3.4.1 Mesh and boundary conditions

A diagram of the mesh and boundary conditions are shown in Figure 3-3. A two-dimensional axisymmetric mesh was designed to take into account the thermal inertia of the alumina tube. Initial modeling work neglected the effect of the alumina tube and was unable to produce realistic results very close to the wall. With a fixed temperature boundary condition on the inner wall, the temperature of the bed near the wall stays unrealistically high. With a fixed radiation temperature, the inner wall temperature was predicted to drop nearly instantaneously. Incorporation of an alumina wall that receives external radiation and extends above and below the bed drastically improved the near wall temperature effects. The length of the wall was chosen to extend far beyond the region that conducts heat into the bed.

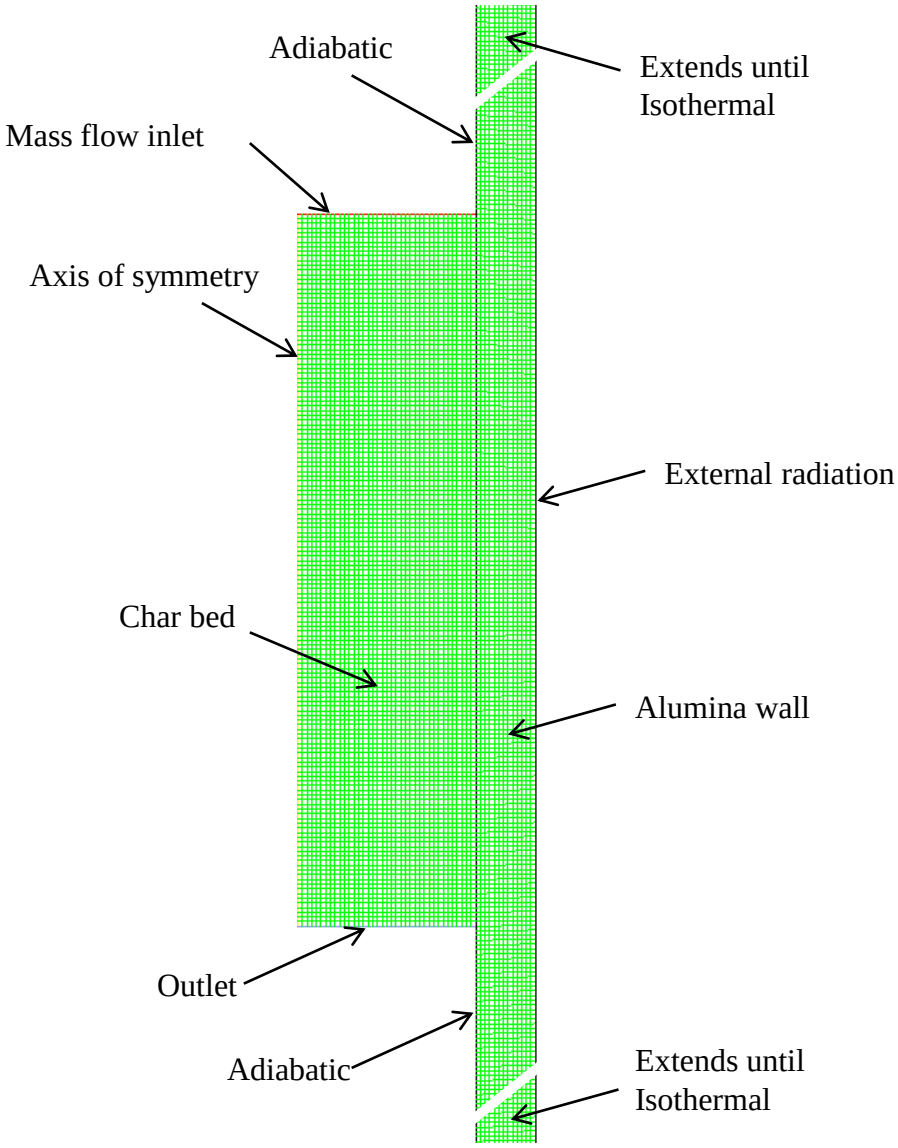

Figure 3-3: Diagram of the mesh and boundary conditions.

Predicting the steady state behavior of a continually replenished bed would be difficult without extensive knowledge of the solid flow characteristics of partially reacted char. Instead, a transient model of a stationary fixed bed was developed. At time $t = 0$, the char bed and alumina walls start at the same temperature as the externally applied radiation. Steam flow at the desired rate crosses the inlet boundary, and the initial steam concentration in the bed is 100%.

3.4.2 Kinectic model

Initial experimental and modeling work highlighted the need for a precise kinetic rate equation. The measured rate of char gasification varies dramatically between different char types and even different measurement techniques. It is nearly impossible to use a rate parameter found in the literature to obtain modeling results that closely match experimental data. Additionally, attempts to measure the kinetic rate under controlled conditions can lead to disappointment if care is not taken to avoid the effects of heat and mass transfer.

The authors tested several different reactor configurations with the intent of measuring the kinetic rate under conditions of known temperature and gas composition at 1000-1150 ºC. Very fast reaction rates were obtained with 1 g of biomass spread over a 4.57 cm diameter mesh. This configuration resulted in a bed approximately 6 mm in depth. It was assumed that at high temperatures the radiative heat transfer to the particles would be sufficient to keep them from appreciably dropping in temperature. The effect of hydrogen inhibition was ignored with the hope that a simple model could answer questions at the proof of concept level. The modeling results using the kinetic rate obtained in this manner failed to adequately match experimental data from fixed bed experiments. Further analysis showed that there were temperature limitations even in a thin bed, and hydrogen produced during the reaction has a strong inhibitory effect on the reaction rate.

Extensive work was performed in an attempt to ensure isothermal conditions and a well-defined hydrogen concentration during rate measurement. A rate equation dependent on the temperature, steam concentration, hydrogen concentration, and degree of conversion was developed. The details of these experiments can be found in Section 2.4. Only the resulting equations will be covered here.

The initial kinetic rate was found to match a Langmuir-Hinshelwood type rate equation. Temperature, steam, and hydrogen concentrations are taken into account. The equation used can be written as,

$$k_0 = \frac{K_1 p_{H_2O}}{1 + K_2 p_{H_2O} + K_3 p_{H_2}}. \tag{10}$$

Where K_1, K_2, and K_3 are calculated using the Arrhenius type expressions

$$K_1 = k_1 \exp(-E_1/RT), \tag{11}$$

$$K_2 = k_2 \exp(-E_2/RT), \tag{12}$$

$$K_3 = k_3 \exp(-E_3/RT). \tag{13}$$

The reaction rate was observed to increase with increasing particle conversion until about 30% of the original mass had been reacted. As many other authors have found, the shape of the curve is well described by the random pore model,

$$r = k_0(1 - X)\sqrt{1 - \varphi \ln(1 - X)}, \tag{14}$$

where k_0 is the kinetic rate at $X = 0$, and φ is a geometric parameter.

This set of equations was shown to fit well with experimental results obtained in the range of 1000-1150 ºC, steam concentrations of 20-100%, and hydrogen concentrations of 0-40%.

3.4.3 Water gas shift

The water gas shift reaction was included using Fluent's built in homogenous reaction mechanism. Water gas shift is the only homogenous reaction that is commonly included in gasification studies [13]. The reaction is modeled with the Arrhenius rate equation with a pre-exponential factor of 2,778 [m^3/s kmol], a temperature exponent of 0, and an activation energy of 12,560 [J/mol] [14].

3.5 Results and Discussion

3.5.1 Mesh validation

A mesh validation test was performed with 1150 ºC external radiation temperature and 2 slpm steam flow. The mesh used for all simulations contains 15,682 elements. For the mesh validation simulation the number of mesh elements was increased by a factor of 4 to 62,728. The variation in CO flow between the two simulations is shown in Figure 3-4.

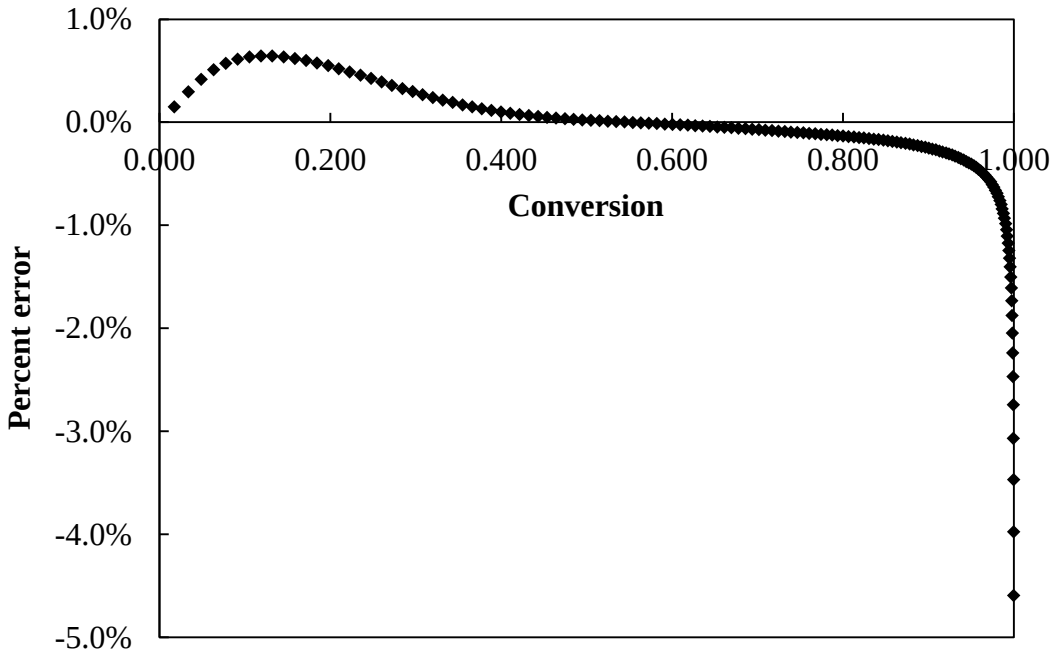

Figure 3-4: Percent error in the CO flow rate vs. conversion for the mesh validation simulation.

The error between the baseline and the refined mesh is less than 1% for conversion values less than 99%. After 99% conversion the CO flow is so small that large percentage variations will have little effect on the overall results.

3.5.2 Flow validation

Experimental tests and simulations were performed under 5 different conditions as shown in Table 3-1. Both temperature and steam flow rate had a large effect on the reaction rate.

Temperature (ºC)	Steam flow (slpm)
1150	2.0
1150	1.0
1150	4.0
1075	2.0
1000	2.0

Table 3-1: Experimental conditions for the model validation experiments.

The main variables tracked during the simulation were the mass flow of carbon containing gases exiting the reactor and the temperature at several locations within the bed. A reference condition of 1150 °C with 2 slpm steam flow was compared to 2 runs at lower temperature and runs with higher and lower steam flow. Figure 3-5 shows the rate of carbon containing gases exiting the reactor vs. time for the reference condition for both the simulation and experimental validation.

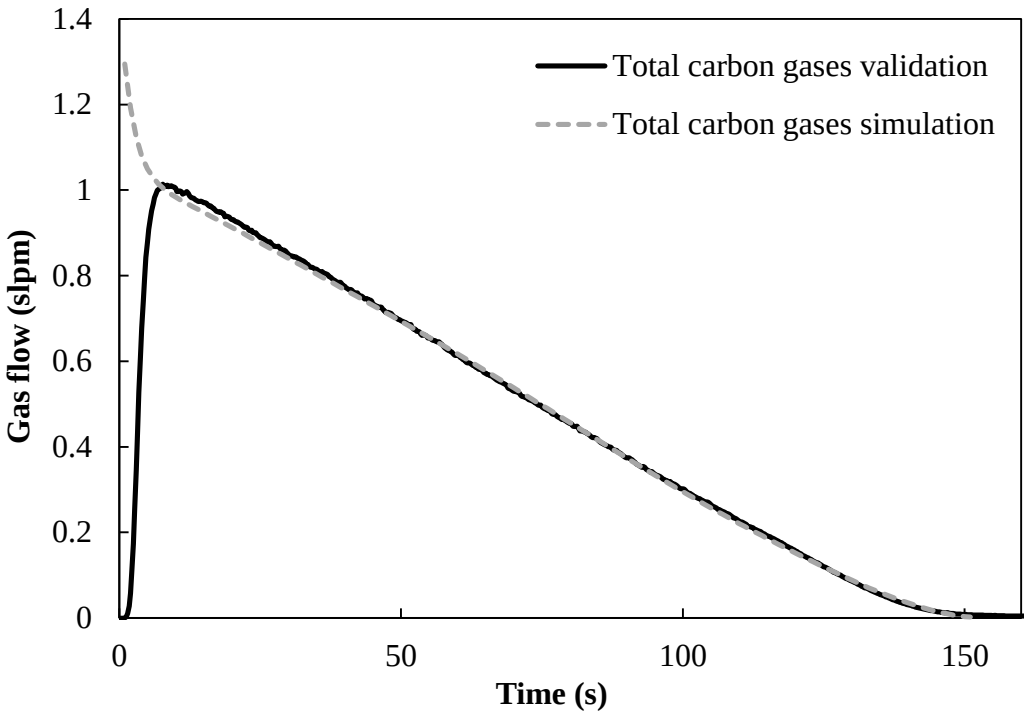

Figure 3-5: Validation and simulation results for steam gasification of switchgrass char at 1150 °C and 2 slpm steam flow.

The simulation matches the experimental data very well for all but the first few seconds of the reaction. This discrepancy is due to the different starting conditions between the model and the experiment. In the model at time $t = 0$ the bed begins at 100% steam concentration and a temperature equal to the external radiation temperature. Under these conditions the reaction rate is temporarily higher until the bed cools due to the reaction. In the experiment, the bed also begins at approximately the external radiation temperature, but due to the flow characteristics of the system, the steam concentration is ramped from 0% to 100% over several seconds. At no point during the experiment is the entire bed at conditions of maximum temperature and steam concentration. Regardless of this initial discrepancy, the simulation is able to predict the flow of carbon containing gases with a high degree of accuracy.

The change in the reaction rate between the ideal conditions used for the kinetic measurement and the full bed is substantial. Figure 3-6 shows the conversion vs. time for the kinetic measurement from previous work at 1150 °C and 100% steam and the full bed run under the same conditions. The reaction rate for the full bed run is significantly slower than the measurements taken under ideal conditions with the same reactor temperature. Heat transfer, low steam concentration and a buildup of hydrogen dominate the reaction, lengthening the time to 90% conversion from 16.6 to 97 seconds.

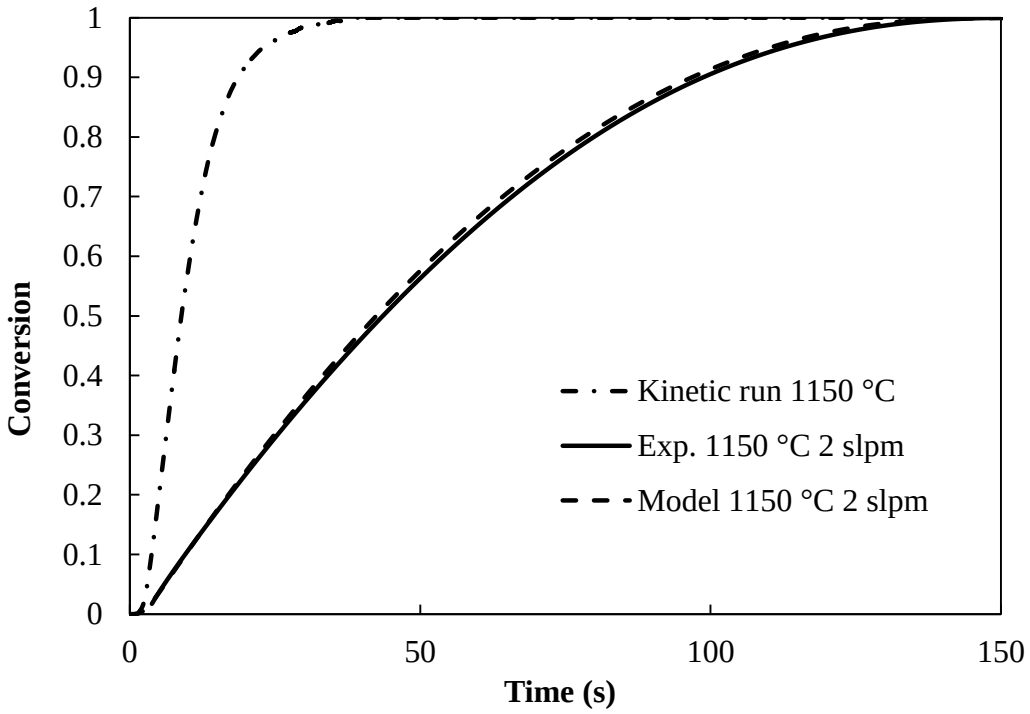

Figure 3-6: Conversion vs. time for the kinetic measurement from previous work at 1150 ºC and 100% steam and the full bed validation and simulation results at 1150 ºC and 2 slpm steam flow. The decrease in the reaction rate due to temperature and gas concentration effects within the full bed is captured well by the model predictions.

The model shows a high degree of accuracy in predicting the overall gasification rate as a function of steam flow. The degree of conversion vs. time at 1150 °C for three different rates of steam flow is show in Figure 3-7. The gasification rate increases substantially at higher steam

flow rates because of the increased steam concentration, decreased hydrogen concentration, and the increased thermal energy carried with the inlet steam. This observation has important implications for reactor design because it highlights the tradeoff between excess steam flow and the volumetric productivity of the reactor.

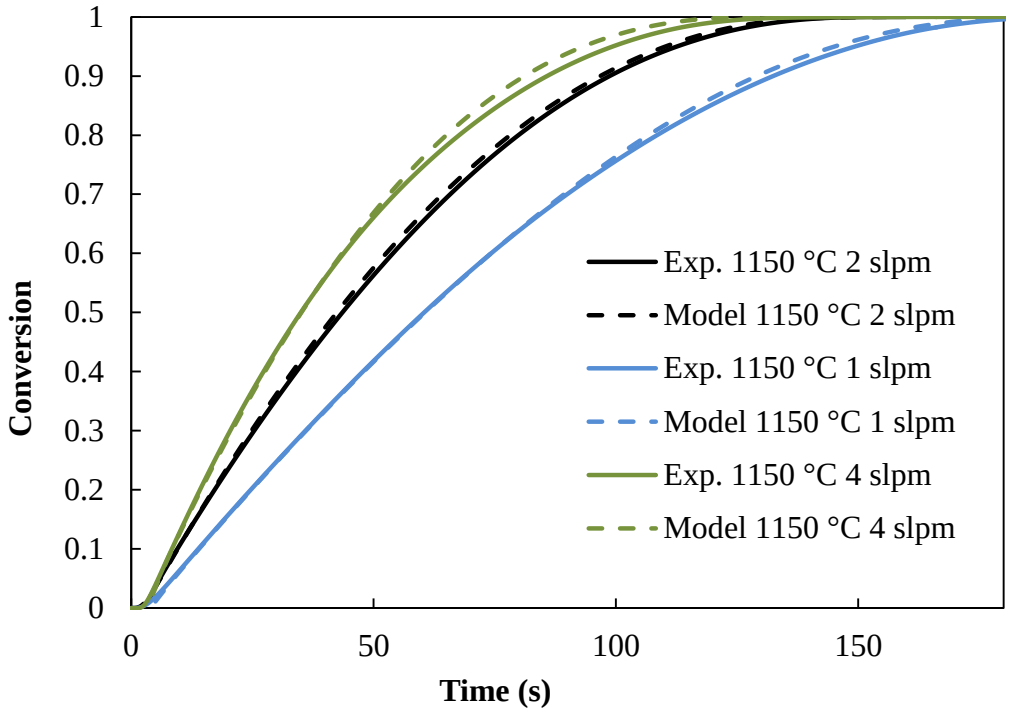

Figure 3-7: Model validation experiments for three different steam flow rates at a furnace temperature of 1150 ºC. The model predicts the overall reaction rate well over a large range of steam flows.

The simulation results fit marginally well over a range of external radiation temperatures. Figure 3-8 shows the conversion vs. time for 3 different temperatures ranging from 1000 ºC to 1150 ºC. The simulation is capable of capturing the decrease in overall reaction rate with a decrease in temperature, but over predicts the reaction rate substantially at lower temperatures. This result is not surprising as the kinetic rate was measured between 1000 ºC and 1150 ºC and all temperatures in the simulation with 1000 ºC external radiation were below this range.

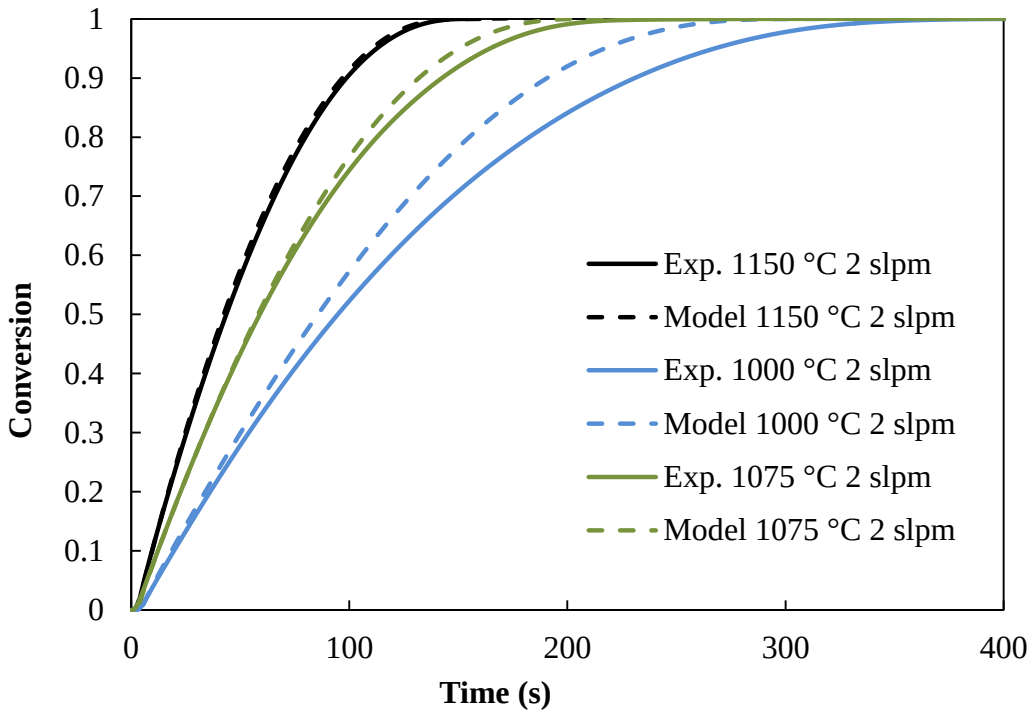

Figure 3-8: Model validation experiments for three different reactor temperatures. The model fits less well at low temperatures because the kinetic rate was developed for temperatures of 1000 ºC or higher. For the experiment performed at a furnace temperature of 1000 ºC, the entirety of the reacting bed quickly cools to well below 1000 ºC.

3.5.3 Temperature validation

The temperature profiles predicted in the simulation fail to match the thermocouple measurements from the experimental validation. Figure 3-9 shows the experimental and simulation results for the temperature vs. time at various locations in the bed. The curve shape follows the same trend, a sharp drop in temperature followed by a slow bottom and a steep return to the radiation temperature. However, the magnitude of the temperature drop is much greater in the simulation.

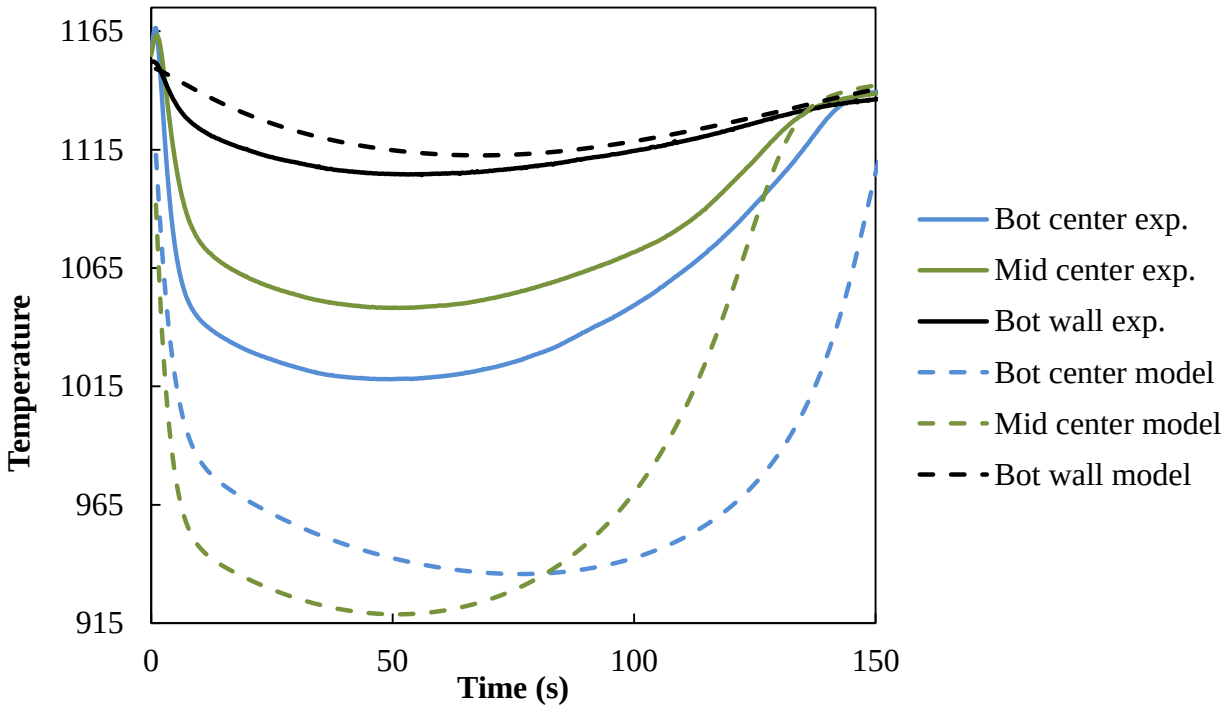

Figure 3-9: Temperature vs. time for the model and validation experiment at 1150 ºC and 2 slpm steam flow. The thermocouples in the experimental setup cannot measure the particle temperature during the reaction. It is likely that the actual particle temperature is very near the temperature predicted by Fluent.

The discrepancy in temperature is most likely due to the endothermic nature of the reaction and the assumption of thermal equilibrium between the particles and the gas. Since the thermocouple itself is not consuming thermal energy, it is likely that it is at a higher temperature than the endothermic particles. On the other hand, the temperature predicted in Fluent is much closer to the particle temperature because it is a heat capacity weighted average of the gas phase and the solid phase. Since the predicted temperature in Fluent is used to calculate the kinetic rate, the close match between predicted and measured conversion suggests that the predicted temperatures have physical relevance.

The above conclusion rests on the reasonable but difficult to verify assumption that the particle temperature in the kinetic measurements was close to the reactor temperature. In the

kinetic measurement experiments 25 g of inert ZrO_2 beads were used with 50 mg or 150 mg biomass char with the larger amount used for the slowest reactions. With the large mass ratio and direct contact between the thermal media and reacting char it is reasonable to believe that the char particles are close to the temperature of the ZrO_2 beads and the initial reactor temperature. In addition, the close match between the measured and predicted kinetic rates in the full bed runs suggest that the kinetic rate expression is suitable for simulations in the range of 1000 ºC to 1150 ºC.

3.5.4 Steam utilization

To further investigate the effect of excess steam flow, several additional simulations were performed. Figure 3-10 shows the percentage of utilized steam vs. the time to 90% conversion. As the steam utilization increases, the overall reaction rate decreases substantially. This behavior is expected because increased steam flow transports more thermal energy into the bed. In addition, a portion of the bed must simultaneously be at a very low steam concentration and high hydrogen concentration to achieve high steam utilization. As a consequence, a high efficiency allothermal gasifier must either be very large in size, or operate in such a way that a large amount of excess steam does not reduce the thermal efficiency.

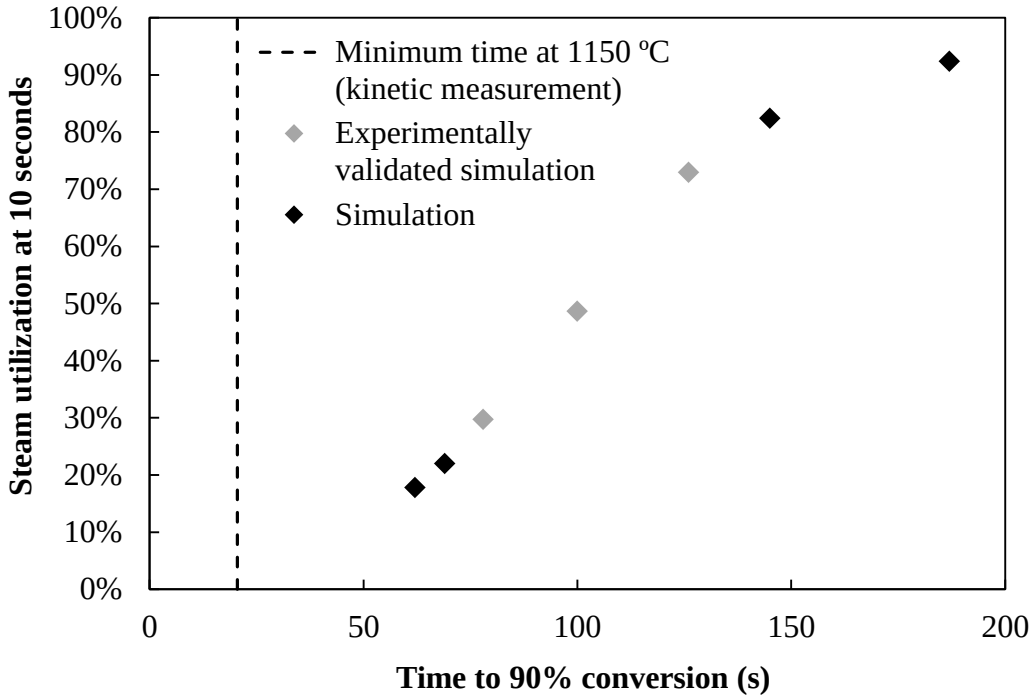

Figure 3-10: Steam utilization after 10 seconds of reaction compared to the time to reach an average of 90% conversion in the bed for a reactor temperature of 1150 ºC. The 90% conversion time from the previous kinetic work is included as a reference. As the steam utilization increases the conversion time increases significantly. Steam flow rates from left to right in slpm: 0.5, 0.75, 1, 2, 4, 6, 8.

3.5.5 Water gas shift

One of the major drawbacks to the current reactor design is the lack of gas composition data for the gases at the exit of the fixed bed. The product gases exiting the bed are free to diffuse into a region of the reactor with a volume many times greater than the reacting bed and an ill-defined temperature profile. Because the water gas shift reaction is a homogenous reaction, it will occur at varying rates within the dead volume. While this does not affect the measured rate of conversion, it does make it impossible to estimate the extent of the water gas shift reaction within the bed.

The predicted level of CO_2 in the gas stream is much lower than the values measured during the experiments. As shown in Figure 3-11, there is a large discrepancy in the ratio of CO

to CO2 between the simulation and validation experiments, but the total flow of carbon containing gases is very close.

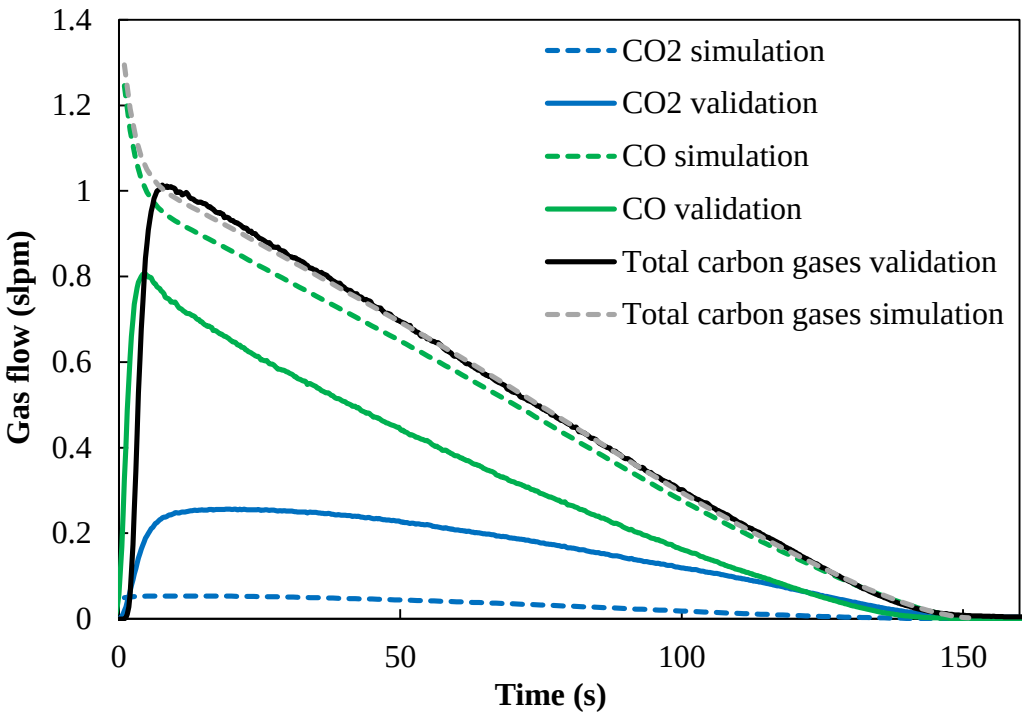

Figure 3-11: Carbon containing product flow for the simulation and validation experiments at 1150 ºC and 2 slpm steam. The large discrepancy in the species distribution is most likely due to the water gas shift reaction occurring in the dead zone beneath the char bed.

The increased level of CO_2 should also correspond to a higher level of hydrogen in the product gas, although difficulties with measuring the hydrogen concentration in real time prevented direct hydrogen measurement. If the majority of the water gas shift reaction in the experimental validation is occurring within the bed rather than below the bed as hypothesized, it could have a large effect on the reaction rate. One mole of hydrogen is produced for every mole of CO converted into CO_2. If the hydrogen is generated within in the bed, it would inhibit the reaction rate and could lead to discrepancies between the model and the validation.

To investigate the effect of an increase in the rate of the water gas shift reaction within the reacting bed, a sensitivity analysis on the pre-exponential factor was performed. The pre-exponential factor for the water gas shift reaction was increased from 2,778 [m^3/s kmol] to 50,000 [m^3/s kmol]. The results for the simulation with A = 50,000 [m^3/s kmol] are compared to the validation experiments in Figure 3-12.

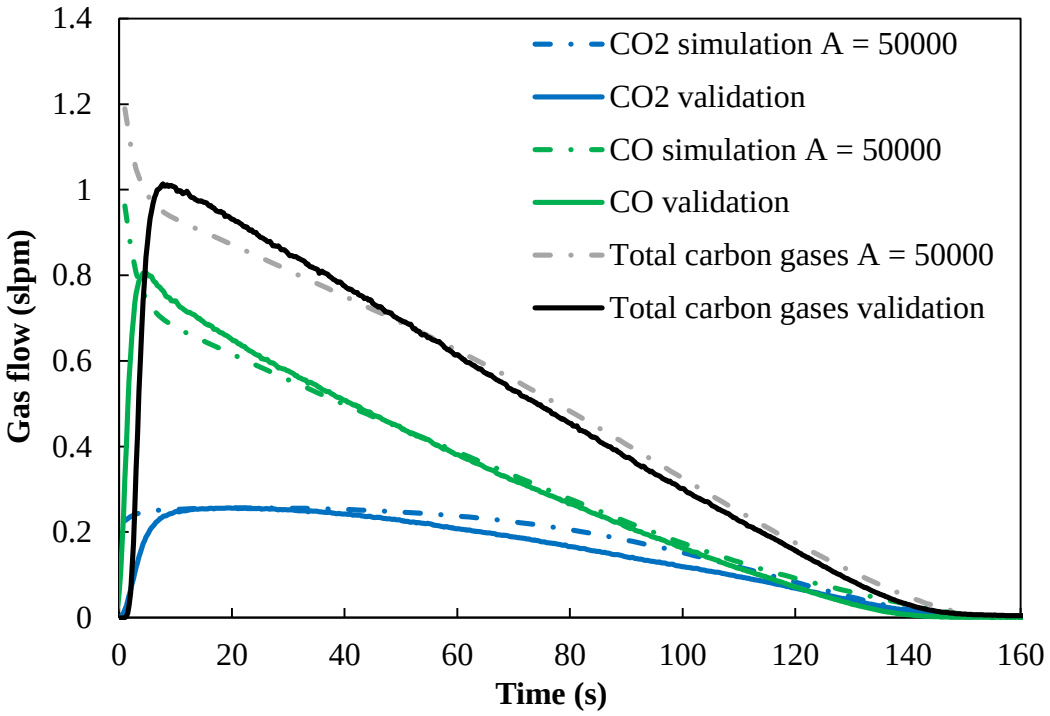

Figure 3-12: Sensitivity analysis for the water gas shift pre-exponential factor. The simulation still closely predicts the overall reaction rate even if all of the water gas shift reaction were occurring within the char bed.

Increasing the rate of water gas shift within the bed only marginally decreases the overall reaction rate. The fit for the total carbon containing gases between the model and the experimental validation is still fairly good, suggesting that the location of the water gas shift reaction in our experimental reactor has only a minimal effect on the reaction rate. One reason the inhibitory effect of increased H_2 from the water gas shift reaction may be minimized is the

increased thermal conductivity of H_2. The minimum temperature in the simulations with increased water gas shift is 20 ºC higher than in the original simulations. This effect is partially due to the slightly slower rate, but may also be due to the higher thermal conductivity of H_2. The potential ability for H_2 to partially mitigate it's inhibitory effect through increased thermal conductivity is an exciting observation, and should be further investigated in future work.

3.5.6 Contour plots

One of the strong points of CFD simulation is the ability to estimate the value of key variables at any location in the reactor. Analysis of contour plots generated from the simulation can help to develop an intuitive feel for the inner workings of the reactor. Gradients in the bed that would be difficult to detect through experimental means can be identified, and future reactor designs can be shaped around the information gained. Figure 3-13 through Figure 3-15 show the progression of the conversion, reaction rate, temperature, steam concentration and hydrogen concentration for the simulation performed at 1150 °C radiation temperature and 2 slpm steam flow. The time points shown are at 5, 50, and 100 seconds.

Figure 3-13 shows the state of the reactor after 5 seconds of reaction. At this point in time the bed is mostly unreacted and the conversion value has little effect on the reaction rate. At the reactor inlet, the temperature and steam concentration are high while the hydrogen and conversion are low. These conditions lead to a reaction rate approaching that measured under ideal conditions, but only at the very inlet to the bed. Further into the bed the temperatre has plumeted nearly 200 °C just 1 cm below the inlet. Only 5 seconds earlier this region of the bed was at the same temperature as the external radiation.

At the 5 second time point the reaction rate is the lowest at the bottom center of the bed. At this location the temperature is not at a minimum, but the lower steam concentration and higher hydrogen concentration causes the reaction rate to be lower than at the temperature minimum. The temperature minimum is located in the upper region of the bed. At 5 seconds it occurs just below the inlet because the highest reaction rates are in the upper region of the bed. Heat transfer from the walls raises the bed temperature in the lower regions where the reaction rate is limited by the gas composition.

As shown in Figure 3-14, after 50 seconds the temperature minimum is approximately 230 ºC below the radiation temperature and it has shifted to a position lower in the bed. The first several millimeters of the bed is now completely reacted, and the contours of the reaction rate look dramatically different. Because the region near the inlet of the bed is fully reacted, no further reaction rate takes place in this area. Further into the bed the first char that the reactant steam reaches is at a very high level of conversion. Based on the Random Pore Model the reaction rate will be very low in this region. Still further into the bed the conversion reaches a region of approximately 30% where the random pore model predicts the highest rate of conversion. By this point the temperature is much lower than the external radiation and some hydrogen is present. These observations explain why no region of the bed is experiencing a reaction rate as high as that seen at the inlet for the 5 second time point.

The radial variation in the reaction rate is somewhat apparent after 5 seconds and much more pronounced after 50 seconds. The region of the bed near the walls is at a higher temperature but similar gas composition compared the center of the reactor. These conditions lead to a higher overall reaction rate along the walls and an inversion in the radial steam concentration gradient from the top to the bottom of the reactor. Near the inlet after 50 seconds

of reaction, the region adjacent to the walls has fully reacted while the center still has some unreacted char. As a consequence, the steam concentration at the top of the reactor is higher near the walls than in the center. Toward the exit of the reactor this concentration gradient has reversed due to the higher reaction rate along the walls over the majority of the bed.

The radial variation in the extent of conversion also decreases the accuracy of the model as regions of the bed become fully reacted. To simplify the model development, the bed properties including porosity are assumed to be constant throughout time. For values of conversion less than 70%, assuming a constant porosity is a reasonable assumption. Mermoud et. Al observed that for the reaction of charcoal and steam, the particle size varies very little up to 50% conversion and most of the original shape and size are retained until 70% conversion [15]. After that point, the particles begin to disintegrate and the porosity of the bed in those regions will change dramatically. It is possible that as the conversion along the walls increases and the porosity decreases, more steam will flow to the walls, further increasing the reaction rate and decreasing the porosity. As such, little confidence should be given to the contour plots in Figure 3-15 due to the high levels of conversion in much of the bed. Since the model still predicts an accurate overall reaction rate at high conversion, the plots were included for comparison purposes.

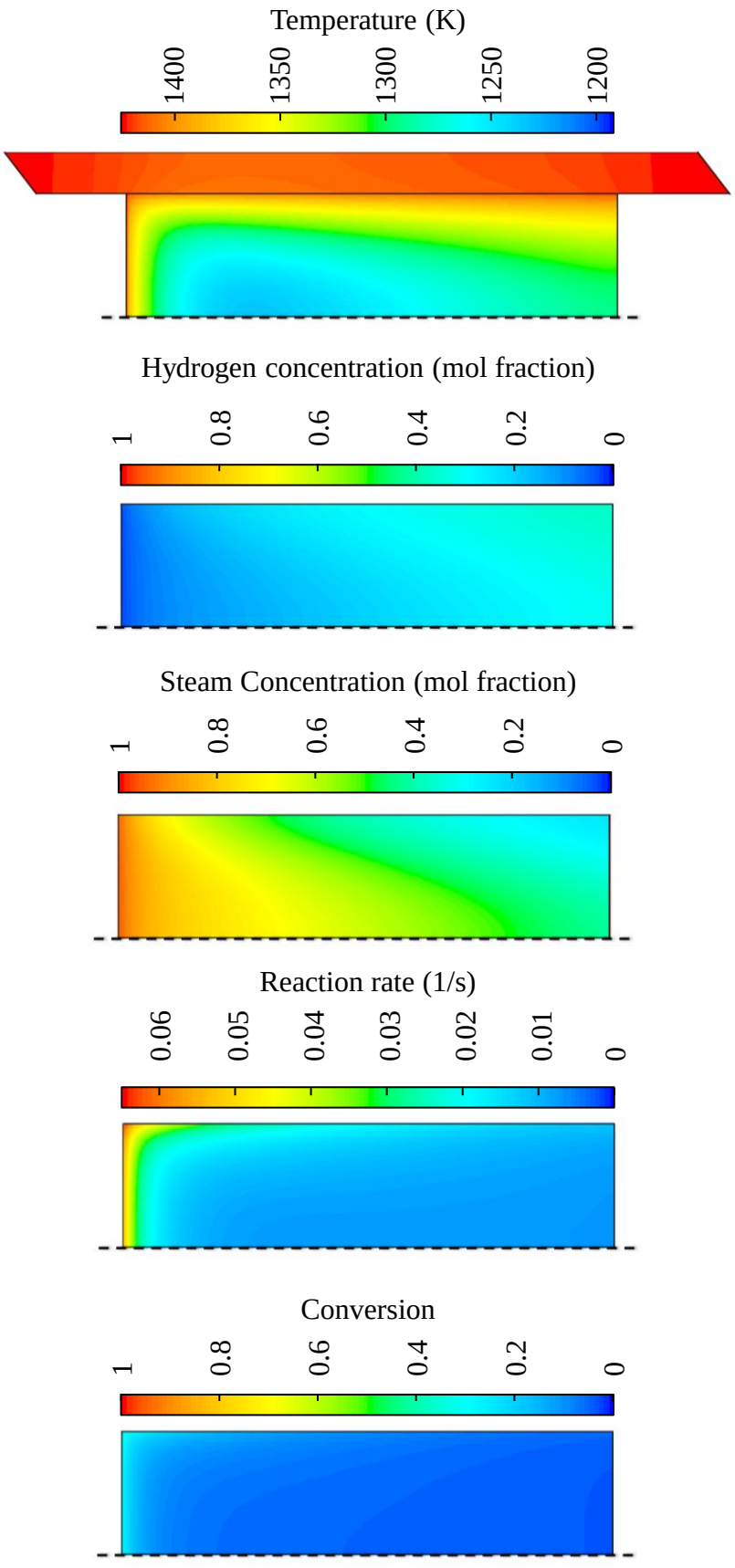

Figure 3-13: Contour plots with axial symmetry for steam gasification of switchgrass char. Steam enters from the top of the figure and product gases exit through the bottom. Time: 5 s; Temperature: 1150 °C; Steam flow: 2 slpm; Char loading: 1 g; Bed height: 3.8 cm.

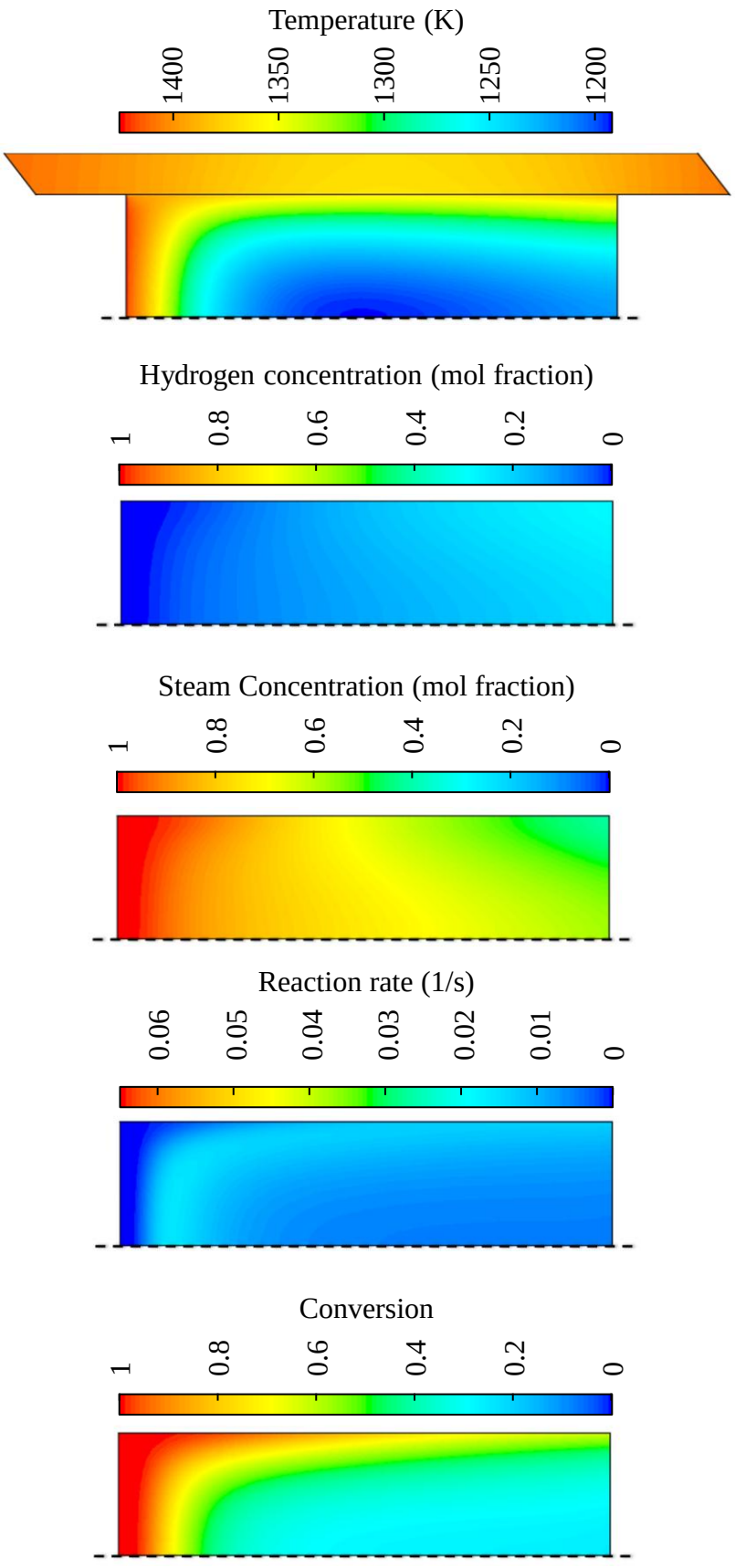

Figure 3-14: Contour plots with axial symmetry for steam gasification of switchgrass char. Steam enters from the top of the figure and product gases exit through the bottom. Time: 50 s; Temperature: 1150 °C; Steam flow: 2 slpm; Char loading: 1 g; Bed height: 3.8 cm.

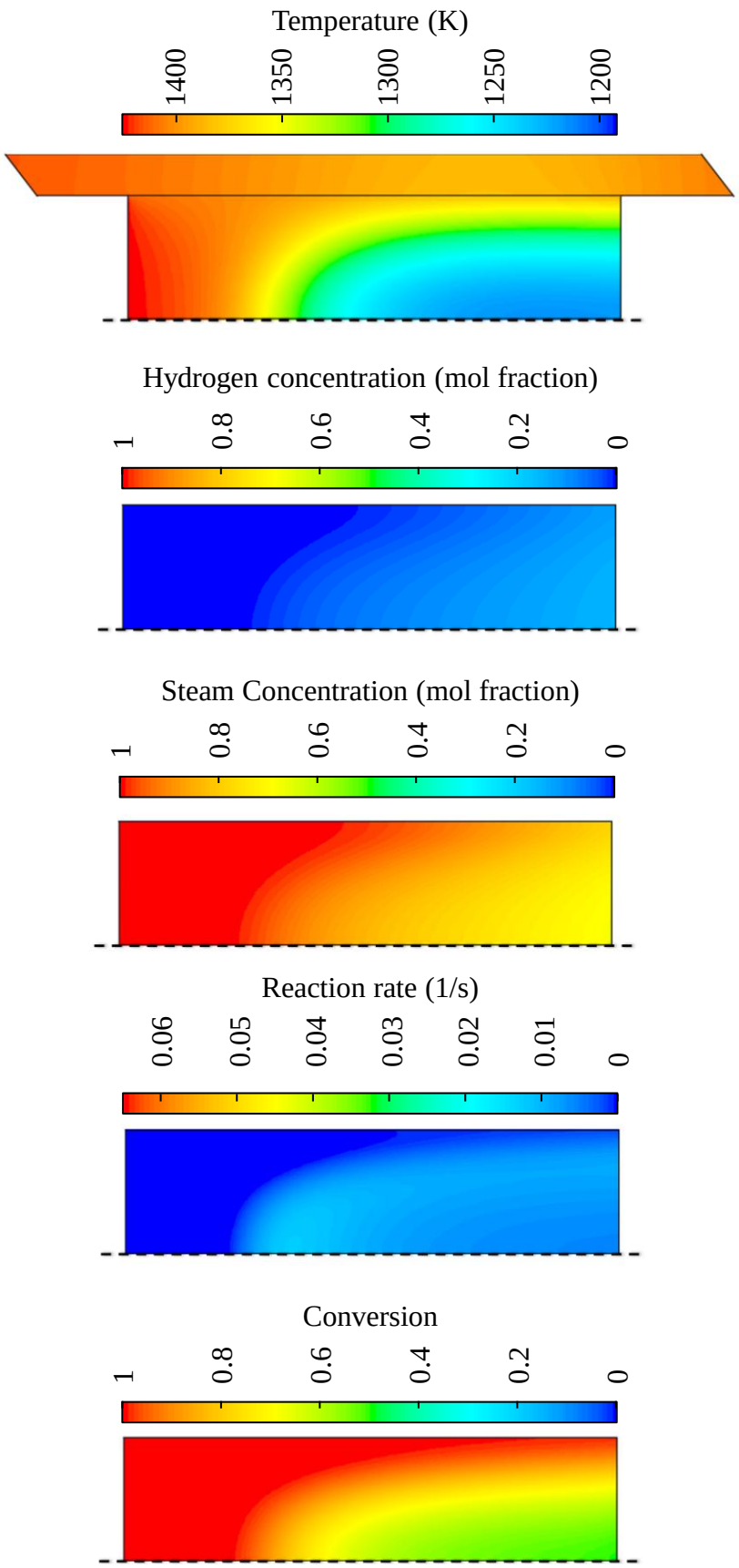

Figure 3-15: Contour plots with axial symmetry for steam gasification of switchgrass char. Steam enters from the top of the figure and product gases exit through the bottom. Time: 100 s; Temperature: 1150 °C; Steam flow: 2 slpm; Char loading: 1 g; Bed height: 3.8 cm.

3.6 Conclusions

A transient CFD model was developed to investigate the steam-char reaction in a fixed reactor. Validation experiments closely matched the simulation results for the flow of carbon containing gases vs. time. The overall reaction rate in a fixed bed configuration was significantly lower the rate measured during kinetic experiments with limited heat transfer resistance and high reactant flow. The inhibition of the reaction rate was primarily due to a temperature decrease of up to 230 ºC in the center of the bed, the consumption of steam, and the buildup of inhibitory hydrogen.

The simulation results also demonstrated that it is very difficult to achieve 100% steam utilization. As the steam flowing through the bed is consumed, the reaction rate decreases both due to a lower concentration of reactant, and a higher concentration of products. In order to achieve high steam utilization while maintaining high thermal efficiency, the reactor must either be large to compensate for slow kinetics, or incorporate recuperative heating with high excess steam flow.

3.7 References

1. Kramreiter, R., et al., *Experimental investigation of a 125 kW twin-fire fixed bed gasification pilot plant and comparison to the results of a 2 MW combined heat and power plant (CHP).* Fuel Processing Technology, 2008. **89**(1): p. 90-102.
2. Murgia, S., M. Vascellari, and G. Cau, *Comprehensive CFD model of an air-blown coal-fired updraft gasifier*. Fuel, (0).
3. Saravanakumar, A., et al., *Numerical modelling of a fixed bed updraft long stick wood gasifier.* Biomass and Bioenergy, 2011. **35**(10): p. 4248-4260.
4. Piatkowski, N., C. Wieckert, and A. Steinfeld, *Experimental investigation of a packed-bed solar reactor for the steam-gasification of carbonaceous feedstocks.* Fuel Processing Technology, 2009. **90**(3): p. 360-366.
5. Richard J, K., *Sunfuels.* Progress in Energy and Combustion Science, 1982. **8**(2): p. 121-134.
6. Melchior, T., et al., *Solar-driven biochar gasification in a particle-flow reactor.* Chemical Engineering and Processing: Process Intensification, 2009. **48**(8): p. 1279-1287.
7. Antal, M.J., et al., *Design and operation of a solar fired biomass flash pyrolysis reactor.* Solar Energy, 1983. **30**(4): p. 299-312.
8. Z'Graggen, A. and A. Steinfeld, *A two-phase reactor model for the steam-gasification of carbonaceous materials under concentrated thermal radiation.* Chemical Engineering and Processing: Process Intensification, 2008. **47**(4): p. 655-662.
9. Umeki, K., et al., *High temperature steam-only gasification of woody biomass.* Applied Energy, 2010. **87**(3): p. 791-798.
10. Umeki, K., T. Namioka, and K. Yoshikawa, *Analysis of an updraft biomass gasifier with high temperature steam using a numerical model.* Applied Energy, 2012. **90**(1): p. 38-45.
11. Di Blasi, C., *Combustion and gasification rates of lignocellulosic chars.* Progress in Energy and Combustion Science, 2009. **35**(2): p. 121-140.
12. Ansys, *Ansys Fluent 12.0 User's Guide*. 2009.
13. Di Blasi, C., *Modeling wood gasification in a countercurrent fixed-bed reactor.* Aiche Journal, 2004. **50**(9): p. 2306-2319.
14. Biba, V., et al., *Mathematical-Model for Gasification of Coal under Pressure.* Industrial & Engineering Chemistry Process Design and Development, 1978. **17**(1): p. 92-98.
15. Mermoud, F., et al., *Experimental and numerical study of steam gasification of a single charcoal particle.* Combustion and Flame, 2006. **145**(1-2): p. 59-79.

3.8 Appendix A: Model Development

The work presented in this appendix was performed by Michael Kruesi under my guidance for the fulfillment of his master's thesis in mechanical engineering at ETH Zurich under Aldo Steinfeld [1]. It has been reproduced here with minor editing to account for references outside of the reproduced material.

3.8.1 Heat transfer model

In the energy equation an effective thermal conductivity is applied for the heat flux within the packed bed. A comparison of a broad variety of different models [2] showed that the model of Yagi and Kunii [3] is suitable for heat conduction calculations of coal with ash deposits at high temperatures. The semi-empirical model of Yagi and Kunii that is followed in this work is a resistance network model. By applying the diffusion approximation for radiation within a solid medium, it includes the radiative conductivity in the network of resistances. The heat transfer within a packed bed can be described as seven mechanisms that can be separated into two terms, a fluid flow independent and a fluid flow dependent term.

Fluid flow independent heat transfer mechanisms:

1. Thermal conduction through solid particle
2. Thermal conduction through contact surface of particles
3. Radiative heat transfer between the surfaces of particles
4. Radiative heat transfer between neighboring voids

Fluid flow dependent heat transfer mechanisms:

5. Thermal conduction through the fluid film near the contact surface of two particles
6. Convective heat transfer, solid-fluid-solid
7. Heat transfer by lateral mixing of fluid

For small Reynolds numbers the boundary layers around the solid particles are thick and the mechanisms 1, 3, 4, and 5 are predominant. However, for large Reynolds numbers, mechanism 7 controls the heat flux in any packed bed. Yagi and Kunii include mechanism 5 in the fluid flow independent term since the effect of the flow has only little effect on the mechanism. The model equation for the effective thermal conductivity k_{eff} consisting of the conductivity for motionless fluids k_{eff}^0 and the conductivity due to lateral mixing of the fluid $(k_{eff})_t$ is

$$k_{eff} = k_{eff}^0 + \left(k_{eff}\right)_t$$

In the case of gas-filled voids the effective conductivity for motionless fluid can be expressed as

$$\frac{k_{eff}^0}{k_g} = \frac{\beta(1-\phi)}{\gamma\left(\frac{k_g}{k_s}\right) + \frac{1}{(1/\varphi) + (D_p h_{rs}/k_g)}} + \phi\beta\frac{D_p h_{rv}}{k_g} \qquad (1)$$

where the radiation heat transfer coefficient through the contact surface is

$$h_{rs} = 0.1952\frac{\varepsilon}{2-\varepsilon}\left(\frac{T}{100}\right)^3$$

where ε is the emissivity. The radiation heat transfer coefficient through the voids is

$$h_{rv} = \left(\frac{0.1952}{1 + \frac{\phi}{2(1-\phi)}\frac{1-\varepsilon}{\varepsilon}}\right)\left(\frac{T}{100}\right)^3$$

For a wide range of packings, parameter β lies between 0.82 and 1. According to existing data, parameter φ can be approximated as $\varphi \approx 0.04$ [2]. In order to get the best fit to the experimental data[1], β was set to 0.9 and γ to 0.7.

In the present case the fluid flow is perpendicular to the direction of the main heat transfer. Although the Reynolds number is small, the effect of the fluid flow is not negligible.

$$\frac{(k_{eff})_t}{k_g} = (\alpha\beta) N_{peM}$$

with $N_{peM} = d_p C_p G / k_g$. G is the mass velocity of the fluid based on the empty tube. For spheres, cylinders, pellets, or broken granules the values of $(\alpha\beta)$ cover a narrow range of 0.1 to 0.14 for the different packing conditions [3]. Since no explicit values for the packed bed of char particles could be found in literature an intermediate value of 0.12 was chosen for $(\alpha\beta)$.

For the solid thermal conductivity in Equation 1 the correlation of Atkinson and Merrick [4] for carbonaceous material was chosen.

$$k_s = (\rho_c / 4155)^{3.5} \sqrt{T} \quad [W/m-K]$$

Although this correlation is not specifically for switchgrass char, it is considered a reasonable approximation for chars with a high carbon content. Based on a composition-dependent correlation for subbituminous chars [5], a true density of $\rho_c = 1656 kg/m^3$ the char was estimated. This correlation was found to give good agreement with the experimental results (Chapter 5.1, Figures 19 and 20 from Michael's thesis [1]). The internal porosity of the particles was not

[1] Experiments were performed in the absence of reaction in a larger bed to fit the thermal conductivity parameters, details can be found in Michael's thesis.

considered and is part of the error. Since the sensitivity of the effective thermal conductivity to the solid thermal conductivity k_s is very small, no further attention was paid to this.

Since no values for emissivity of switchgrass char could be found, the emissivity ε was assumed to be 0.92, the same as the one from straw char [6]

3.8.2 Reference Enthalpy and Reaction Enthalpy of Gasification

The reference enthalpy of the used biomass was calculated based on the higher heating value (HHV) and the composition of the biomass $C_1H_xO_yS_uN_v$ (Table 9, Michael's thesis [1]). For the combustion reaction

$$C_1H_xO_yS_uN_v + \left(2 + \frac{x}{4} - \frac{y}{2} + u\right) \cdot O_2 \rightarrow \frac{x}{2} \cdot H_2O + CO_2 + u \cdot SO_2 + \frac{v}{2} \cdot N_2 \qquad (2)$$

the enthalpy of combustion per mole of biomass ($C_1H_xO_yS_uN_v$) can be written as

$$\Delta H^0_{combustion} = HHV \cdot M_{C_1H_xO_vS_uN_v}$$

where the molar mass is defined as

$$M_{C_1H_xO_vS_uN_v} = M_C + x \cdot M_H + y \cdot M_O + u \cdot M_S + v \cdot M_N$$

The standard enthalpy of the biomass $\Delta_f H^0_{C_1H_xO_yS_uN_v}$ can then be derived from the standard enthalpies of the combustion reaction (Equation 2).

$$\begin{aligned}\Delta_f H^0_{C_1H_xO_yS_uN_v} = {} & \frac{x}{2} \cdot \Delta_f H^0_{H_2O(liq)} + \Delta_f H^0_{CO_2} + u \cdot \Delta_f H^0_{SO_2} + \frac{v}{2} \cdot \Delta_f H^0_{N_2} \\ & - \left(2 + \frac{x-y}{2}\right) \cdot \Delta_f H^0_{O_2} + \Delta H^0_{combustion}\end{aligned} \qquad (3)$$

Since the standard enthalpies of elementary substances are 0, Equation 3 can be simplified to

$$\Delta_f H^0_{C_1H_xO_yS_uN_v} = \frac{x}{2}\cdot\Delta_f H^0_{H_2O(liq)} + u\cdot\Delta_f H^0_{SO_2} + \Delta_f H^0_{CO_2} + \Delta H^0_{combustion}$$

Based on the standard enthalpy of the switchgrass char the reaction enthalpy of the gasification reaction can be determined. Equation 4 describes the simplified complete steam gasification of the switchgrass char.

$$C_1H_xO_yS_uN_v + (1-y)\cdot H_2O \rightarrow \left(1+\frac{x}{2}-y-u\right)\cdot H_2 + CO + u\cdot H_2S + \frac{v}{2}\cdot N_2 \qquad (4)$$

The enthalpy change for this reaction can is

$$\Delta H^0_{gasification} = \Delta_f H^0_{CO} + u\cdot\Delta_f H^0_{H_2S} - (1-y)\Delta_f H^0_{H_2O} - \Delta_f H^0_{C_1H_xO_yS_uN_v}$$

In the present case the gasification enthalpy on a daf basis was found to be

$$\Delta H^0_{gasification} = 115\text{kJ/mol} = 8.6234 MJ/kg_{char}$$

The resulting source term to be introduced in the energy equation is

$$S^h_f = -\dot{m}Y_{char\,consumption}\cdot\Delta H^0_{gasification}$$

Although sulfur is not included in the simplified chemistry applied in this model, the reaction enthalpy of sulfur is considered.

3.8.3 Heat Capacity

The heat capacity of the switchgrass char was estimated following the approach described by Merrick [7]. The model applies the Einstein form of the quantum theory specific heat description for solids. The theory assumes that all atoms in the solid oscillate independently in three directions with a common characteristic frequency. This leads to a specific heat for dry and ash free (daf) char given by

$$c_{daf} = 3 \cdot \frac{R}{a} g_1(z)$$

where

$$g_1 = \frac{\exp(z)}{\left(\frac{\exp(z)-1}{z}\right)^2}$$

The mean atomic weight a is defined as

$$\frac{1}{a} = \sum_{i=1}^{5} \frac{y_i}{M_i}$$

where y_i is the mass fraction of carbon, hydrogen, oxygen, nitrogen and sulfur on a daf basis.

$$z = \frac{\Theta}{T} = \frac{1200K}{T}$$

The effect of ash was included by assigning the following specific heat to the ash.

$$c_{ash} = 754 + 0.586 \cdot (T - 273.15) \qquad [J/kg\,K]$$

By assuming additivity, the specific heat of the char can be expressed as

$$C = \sum_i w_i c_i$$

w_i is the mass fraction of as received char of daf char, ash and moisture. Since the present model assumes that the char is completely dry by the time the experiment is started only the mass fraction of daf char and ash are considered.

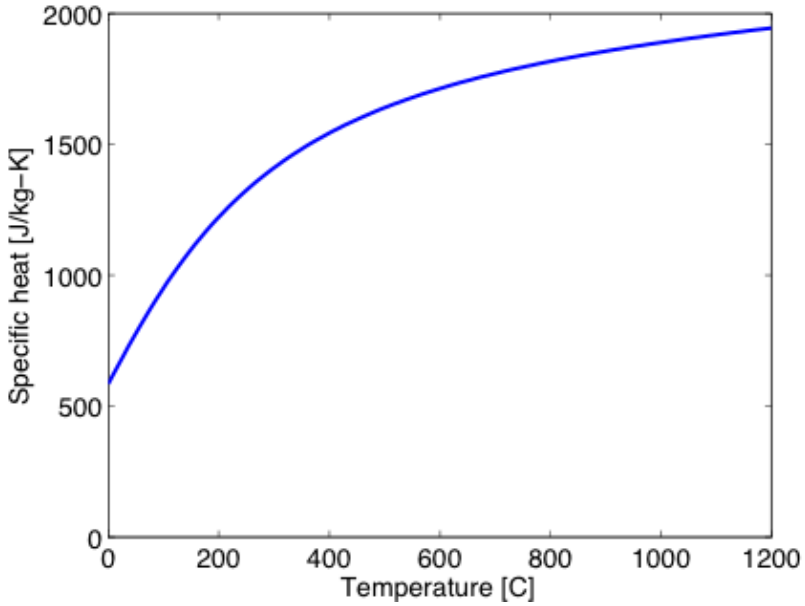

Figure 3-16 Specific heat switchgrass char.

For the implementation of the specific heat into Fluent the formula for the specific heat was evaluated over the temperature and stored as a polynomial. The polynomial coefficients for the switchgrass char can be found in Table 3-. Figure 3-16 depicts the specific heat of the switchgrass char in dependence on the temperature.

Table 3-2 Polynomial coefficients specific heat switchgrass char

$$C_p = A + BT + CT^2 + DT^3 + ET^4 \quad [J/kg\,K]$$

A	B	C	D	E
-1.1235e+03	8.6873	-0.0104	5.9015e-06	-1.2771e-09

3.8.4 Momentum Conservation

In the porous media model the packed bed is not physically present. Instead, a momentum source term is added to the governing momentum equation to take the resistance of the medium

into account. Fluent defines the source terms as shown in Equation 5 below. S_i is the source term for the *i*-th (x or y) momentum equation. It contains a viscous loss term (1st term RHS) and an inertial loss term (2nd term RHS).

$$S_i = -\left(\sum_j D_{ij} \mu v_{sf,j} + \sum_j C_{ij} \frac{1}{2} \rho |v_{sf}| v_{sf,j} \right) \quad (5)$$

The introduced momentum sink represents the pressure gradient in the porous media. The pressure gradient depends upon the superficial velocity, which is defined as

$$v_{sf} = \phi v_{physical}$$

where ϕ is the macro porosity.

In the case of an isotropic porous medium, which is assumed here, Equation 5 simplifies to

$$S_i = -\left(\frac{\mu}{\alpha} v_{sf,i} + C_2 \frac{1}{2} \rho |v_{sf}| v_{sf,i} \right) \quad (6)$$

where α is the permeability and C_2 the internal resistance factor.

In order to specify the permeability and the internal resistance factor, the flow regime has to be determined. An interstitial Reynolds number can be used to characterize the flow regime in fixed beds.

$$\mathrm{Re}_{inter} = \frac{D_p \frac{v_{sf}}{\phi} \rho_f}{\mu}$$

The flow regime can be described as creeping, viscous-inertial, or turbulent (Figure 3-17):

$\mathrm{Re}_{inter} \leq 1$ creeping or Darcian regime

$1 < \mathrm{Re}_{inter} < 500$ nonlinear-laminar or viscous-inertial regime

$\mathrm{Re}_{inter} \geq 500$ turbulent regime

The boundaries of the different flow regimes cannot be seen as sharp boundaries since the transition between the different regimes is gradual. In our case the interstitial Reynolds number lies in the lower end of the viscous-inertial regime ($\mathrm{Re}_{inter} \approx 5$). In this regime both viscous and inertial forces affect the fluid dynamics. The pressure drop depends nonlinearly on fluid velocity but the flow is still laminar. Therefore, a laminar solution of the flow through the packed bed of biomass was computed. [8]

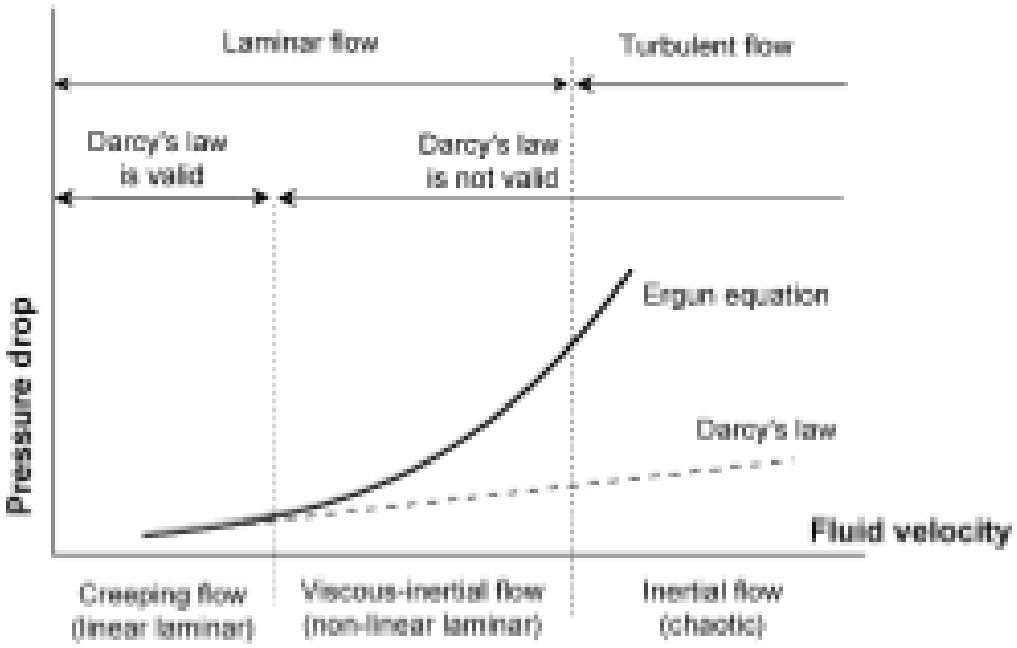

Figure 3-17 Characterization of different hydrodynamic regimes in fixed beds by means of pressure drop–flow rate behavior [8]

As mentioned previously the flow through the bed is in the viscous-inertial regime. In this regime the simple Darcian law (Equation 7) is not valid anymore (Figure 3-).

$$\nabla p = -\frac{\mu}{\alpha} v \qquad (7)$$

Since the Reynolds numbers is greater than 1 ($\mathrm{Re}_{inter} > 1$) inertial effects need to be accounted for in the momentum equation. The correlation of Ergun [9] was chosen (Equation 8) to derive appropriate constants for the permeability and the inertial resistance factor in Equation 6. The Ergun equation is applicable over a wide range of Reynolds numbers and many types of packings. In the semi-empirical correlation, viscous losses and kinetic energy losses are assumed to be additive.

$$\frac{|\Delta p|}{L} = \frac{150\mu}{D_p^2}\frac{(1-\phi)^2}{\phi^3} v_{sf} + \frac{1.75\rho}{D_p}\frac{(1-\phi)}{\phi^3} v_{sf}^2 \quad (8)$$

The representative particle diameter D_p is defined as the diameter of a sphere with the same surface to volume ratio as the particles present in the reactor. ϕ is the macro porosity of the packed bed. [8, 10, 11]

This leads to a permeability of

$$\alpha = \frac{D_p^2}{150}\frac{\phi^3}{(1-\phi)^2}$$

and a viscous loss coefficient of

$$C_2 = \frac{3.5}{D_p}\frac{(1-\phi)}{\phi^3}$$

to be implemented in Equation 6.

3.8.5 References

1. Kruesi, M., *Solar steam gasification of switchgrass char in an externally heated tubular reactor*, MSc. thesis, ETH - Swiss Federal Institute of Technology Zurich, 2010.
2. Zbogar, A., et al., *Heat transfer in ash deposits: A modelling tool-box.* Progress in Energy and Combustion Science, 2005. **31**(5-6): p. 371-421.
3. Yagi, S. and D. Kunii, *Studies on Effective Thermal Conductivities in Packed Beds.* Aiche Journal, 1957. **3**(3): p. 373-381.
4. Atkinson, B. and D. Merrick, *Mathematical-Models of the Thermal-Decomposition of Coal, 4. Heat-Transfer and Temperature Profiles in a Coke-Oven Charge.* Fuel, 1983. **62**(5): p. 553-561.
5. Parkash, S., *True Density and Elemental Composition of Subbituminous Coals.* Fuel, 1985. **64**(5): p. 631-634.
6. Fjellerup, J., et al., *Heat transfer in a fixed bed of straw char.* Energy & Fuels, 2003. **17**(5): p. 1251-1258.
7. Merrick, D., *Mathematical-Models of the Thermal-Decomposition of Coal .2. Specific-Heats and Heats of Reaction.* Fuel, 1983. **62**(5): p. 540-546.
8. Hlushkou, D. and U. Tallarek, *Transition from creeping via viscous-inertial to turbulent flow in fixed beds.* Journal of Chromatography A, 2006. **1126**(1-2): p. 70-85.
9. Ergun, S., *Fluid Flow through Packed Columns.* Chemical Engineering Progress, 1952. **48**(2): p. 89-94.
10. Fluent, Inc., *Fluent 6.3 User's Guide*. 2006.
11. McCabe, W.L., J.C. Smith, and P. Harriott, *Unit operations of chemical engineering*. 7th ed. McGraw-Hill chemical engineering series. 2005, Boston: McGraw-Hill. xxv, 1140 p.

Chapter 4 A Novel Brush Feeder for the Pneumatic Delivery of Small Particles at Steady Feed Rates

4.1 Abstract

A novel particle feeding system capable of pneumatically dispensing dispersed particles at low and consistent feed rates has been developed. The feeder is based on a rotating brush that continually cleans the outlet orifice in a hopper filled with particles. The system was designed specifically for biomass particles that have been milled and sieved to less than 150 μm as a feedstock for laboratory scale aerosol flow reactors. This feedstock often contains a large fraction of high aspect ratio particles that form obstructions in many conventional feeding systems. In addition to biomass, the feeder has successfully fed all particles less than 150 μm that have been tested. Feed rates varying from 4.25 to 2420 mg/min have been obtained with spray dried algae at a constant carrier gas flow of 0.75 slpm, and steady and consistent feeding with milled switchgrass has been demonstrated. The design, construction, and preliminary testing of the feeding system are presented in this paper.

4.2 Introduction

Feeding of dispersed particulate matter to laboratory scale reactors is a problem that has resisted a universal solution for decades. The highly diverse range of properties that small solid particles exhibit often prevents one design from working with many different particle types [1]. Many researchers have found themselves unexpectedly in the field of feeder design when their original topic was some other aspect of solids processing. For a wide range of laboratory scale processes, the suitability of the data collected is primarily determined by the quality of the particle feeding system. In many cases, optimization of the feeder can dramatically increase the quality of measurements.

A particular challenge is the measurement of steam gasification reaction kinetics for fine biomass particles (<150 μm size fraction) at high reaction temperatures (> 1000^{o}C). The particles must be rapidly heated and then held at temperature for short residence times on the order of fractions of a second to several seconds. A most suitable reactor for carrying out this type of reaction is the drop tube reactor (DTR) where particles entrained in a stream of reactant gas flow downward through a heated transport tube. High rates of heat and mass transfer are achieved if the particles can be well dispersed in the reactant stream. Otherwise, the feeding of aggregates results in stochastic mass/heat transfer resistances that are rate limiting and intrinsic kinetics cannot be measured directly. For optimal performance, it is extremely desirable to be able to feed a steady stream of dispersed particles independent of the amount of carrier gas flow. Limited carrier gas flow gives more flexibility in the range of residence times and reactant concentrations that is achievable.

Some biomass types can be difficult to feed due to their light, fluffy nature. Others contain a high fraction of high aspect ratio particles. All contain a wide range of particle sizes when

prepared by conventional milling and sieving processes. Since particle size can have a large effect on the reaction rate, it is important that size separation does not take place inside the feeder. Many different feeder designs were considered, but all are non-ideal in some aspect for this difficult to feed particle group.

Fluidized bed feeders (FBF) are commonly used as laboratory feeders and especially in situations where an agglomerative power must be broken up before feeding [2-4]. The powder is loaded into a bed and sometimes mixed with a milling media to aid in fluidization. Fluidization gas is flowed into the bed and a stream of gas and particles is extracted. While FBFs have proven reliable in many applications, the high aspect ratio particles present in many biomass types proved exceedingly difficult to fluidize on a small scale. Additionally, it is difficult to ensure that no size separation takes place within the bed.

Another class of feeders relies on a suction tube that is progressively moved toward a bed of particles. Examples of this type of feeder are the moving cup and rotary table feeder [4-6]. These designs are advantageous because particles are presented to the feeder outlet at a steady rate regardless of their size and morphology. Size separation in the feeder is completely eliminated with this approach. Unfortunately, clogging at the inlet of the suction tube is a major concern with many biomass types, and maintaining a pressurized and air-free environment with sliding seals is difficult.

Screw and rotary valve feeders have also been used in a wide range of applications [7, 8]. In processes where high flow rates are needed and where particle agglomeration and pulsation of flow are not issues, such feeders are often the best choice. For kinetic measurements in a DTR,

agglomeration and pulsation of flow can severely affect the heat and mass transfer, and obtaining small and precise flows is difficult.

Vibratory feeders have also been used to successfully feed particles in laboratory conditions [8]. These designs are based on a conical hopper attached to a vibrating platform. Vibration of the particle bed provides fluidization like conditions and a steady stream of particles may be extracted from the bottom of the hopper. Unfortunately, feeding of small agglomerative particles can be difficult, and feeding of particles with a high aspect ratio can be nearly impossible if they form a bridged network inside the hopper.

To combat the difficulties listed above, a novel brush based feeding system was developed. This paper details the design of the feeding system and presents some initial testing with a several particle types.

4.3 Feeder design

4.3.1 Design constraints

Many different prototype feeding systems were developed and tested for their performance with biomass feedstocks. The feeders were tested against the following criteria:

1. Steady particle flow over long periods of time.
2. Ability to feed paritcles up to 150 μm in diameter.
3. Limited clogging with high aspect ratio particles.
4. Operates with approximately 1 slpm carrier gas flow.
5. Operate at pressures up to 4 psi with an air-free environment.
6. Feed at least 120 mg/min.
7. Gravimetric measurement of real time feed rate.

8. Limited size/morphology separation in feeder.

4.3.2 Vibratory feeder testing

Initial testing with a vibrating hopper showed marginal results. An extensive experimental campaign was carried out using particles ranging in size from 150 μm to 2 mm. A hopper with sloped sides and a 12.7 mm outlet tube was attached to a vibrating platform as shown in Figure 4-1. The hopper is loaded though a rear port with an O-ring seal. The top of the hopper is equipped with an inlet to allow purge gas to be passed through the particle bed. Initial testing showed that the particle flow rate at a constant vibration rate was highly erratic and frequently ceased altogether. Without visual inspection there was no way to guarantee that particles were flowing into the reactor system.

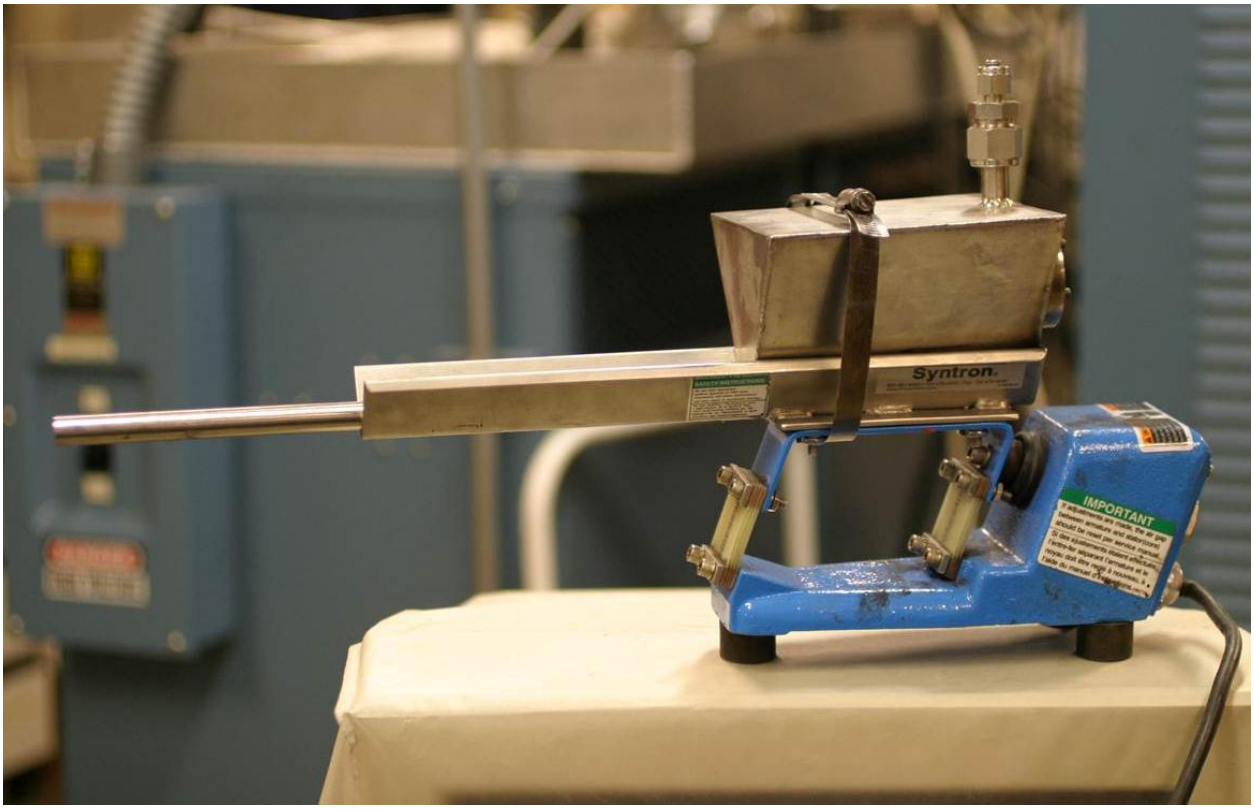

Figure 4-1: Photo of the vibratory feeder. A sloped-wall hopper is attached to a vibrating platform to dispense particles from the bottom of the hopper. Purge gas may be flowed through the bed from the top of the hopper.

In order to continuously monitor the flow rate of particles leaving the feeder a clear piece of vinyl tubing was used to connect the feeder outlet to the reactor system. The tubing was fitted over the feeder outlet and reactor inlet and sealed with hose clamps. Because the inlet to the reactor is high above the laboratory floor and the particles must be able to freely fall into the reactor, a webcam was positioned such that the operator could view the vinyl tubing through a window on the control computer. The vibration rate was manually and continuously adjusted based on a visual inspection of the particles falling through the vinyl tube. If the feeder became clogged, pulsing the vibration rate to the maximum could usually restore particle flow. Due to the high variability of particle flow rate, experiments were carried out for anywhere from 20 to 45 minutes, a seemingly endless amount of time for the operator to be monitoring the flow and adjusting the vibration rate.

Even with the above listed disadvantages, an experimental campaign was performed to test the effect of several variables on the degree of conversion using milled corn stover. Data from a typical run are shown in Figure 4-2. Gas composition was determined by NDIR for the CO and CO_2 and by mass spec for H_2 on selected runs. Large fluctuations in the concentration of product gases indicated that large variations in particle flow were occurring and a more suitable method of feeding was needed. Additionally, the results indicated that particle size had a huge effect on the degree of conversion. Given the limited residence time of the laboratory scale aerosol flow reactor the degree of conversion was limited to about 80% for particles larger than 150 μm. To achieve high conversion in a small reactor we would need to be able to feed particles that were smaller than 150 μm.

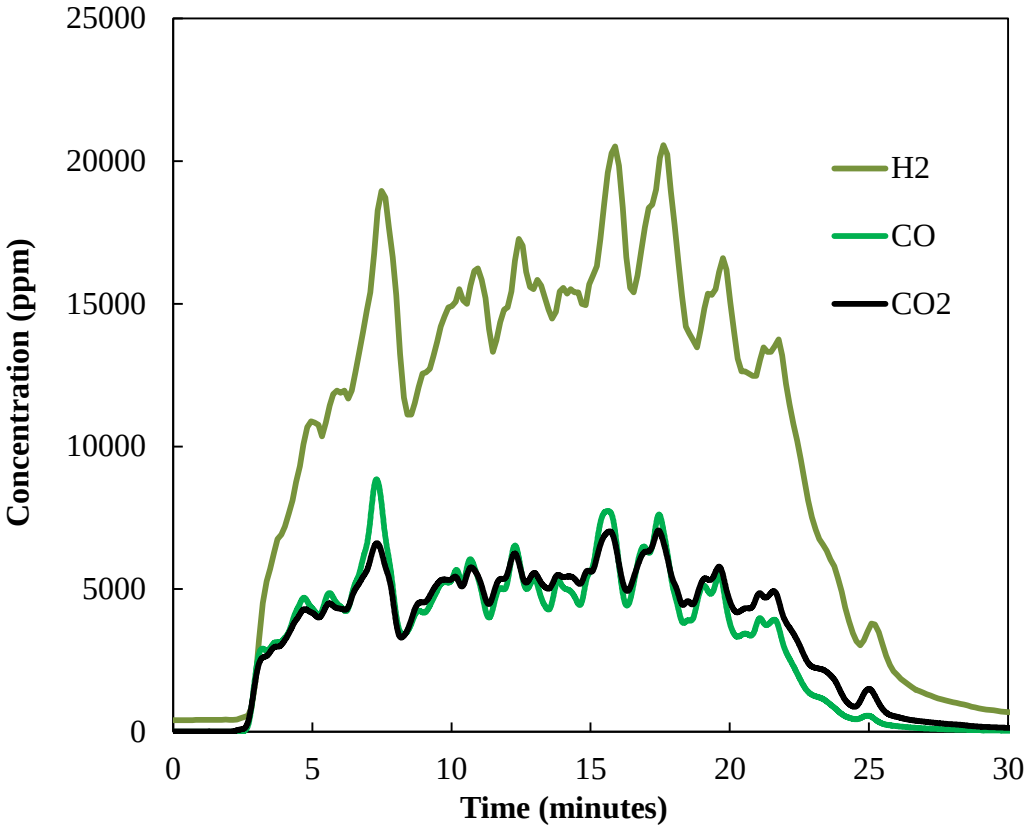

Figure 4-2: Gas concentration vs. time for a gasification run using the vibratory feeder. Large variations in the product gas concentration are due to variability in the particle feed rate.

The marginal effectiveness of the vibratory feeder and the lack of a commercially available replacement led to an extended effort to improve the hopper and particle entrainment system while maintaining the use of the vibratory platform. Several prototypes were developed that were designed to prevent the agglomeration issues seen with the original hopper when using small particles. The results with algae were mildly encouraging, but milled terrestrial plants such as corn stover and switchgrass proved impossible to feed consistently. The fibrous nature of these terrestrial plants leads to a high fraction of rod-like particles after conventional milling processes. These particles with lengths up to a millimeter would quickly accumulate at the outlet of the hopper to form a bridged network that completely restricts particle flow. In the end the vibrating platform was abandoned and the feeding system was completely redesigned.

4.3.3 Brush feeder design

To combat the issue of bridging over the outlet, a novel feeder was designed such that the outlet is the minimum point of restriction and is continually cleaned. A diagram of the feeder is shown in Figure 4-3. A goat hair brush is enclosed in a fully sealed hopper. The brush covers the inlet and outlet holes in the bottom of the feeder. A motor is enclosed in a separately sealed housing that turns the brush at 0-100 rpm. As the brush rotates, particles percolate down through the bristles and are swept into the outlet hole by the carrier gas. The brush head may be equipped with wipers to continually disturb the particle bed to prevent bridging in the hopper. The top and bottom caps are held together with 4 threaded rods not shown in the figure.

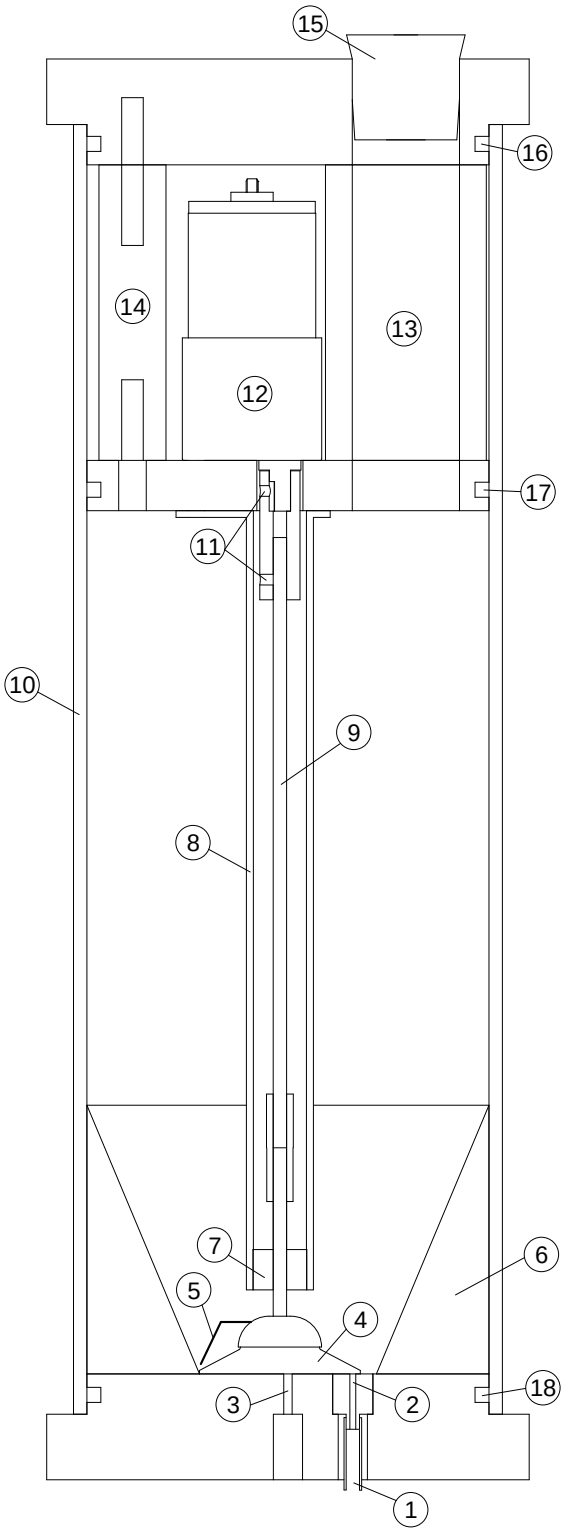

Figure 4-3: Cross sectional view of the rotary brush feeder. (1) Gas and particles outlet; (2) Outlet orifice; (3) Carrier gas inlet; (4) Goat hair brush; (5) Wiper; (6) Aluminum conical insert; (7) Brass bearing; (8) Protective housing for driveshaft; (9) Driveshaft; (10) Acrylic housing; (11) Set screws; (12) Drive motor; (13) Particle loading port; (14) Support for motor mount (1 of 3); (15) Particle loading port stopper; (16), (17), (18) O-ring seals.

For easy to feed spherical particles, the design work ends at the exit orifice of the feeder. From here a 1/8” O.D. tube is used to pneumatically transport the particles to the reactor. For particles with a high aspect ratio, it is much more difficult to prevent bridging where the 1/8” feed tube must be coupled. In an ideal application there are at least two connections to be made, one where the flexible tube connects to the feeder, and the other where the metal reactor tube connects to the flexible tube. Clogging at the feeder outlet was solved by machining the brass outlet orifice to have a nipple that the flexible tube can slide over as shown in Figure 4-4.

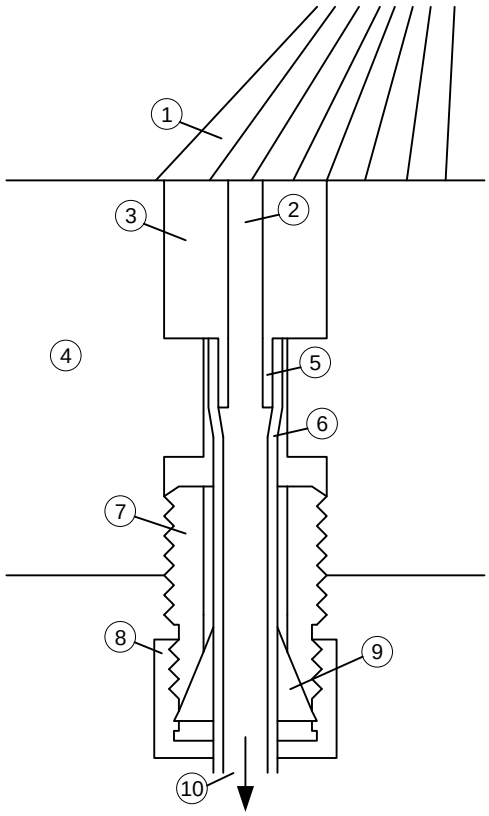

Figure 4-4: Diagram of the exit orifice assembly: (1) Brush; (2) Exit orifice; (3) Exchangeable brass piece; (4) Feeder base; (5) Machined nipple; (6) Flexible outlet tube; (7) Swagelok fitting; (8) Swagelok nut; (9) Swagelok ferrule; (10) Particle and gas exit.

The tube is then held in place with a bored through threaded Swagelok fitting that is screwed into the outlet port. The coupling at the transition between the flexible tube and the metal tubing is a

Swagelok coupling. This coupling performs satisfactorily under most conditions, but occasionally clogs with high aspect ratio particles.

The feeder is loaded with biomass from the top through a feeding port that passes through the motor enclosure. This port is sealed with either an expandable stopper for low pressures, or a screw plug for higher pressure. Because the entire feeder is sealed, the operating pressure is only limited by the materials of construction. With the current polycarbonate housing, pressures up to 35 psi have been tested. Polycarbonate was chosen for its shatter resistance and the ability to visually inspect the bed behavior.

The feeder is placed on a lab balance with 10 mg precision and is enclosed in an acrylic housing. A housing is needed to prevent air currents in the lab from affecting the balance reading as shown in Figure 4-5. Long lengths of pliable 1/8” tubing and coiled copper wire make the gas and electrical connections to the housing. It is important to ensure that the connections have limited residual strain to reduce drift in the balance reading. The motor housing is equipped with gas connections for purging. The feeder must be fully purged with the desired carrier gas before use to prevent changes in weight due to displacement of air. If argon is used as the carrier gas, a weight change of up to a gram is possible as the chamber is purged.

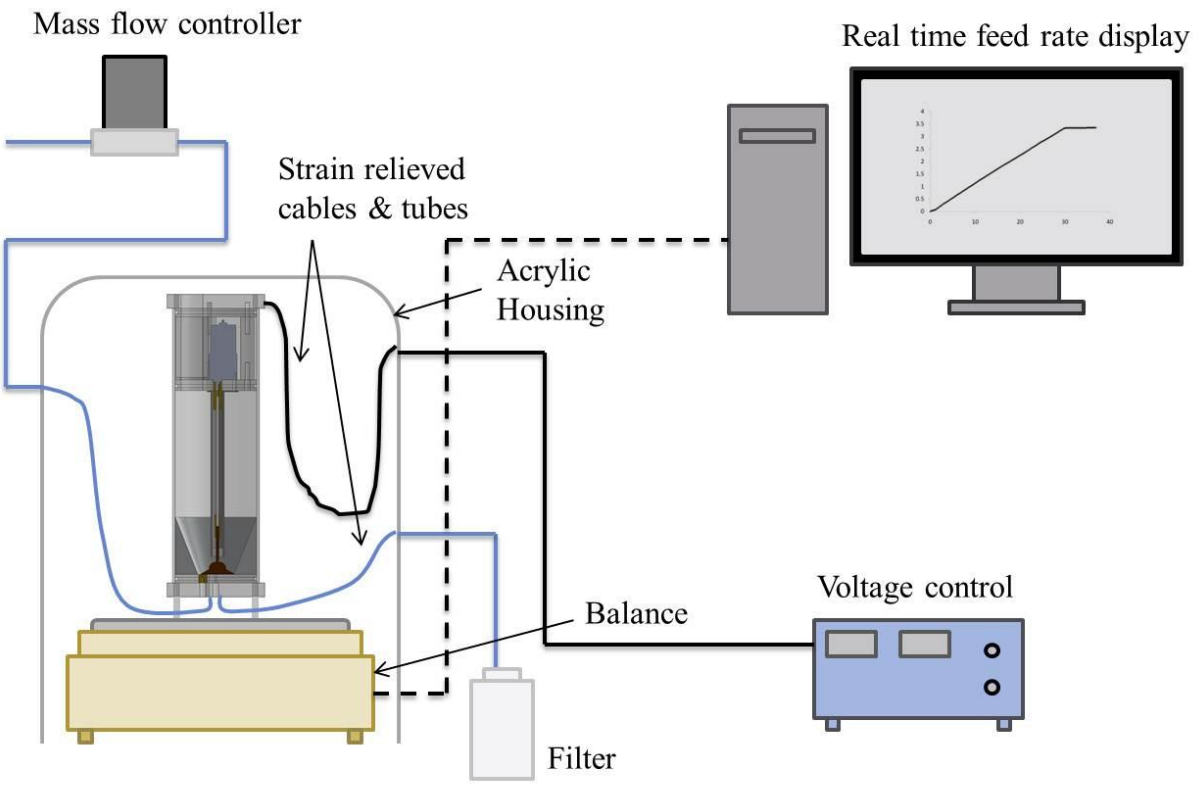

Figure 4-5: Diagram of the brush feeder system. A mass flow controller supplies gas to the base of the feeder through strain relieved tubing. For testing purposes the outlet of the feeder is connected to a filter assembly. The rotational velocity of the brush is controlled by the voltage setting. The balance reading is recorded by Labview and the real-time feed rate is calculated.

The balance value is recorded by a Labview program to analyze the data in real-time. The feed rate is continually calculated based on a user defined number of previous points, and the current balance reading is plotted on a chart. While not currently implemented, it would be possible to create a feedback loop to set the motor speed based on a desired feed rate.

4.3.4 Methods of feed rate adjustment

A multitude of adjustment mechanisms were built into the design to facilitate testing of a wide range of particle types. A list of adjustable parameters, the difficulty of adjustment, and the scale of the potential change in feed rate are listed in Table 4-1.

Adjustment	Difficulty	Magnitude
Brush speed	Easiest	Medium
Screw position	Easy	Small
Bottom plate rotation	Medium	Large
Orifice size	Medium	n/a
Brush shaft length	Hard	Large

Table 4-1: Methods of feed rate adjustment

The easiest mechanism to adjust the feed rate is the rotational speed of the brush. As the brush speed increases, the rate at which particles are swept over the outlet orifice is increased and more particles exit the feeder. To facilitate the movement of new particles down through the bristles of the brush, an adjustable screw protrudes into the bristles. As the bristles pass over the top of the screw the added resistance causes them to spread apart, allowing particles to advance towards the bottom of the brush. This screw is adjustable from the bottom of the feeder.

Macro adjustment of the feed rate can be controlled through three different mechanisms. The first and easiest method of adjustment is the rotational position of the base plate. The radial position of the outlet orifice with respect to the brush has a dramatic effect on the number of particles that exit the feeder. Engineering a method to move the location of the orifice would be difficult. Instead, the motor, drive shaft, and brush are located slightly off-center to allow for radial positioning of the outlet by rotating the baseplate with respect to the motor housing. Because the baseplate has 4 bolt holes in a square pattern, 4 different positions are possible. Another mechanism to vary the distance between the edge of the brush and the exit orifice is the drive shaft length. By lengthening the shaft, the brush is splayed out against the bottom plate. At the same time, the angle and density of the bristles change such that the bristles are more closely packed and oriented closer to horizontal. The final mechanism for adjustment is the size of the

outlet orifice. The orifice is designed as a removable brass insert to facilitate easy changes in diameter or shape.

4.4 Results and discussion

The performance of the feeder exceeded expectations on all fronts. All of the design criteria in Section 4.3.1 have either been met or exceeded. Numerous different organic and inorganic particles have been successfully fed using the rotating brush design and no particles in the <150 μm diameter range have proven impossible to feed.

While steady feeding was attainable with all test particles, several areas of sensitivity were identified. As mentioned in the design section, the most difficult issue to overcome is the clogging of high aspect ratio particles in the downstream transport tube. In almost every instance where particle flow ceased it was due to clogging in the unions that connected the 1/8” transport tube to the reactor system. In cases where particle flow through the outlet orifice decreased or stopped it was always due to bridging in the hopper. Small adjustments to the wiper located above the brush and connected to the drive shaft were able to eliminate this problem.

Maintaining an accurate measurement of the mass of particles still in the feeder was also difficult at times. Before the protective housing was installed small air disturbances caused by the building ventilation system and movement in the lab would cause discrepancies in the reading. Installing an acrylic housing completely eliminated the effect of air currents, but it is important to ensure that all connections between the feeder and the housing are as simple as possible. The plastic gas lines and copper electrical connections should be at least several inches long to reduce the amount of force they can exert and they should touch the feeder and the housing in only two locations. Before feeding is started, the balance reading must be allowed to

stabilize, sometimes taking up to several minutes to relieve strain in the plastic lines and purge the air from the feeder. Once feeding has started, large changes in the total system pressure can also affect the balance reading by changing the forces exerted by the plastic tubing.

Spray dried algae was tested over a large range of feeder settings and performed very well under all conditions. An SEM image of the particle feed is shown in Figure 4-6.

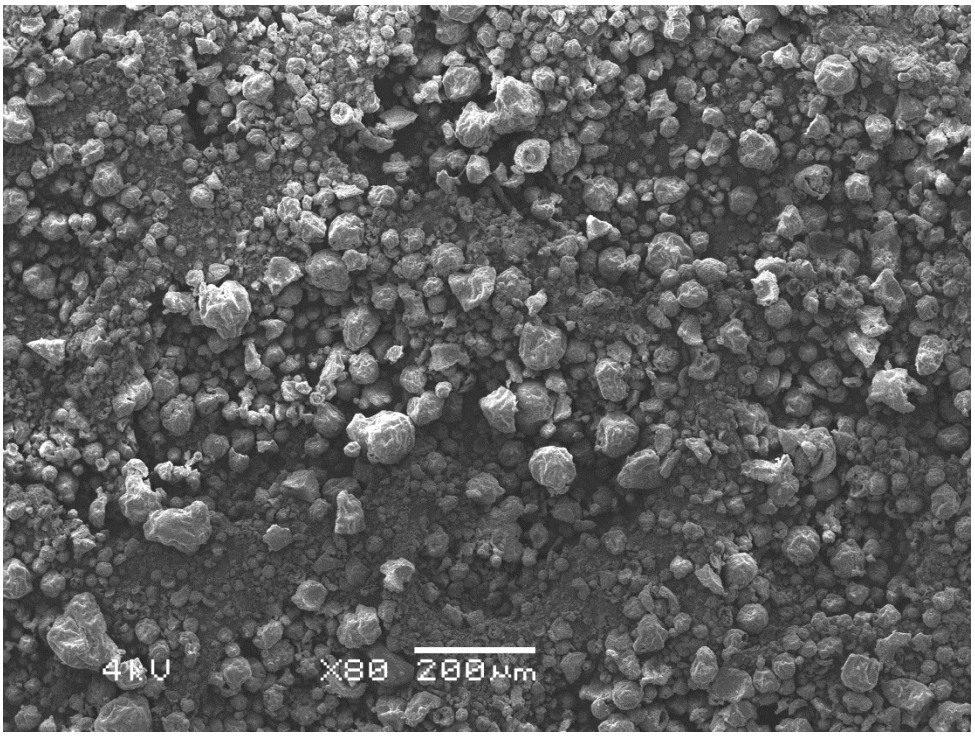

Figure 4-6: SEM image of the algae particles.

All adjustable parameters were varied and tested to their maximum settings other than the outlet orifice size. Mass fed vs. time plots for three different settings are shown in Figure 4-7 and Figure 4-8. Steady particle flow was achieved at feed rates varying over several orders of magnitude from 0.07 to 40.3 mg/s. The experiments were carried out with a carrier gas flow of 0.75 slpm corresponding to particle loadings of 0.0056 to 3.22 kg/m^3.

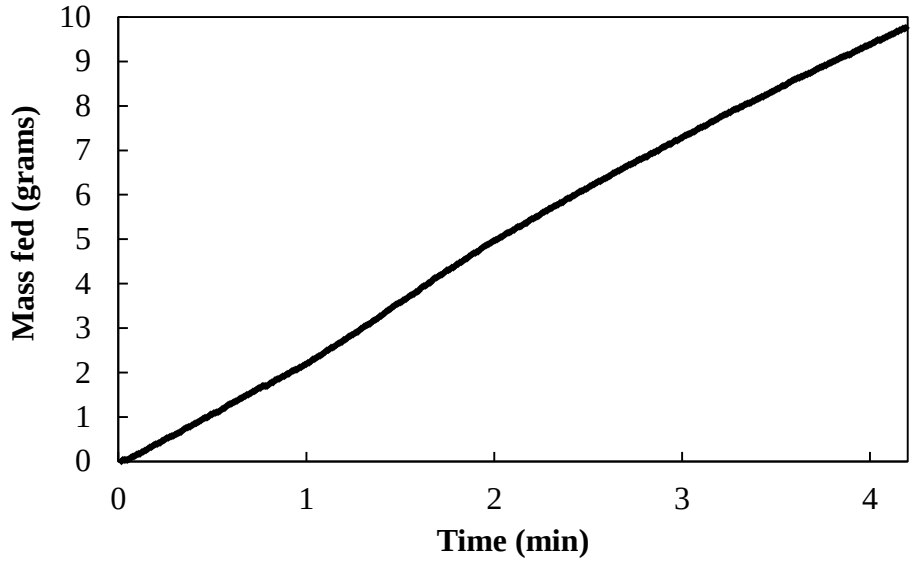

Figure 4-7: Mass fed vs. time for high-flow settings with algae feedstock. Feed rate: 2421 mg/min

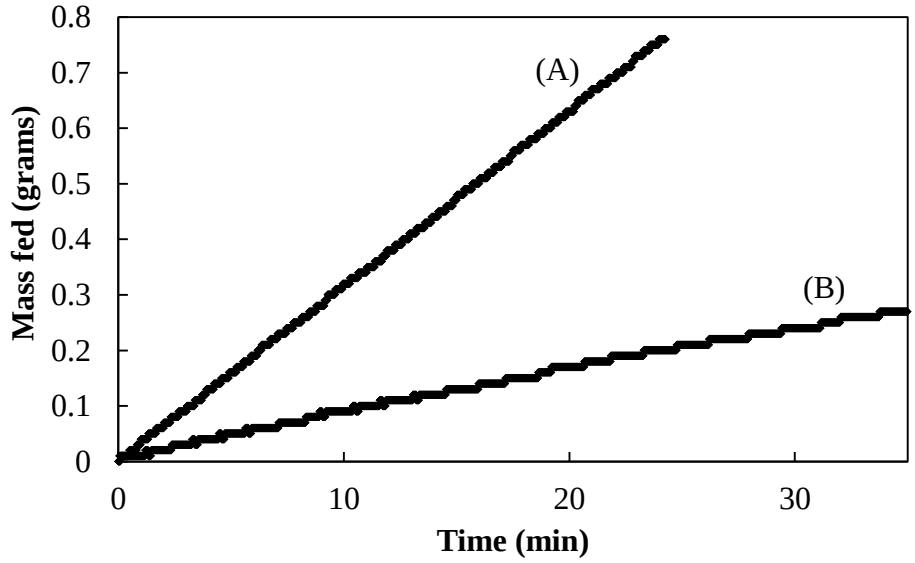

Figure 4-8: Mass fed vs. time for medium and low flow settings with algae feedstock. (A) 31.5 mg/min. (B) 7.60 mg/min.

Switchgrass was milled and sieved to <150 μm particles and tested under a limited set of conditions. An SEM of the processed switchgrass is shown in Figure 4-9.

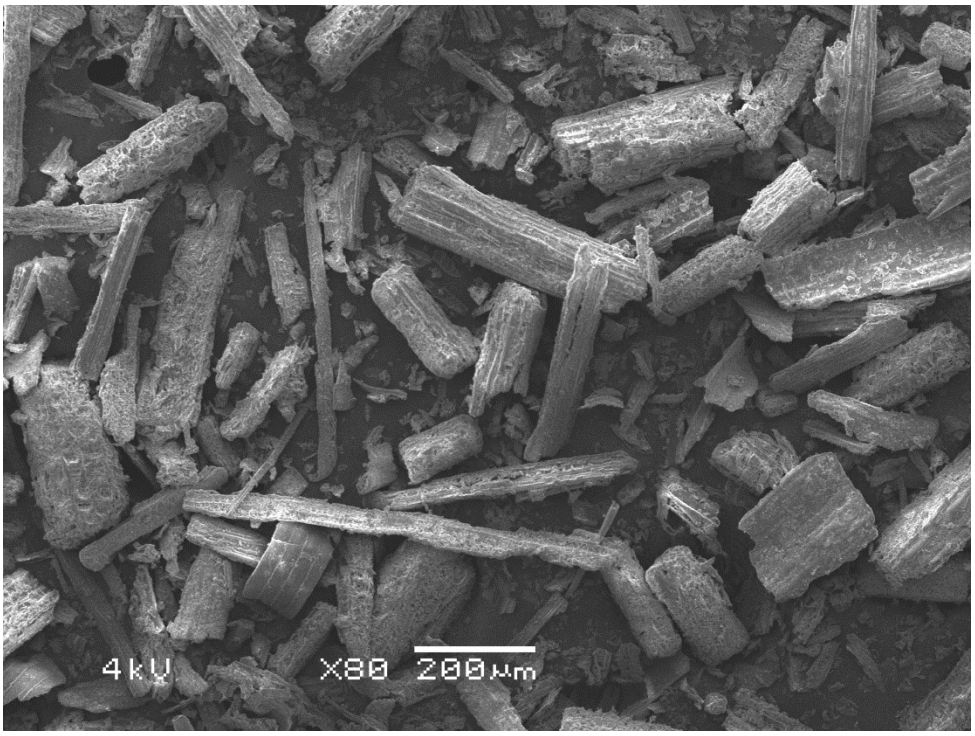

Figure 4-9: SEM image of switchgrass particles.

Mass fed vs. time for three different rotational speeds is shown in Figure 4-10. Careful positioning of the wiper was necessary to prevent bridging just above the outside edge of the brush. Without the wiper in place, a small void would form preventing the edge of the brush from being replenished with particles.

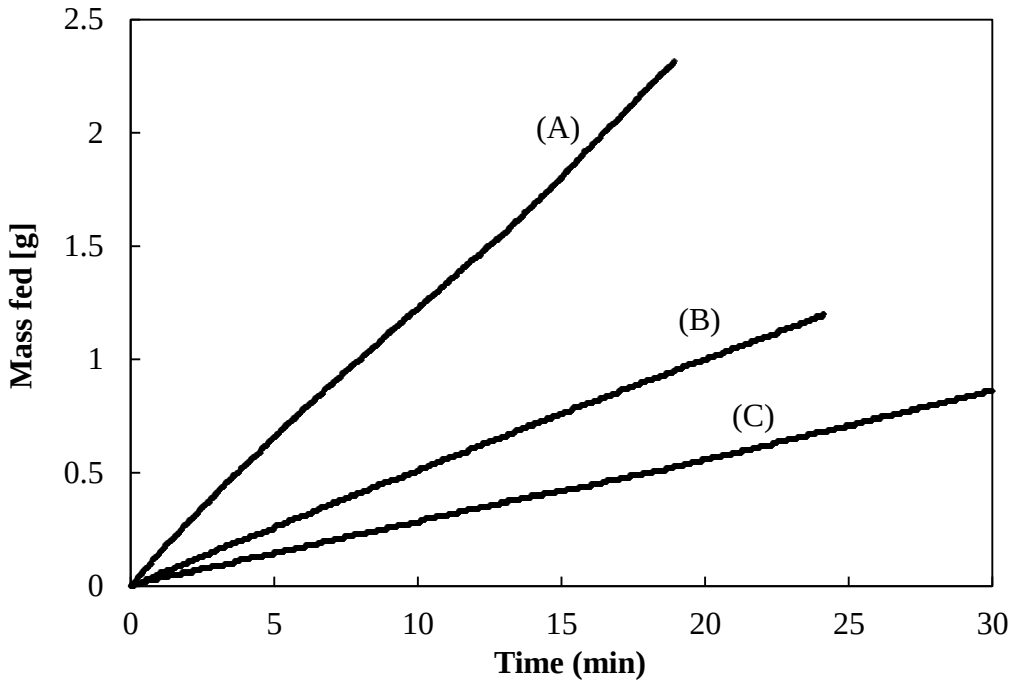

Figure 4-10: Mass fed vs. time for three different voltage settings with milled switchgrass. (A) 118 mg/min; (B) 49.6 mg/min; (C) 28.4 mg/min.

Proof of concept feeding was performed with many other particle types including spent barley grains, rice hulls, acetylene black, and alumina. All particles were less than 150 μm in diameter and all were able to be fed at steady feed rates over long periods of time. Laser imaging was performed for algae, acetylene black and alumina using an Oxford Lasers 6301 particle sizing system. Images were taken just after the outlet of the 1/8" feed tube and are shown in Figure 4-11. High levels of dispersion were obtained for all three feedstocks.

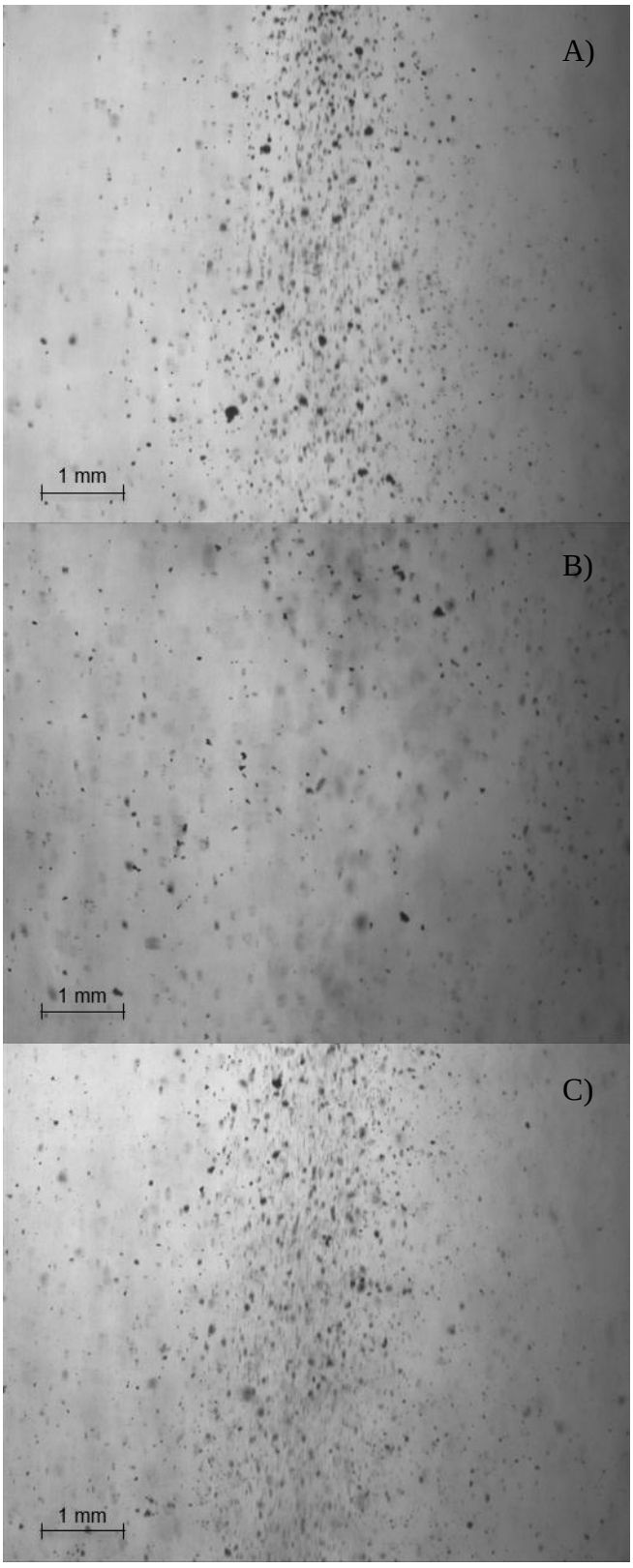

Figure 4-11: Laser images taken just after the outlet of the feed tube using the rotary brush feeder. A) Spray dried Algae; B) Acetylene black; C) Alumina.

4.5 Conclusions

A novel particulate feeding system based on a rotating brush was developed to support kinetic measurements in a drop tube reactor. The feeding system has performed well with all feedstocks tested to date. Steady flow over long time periods and with high levels of dispersion has been demonstrated. An added advantage of the brush feeder is the ability to feed rod like particles with high aspect ratios.

4.6 References

1. T.W, D., *The production of concentrated powder suspensions at low flow rates.* Powder Technology, 1985. **42**(3): p. 249-253.
2. Francis, T.M., et al., *An investigation of a fluidized bed solids feeder for an aerosol flow reactor.* Powder Technology, 2010. **199**(1): p. 70-76.
3. Suri, A. and M. Horio, *A novel cartridge type powder feeder.* Powder Technology, 2009. **189**(3): p. 497-507.
4. Gullett, B.K. and G.R. Gillis, *Low Flow-Rate Laboratory Feeders for Agglomerative Particles.* Powder Technology, 1987. **52**(3): p. 257-260.
5. Buchanan, J.S. and H.J. Schoennagel, *Moving Cup Particulates Feeder Used in Laboratory Fcc Unit.* Powder Technology, 1994. **78**(3): p. 281-285.
6. Reist, P.C. and L. Taylor, *Development and operation of an improved turntable dust feeder.* Powder Technology, 2000. **107**(1-2): p. 36-42.
7. Mehmet Yasar, G., *Design improvements on rotary valve particle feeders used for obtaining suspended airflows.* Powder Technology, 2004. **139**(1): p. 76-80.
8. Tardos, G.I. and Q. Lu, *Precision dosing of powders by vibratory and screw feeders: an experimental study.* Advanced Powder Technology, 1996. **7**(1): p. 51-58.

Chapter 5 Conclusions and Future Direction

5.1 Conclusions

A novel, low cost experimental system for measuring high temperature steam-char kinetics was developed. The goal of developing this system was to provide an easy way to obtain high quality kinetic rate data for endothermic gasification reactions that are very rapid. The motivation to obtain such data comes from the application of concentrated solar power to biomass gasification.

The novel measurement technique developed in this work was based on a modified fixed bed design. A large amount of inert thermal media was used to limit the temperature drop during the reaction so that the bed could be assumed to be isothermal. A high rate of reactant flow was forced through the bed to approximate conditions of constant gas concentration.

Under these optimized reaction conditions, the reaction rate of switchgrass char at 1150 °C was far too rapid to use conventional methods such as gas chromatography to monitor the reaction rate. Initial experiments using a non-dispersive infrared (NDIR) analyzer showed that even real-time measurements with a factory configured NDIR were too slow to capture the shape of the curve for the most rapid reaction rates.

While analyzing the data from the NDIR experiments we observed that the outlet flow meter on the system responded very rapidly to changes in the gasification rate. After further analysis it was determined that the flow meter alone could provide a measurement of the reaction rate with a fast response time and high temporal resolution, provided the CO_2 was removed from

the gas stream. If the CO_2 is not removed, large changes in the CO/CO_2 ratio due to the water gas shift reaction can affect the results.

Further work with the NDIR measurement system decreased the response time to a point where reasonable data could be collected and used as a comparison to the gas flow measurement technique. The two methods produced very similar results, with the response time of the gas flow measurement technique being slightly better for the fastest reaction rates. The results were particularly striking considering that the price of the NDIR is roughly 30 times that of the flow meter.

The gas flow measurement technique was then used to collect data over a range of operating conditions that are relevant to solar thermal gasifiers. Using the collected data, an empirical kinetic rate expression was developed based on the Random Pore Model (RPM) for the dependence on the degree of conversion, and a Langmuir-Hinshelwood type expression to predict the initial kinetic rate. The Langmuir-Hinshelwood expression is capable of estimating the initial kinetic rate based on the temperature, steam concentration and hydrogen concentration.

Using the empirical kinetic rate expression, a computational fluid dynamics (CFD) model was developed to assess the feasibility of an externally heated allothermal fixed bed gasifier. A two-dimensional axisymmetric model of our laboratory scale fixed bed reactor was developed using the commercially available Ansys Fluent software package. The presence of the fixed bed was incorporated using Fluent's porous media model with user defined functions (UDFs) to account for the heat and mass source terms.

The Fluent model was experimentally validated using our fixed bed reactor with a 1 gram loading of switchgrass char. This amount of char fills a bed approximately 19 mm in diameter

and 38 mm deep. Even with this very small bed, the overall reaction rate of the bed was much lower than that measured during the kinetic experiments with identical reactor temperatures and inlet steam concentrations. The inhibition of the reaction rate was primarily due to the effects of heat transfer, consumption of steam, and a buildup of inhibitory hydrogen.

Further investigation was performed to determine the effect of the steam flow rate on the overall reaction rate within the fixed bed. Simulations were performed outside of the range of experimental validation to estimate the dependency of the steam utilization on the time for the bed to reach an average conversion of 90%. While an industrial reactor would not operate in a batch fixed bed mode as done in our experiments and simulations, the steam utilization after 10 seconds of reaction was used to approximate the conditions in a continually replenished fixed bed. The time to 90% conversion was found to be highly dependent on the steam flow rate, and by extension the steam utilization at 10 seconds. A steam utilization value of 92% was achieved with a time to 90% conversion of 187 seconds, whereas the utilization drops to 18% to achieve 90% conversion after 62 seconds. As a comparison, the kinetic experiments with the same reactor temperature and inlet steam concentration were 90% complete in 20.5 seconds.

The steam utilization results were striking in that they highlight the tradeoff between high volumetric reactor productivity, and excess steam flow. To design an externally heated allothermal gasifier to be very efficient, the reactor volume must either be large, or else it must incorporate excess steam flow with heat recuperation.

In addition to the work done with switchgrass char, a novel particulate feeding system capable of delivering a consistent stream of particles to an aerosol flow reactor was developed. To the author’s knowledge, the kinetics of biomass gasification for very small particles can only

be measured in an aerosol flow reactor. To obtain quality kinetic data, a very consistent stream of particles must be delivered with a minimal amount of carrier gas flow.

A novel brush based feeding system was developed after numerous failed attempts to deliver particles with a vibrating hopper. The brush feeder is designed such that the outlet of a hopper is the minimum restriction between the feeding device and the reactor, and a rotating brush continually sweeps the outlet clean.

The brush feeder has performed exceptionally well with all particle matter less than 150 μm in diameter, including milled biomass containing a large number of high aspect ratio particles that are difficult to feed.

5.2 Future work

The gas flow measurement technique combined with the modified fixed bed described in this thesis provide a method for measuring kinetics under conditions with reduced heat transfer resistance. It is impossible to completely eliminate the temperature differential between the particles and the reactor temperature, and future work should be done to estimate the temperature of the particles during the kinetic measurements. The assumption made in this work is that the particles are maintained at the initial bed temperature by means of intimate contact with a large reservoir of inert thermal media. It is difficult to verify that assumption due to the complicated geometry of the system, and the difficult to quantify contact area between the thermal media and the reacting char.

The empirical rate expression developed in Chapter 2 is valuable for researchers that are developing CFD models of potential reactor designs to be used with a yet to be determined biomass source. For reactors designed to operate with a specific type of biomass, it would be

valuable to know how the kinetic rate differs from the empirical rate expression for switchgrass char. Studies could be performed with various other char types to determine which parts of the model remain the same and which parts must be modified when the feedstock changes. It is possible that the geometric factor in the Random Pore Model, or various constants in the Langmuir-Hinshelwood fit are constant over certain broad categories of biomass. If the number of fitted values can be reduced, fewer experimental points will be needed to develop a rate expression for an arbitrary char source.

The computational fluid dynamics model makes two simplifying assumptions that should be investigated in more depth. First, the porosity and other bed properties other than density are assumed to be constant. The porosity can have a major effect on the gas flow in the bed, and a positive feedback loop may result near the walls. The char near the walls is hotter than the char in the center and reacts at a faster rate. As this char approaches 70% conversion it will begin to disintegrate and more of the steam flow will be directed to the region near the walls, further increasing the reaction rate. The model was still capable of predicting the reaction rate at high conversion, but little attention should be paid to the details inside the bed at high conversion unless the effect of increasing porosity with increasing conversion is included.

Second, the model assumes that the particle and gas phases are at equal temperatures. Because the reaction is endothermic, and the temperature results between the model and the thermocouples in the bed do not match, it is likely that this assumption is not valid. Further investigations using the simple model presented in this work should include two separate phases with a heat transfer coefficient between them to represent the interaction between the char and gas phase.

The rotary brush feeder results with milled switchgrass are very encouraging, but further work should be done to reduce blockages in the tubes used to connect the feeder to the reactor. The use of the rotating brush has completely eliminated blockages at the outlet of the hopper, but occasionally particles accumulate in the couplings used to connect the feeder to the reactor system. To eliminate this issue, a specially designed coupling should be fabricated to provide a smooth transition between the feeder tube and the reactor inlet tube. One way the coupling could be designed is with a bored through Swagelok fitting. If the receiving tube had an inward taper and the feeder tube was tapered in the opposite direction, the two tubes could directly couple in the middle of the bored through fitting. Gas sealing would still be provided by the Swagelok ferrules, but the extra edges inside the coupling would be eliminated. It is conceivable that this modification could fix all clogging issues encountered with milled switchgrass.

Bibliography

Annual Energy Review 2010. 2010, U.S. Energy Information Administration.

Ahmed, I.I. and A.K. Gupta, *Kinetics of woodchips char gasification with steam and carbon dioxide.* Applied Energy, 2011. **88**(5): p. 1613-1619.

Alevanau, A., et al., *Parameters of high temperature steam gasification of original and pulverised wood pellets.* Fuel Processing Technology, 2011. **92**(10): p. 2068-2074.

Ansys, *Ansys Fluent 12.0 User's Guide*. 2009.

Antal, M.J., et al., *Design and operation of a solar fired biomass flash pyrolysis reactor.* Solar Energy, 1983. **30**(4): p. 299-312.

Atkinson, B. and D. Merrick, *Mathematical-Models of the Thermal-Decomposition of Coal, 4. Heat-Transfer and Temperature Profiles in a Coke-Oven Charge.* Fuel, 1983. **62**(5): p. 553-561.

Bhatia, S.K. and D.D. Perlmutter, *A Random Pore Model for Fluid-Solid Reactions .1. Isothermal, Kinetic Control.* Aiche Journal, 1980. **26**(3): p. 379-386.

Biagini, E., M. Cioni, and L. Tognotti, *Development and characterization of a lab-scale entrained flow reactor for testing biomass fuels.* Fuel, 2005. **84**(12-13): p. 1524-1534.

Biba, V., et al., *Mathematical-Model for Gasification of Coal under Pressure.* Industrial & Engineering Chemistry Process Design and Development, 1978. **17**(1): p. 92-98.

Buchanan, J.S. and H.J. Schoennagel, *Moving Cup Particulates Feeder Used in Laboratory Fcc Unit.* Powder Technology, 1994. **78**(3): p. 281-285.

Colomba, D.B., *Combustion and gasification rates of lignocellulosic chars.* Progress in Energy and Combustion Science, 2009. **35**(2): p. 121-140.

Cox, P.M., et al., *Acceleration of global warming due to carbon-cycle feedbacks in a coupled climate model.* Nature, 2000. **408**(6809): p. 184-187.

Di Blasi, C., *Modeling wood gasification in a countercurrent fixed-bed reactor.* Aiche Journal, 2004. **50**(9): p. 2306-2319.

Di Blasi, C. and C. Branca, *Kinetics of primary product formation from wood pyrolysis.* Industrial & Engineering Chemistry Research, 2001. **40**(23): p. 5547-5556.

Ergun, S., *Fluid Flow through Packed Columns.* Chemical Engineering Progress, 1952. **48**(2): p. 89-94.

Fjellerup, J., et al., *Heat transfer in a fixed bed of straw char.* Energy & Fuels, 2003. **17**(5): p. 1251-1258.

Fluent, Inc., *Fluent 6.3 User's Guide*. 2006.

Francis, T.M., et al., *An investigation of a fluidized bed solids feeder for an aerosol flow reactor.* Powder Technology, 2010. **199**(1): p. 70-76.

Fushimi, C., T. Wada, and A. Tsutsumi, *Inhibition of steam gasification of biomass char by hydrogen and tar.* Biomass and Bioenergy, 2011. **35**(1): p. 179-185.

Gadsby, J., C.N. Hinshelwood, and K.W. Sykes, *The Kinetics of the Reactions of the Steam-Carbon System.* Proceedings of the Royal Society of London Series a-Mathematical and Physical Sciences, 1946. **187**(1009): p. 129-151.

Gao, N., et al., *Hydrogen-rich gas production from biomass steam gasification in an updraft fixed-bed gasifier combined with a porous ceramic reformer.* International Journal of Hydrogen Energy, 2008. **33**(20): p. 5430-5438.

Gregg, D.W., et al., *Solar gasification of coal, activated carbon, coke and coal and biomass mixtures.* Solar Energy, 1980. **25**(4): p. 353-364.

Gullett, B.K. and G.R. Gillis, *Low Flow-Rate Laboratory Feeders for Agglomerative Particles.* Powder Technology, 1987. **52**(3): p. 257-260.

Han, J. and H. Kim, *The reduction and control technology of tar during biomass gasification/pyrolysis: An overview.* Renewable and Sustainable Energy Reviews, 2008. **12**(2): p. 397-416.

Hayashi, J.i., et al., *Rapid conversion of tar and char from pyrolysis of a brown coal by reactions with steam in a drop-tube reactor.* Fuel, 2000. **79**(3-4): p. 439-447.

Henriksen, U., et al., *The design, construction and operation of a 75 kW two-stage gasifier.* Energy, 2006. **31**(10-11): p. 1542-1553.

Hlushkou, D. and U. Tallarek, *Transition from creeping via viscous-inertial to turbulent flow in fixed beds.* Journal of Chromatography A, 2006. **1126**(1-2): p. 70-85.

Huang, Z.M., et al., *Kinetic studies of char gasification by steam and CO2 in the presence of H-2 and CO.* Fuel Processing Technology, 2010. **91**(8): p. 843-847.

Huber, G.W., S. Iborra, and A. Corma, *Synthesis of transportation fuels from biomass: Chemistry, catalysts, and engineering.* Chemical Reviews, 2006. **106**(9): p. 4044-4098.

Huttinger, K.J. and W.F. Merdes, *The Carbon-Steam Reaction at Elevated Pressure - Formations of Product Gases and Hydrogen Inhibitions.* Carbon, 1992. **30**(6): p. 883-894.

Jamil, K., J.-i. Hayashi, and C.-Z. Li, *Pyrolysis of a Victorian brown coal and gasification of nascent char in CO2 atmosphere in a wire-mesh reactor.* Fuel, 2004. **83**(7-8): p. 833-843.

Klose, W. and M. Wolki, *On the intrinsic reaction rate of biomass char gasification with carbon dioxide and steam.* Fuel, 2005. **84**(7-8): p. 885-892.

Kramreiter, R., et al., *Experimental investigation of a 125 kW twin-fire fixed bed gasification pilot plant and comparison to the results of a 2 MW combined heat and power plant (CHP).* Fuel Processing Technology, 2008. **89**(1): p. 90-102.

Kruesi, M., *Solar steam gasification of switchgrass char in an externally heated tubular reactor*, in *Mechanical Engineering*. 2010, ETH - Swiss Federal Institute of Technology Zurich.

Lédé, J., *Solar thermochemical conversion of biomass.* Solar Energy, 1999. **65**(1): p. 3-13.

Lichty, P., et al., *Rapid high temperature solar thermal biomass gasification in a prototype cavity reactor.* Journal of Solar Energy Engineering-Transactions of the Asme, 2010. **132**(1).

Luo, S., et al., *Hydrogen-rich gas from catalytic steam gasification of biomass in a fixed bed reactor: Influence of particle size on gasification performance.* International Journal of Hydrogen Energy, 2009. **34**(3): p. 1260-1264.

Lussier, M.G., Z. Zhang, and D.J. Miller, *Characterizing rate inhibition in steam/hydrogen gasification via analysis of adsorbed hydrogen.* Carbon, 1998. **36**(9): p. 1361-1369.

Mark E, D., *The Fischer–Tropsch process: 1950–2000.* Catalysis Today, 2002. **71**(3-4): p. 227-241.

Marquez-Montesinos, F., et al., *CO2 and steam gasification of a grapefruit skin char.* Fuel, 2002. **81**(4): p. 423-429.

Matsumoto, K., et al., *Gasification reaction kinetics on biomass char obtained as a by-product of gasification in an entrained-flow gasifier with steam and oxygen at 900-1000 °C.* Fuel, 2009. **88**(3): p. 519-527.

McCabe, W.L., J.C. Smith, and P. Harriott, *Unit operations of chemical engineering*. 7th ed. McGraw-Hill chemical engineering series. 2005, Boston: McGraw-Hill. xxv, 1140 p.

Mehmet Yasar, G., *Design improvements on rotary valve particle feeders used for obtaining suspended airflows.* Powder Technology, 2004. **139**(1): p. 76-80.

Melchior, T., et al., *Solar-driven biochar gasification in a particle-flow reactor.* Chemical Engineering and Processing: Process Intensification, 2009. **48**(8): p. 1279-1287.

Mermoud, F., et al., *Experimental and numerical study of steam gasification of a single charcoal particle.* Combustion and Flame, 2006. **145**(1-2): p. 59-79.

Merrick, D., *Mathematical-Models of the Thermal-Decomposition of Coal .2. Specific-Heats and Heats of Reaction.* Fuel, 1983. **62**(5): p. 540-546.

Messenbock, R., D.R. Dugwell, and R. Kandiyoti, *CO2 and steam-gasification in a high-pressure wire-mesh reactor: the reactivity of Daw Mill coal and combustion reactivity of its chars.* Fuel, 1999. **78**(7): p. 781-793.

Muhlen, H.J., K.H. Vanheek, and H. Juntgen, *Kinetic-Studies of Steam Gasification of Char in the Presence of H-2, Co2 and Co.* Fuel, 1985. **64**(7): p. 944-949.

Murgia, S., M. Vascellari, and G. Cau, *Comprehensive CFD model of an air-blown coal-fired updraft gasifier.* Fuel, (0).

Nipattummakul, N., et al., *High temperature steam gasification of wastewater sludge.* Applied Energy, 2010. **87**(12): p. 3729-3734.

Ollero, P., et al., *Diffusional effects in TGA gasification experiments for kinetic determination.* Fuel, 2002. **81**(15): p. 1989-2000.

Parkash, S., *True Density and Elemental Composition of Subbituminous Coals.* Fuel, 1985. **64**(5): p. 631-634.

Piatkowski, N., C. Wieckert, and A. Steinfeld, *Experimental investigation of a packed-bed solar reactor for the steam-gasification of carbonaceous feedstocks.* Fuel Processing Technology, 2009. **90**(3): p. 360-366.

Reist, P.C. and L. Taylor, *Development and operation of an improved turntable dust feeder.* Powder Technology, 2000. **107**(1-2): p. 36-42.

Richard J, K., *Sunfuels.* Progress in Energy and Combustion Science, 1982. **8**(2): p. 121-134.

Saravanakumar, A., et al., *Numerical modelling of a fixed bed updraft long stick wood gasifier.* Biomass and Bioenergy, 2011. **35**(10): p. 4248-4260.

Simone, M., et al., *Evaluation of global biomass devolatilization kinetics in a drop tube reactor with CFD aided experiments.* Fuel, 2009. **88**(10): p. 1818-1827.

Smolinski, A., K. Stanczyk, and N. Howaniec, *Steam gasification of selected energy crops in a fixed bed reactor.* Renewable Energy, 2010. **35**(2): p. 397-404.

Suri, A. and M. Horio, *A novel cartridge type powder feeder.* Powder Technology, 2009. **189**(3): p. 497-507.

T.W, D., *The production of concentrated powder suspensions at low flow rates.* Powder Technology, 1985. **42**(3): p. 249-253.

Tardos, G.I. and Q. Lu, *Precision dosing of powders by vibratory and screw feeders: an experimental study.* Advanced Powder Technology, 1996. **7**(1): p. 51-58.

Umeki, K., T. Namioka, and K. Yoshikawa, *Analysis of an updraft biomass gasifier with high temperature steam using a numerical model.* Applied Energy, 2012. **90**(1): p. 38-45.

Umeki, K., et al., *High temperature steam-only gasification of woody biomass.* Applied Energy, 2010. **87**(3): p. 791-798.

Yagi, S. and D. Kunii, *Studies on Effective Thermal Conductivities in Packed Beds.* Aiche Journal, 1957. **3**(3): p. 373-381.

Yan, F., et al., *Hydrogen-rich gas production by steam gasification of char derived from cyanobacterial blooms (CDCB) in a fixed-bed reactor: Influence of particle size and residence time on gas yield and syngas composition.* International Journal of Hydrogen Energy, 2010. **35**(19): p. 10212-10217.

Z'Graggen, A., et al., *Hydrogen production by steam-gasification of petroleum coke using concentrated solar power--II Reactor design, testing, and modeling.* International Journal of Hydrogen Energy, 2006. **31**(6): p. 797-811.

Z'Graggen, A. and A. Steinfeld, *A two-phase reactor model for the steam-gasification of carbonaceous materials under concentrated thermal radiation.* Chemical Engineering and Processing: Process Intensification, 2008. **47**(4): p. 655-662.

Zbogar, A., et al., *Heat transfer in ash deposits: A modelling tool-box.* Progress in Energy and Combustion Science, 2005. **31**(5-6): p. 371-421.